STUDIES OF SOMATOSENSORY AND PAIN NEURAL CIRCUITS WITH HIGH FIELD FUNCTIONAL MRI

By

Elizabeth Ann Stringer

Dissertation

Submitted to the Faculty of the

Graduate School of Vanderbilt University

in partial fulfillment of the requirements

for the degree of

DOCTOR OF PHILOSOPHY

in

Neuroscience

December, 2010

Nashville, Tennessee

Approved:

Professor Stephen Bruehl

Professor Li Min Chen

Professor John C. Gore

Professor Jon Kaas

Professor Ronald Wiley

For my grandfather, John Charles Katz

ACKNOWLEDGMENTS

This research would not have been possible without the financial support of the National Institutes of Health through grants awarded to my advisor, Dr. John C. Gore. Most significantly the EB000461 grant has supported my research on the 7-T MR scanner for the last three years, and the T32 EB003817 predoctoral training grant supported two years of my research.

I must acknowledge and thank my advisor Dr. Gore for taking a chance on me when I was a first year graduate student. He provided the finances that allowed me to acquire data whenever I needed to, procure new equipment, travel to conferences, and the list goes on. My research could not have been accomplished without the Vanderbilt University Institute of Imaging Science's (VUIIS) 7-T scanner and the group of interdisciplinary scientists that keep it operational for human research. None of this would have been possible without Dr. Gore's vision.

I thank my committee members for encouraging me in my research. Their genuine interest in my projects has served as wonderful motivation. Dr. Li Min Chen has been a co-advisor to me and has taught me a great deal about sensory systems and manuscript writing, and her guidance has been critical to my development as a scientist. Dr. Ronald Wiley, my committee chair, has let me participate in his lab meetings and taught me to appreciate the complexity of the pain system, of which previously I had had only a superficial understanding. My other committee members, Dr. Stephen Bruehl and Dr. Jon Kaas, have each met with me on multiple occasions to assess my data, answer questions, and offer positive outlooks on the future.

Although not on my committee, Dr. Robert Friedman has given me his unwavering support and has taught me so much about science from electronics to physiology. Much of the data was acquired with Dr. Friedman's help, and he developed

the electronics we used in our studies. He has been a true mentor to me and I thank him for all his time and efforts.

I thank the many members of the VUIIS that have helped me along the way. Specifically Dr.'s Christopher Gatenby, Baxter Rogers, Allen Newton, and Robert Barry have all been integral in data acquisition, analysis, and interpretation. The VUIIS MR technologists have all helped with screening subjects and getting subjects into the scanner for data acquisition. Nancy Hagans is our administrator extraordinaire and has assisted me in many things over the last six years.

My family and friends have been so supportive of me during my graduate school experience, and I never would have made it through without them. My cousin Christina Rodriguez was the best roommate I could ask for and did her best to get me to balance the work with some fun. My cousin Christina Stringer has been my dissertation writing partner and without her support I'm not sure I would have had the motivation to "put pen to paper." My sister and best friend, Marie Yeagle, my brother-in-law, Jeremy Yeagle, my grandparents, Nancy and John Katz, and my parents, Pete and Bella Stringer, have been the most encouraging cheerleading section. They have made this document possible by persuading me not to give up time and time again. And last but not least, I thank Trey House for his unconditional love.

TABLE OF CONTENTS

LIST OF FIGURES

Figure **Page**

CHAPTER I

INTRODUCTION

The primary somatosensory cortex (SI) plays a principal role in the processing of both somatosensory and pain information. The organization and function of this cortical region have been studied for over a century using anatomical (e.g. lesions and antero- and retrograde staining) and physiological methods (e.g. single and multiunit electrical recordings). While these invasive techniques give us insight into the architecture of the human cortex and are practical for studies in most mammalian species, they are unfeasible approaches to studying this region in most people. With the advent of ultra-high field (7 Tesla) non-invasive magnetic resonance imaging (MRI) scientists are now able to study the cortex with the resolution and precision once only available by invasive techniques. In this work we use 7 T MRI to explore how human SI responds to and processes somatosensory and noxious stimuli.

Primary Somatosensory Cortex

The somatosensory cortices vary greatly across mammals in size, number, and functional representation. Despite inter-species differences, all mammals possess a systematic representation of contralateral cutaneous receptors known as the primary somatosensory cortex (SI). SI is located posterior to the central sulcus (CS) on the postcentral gyrus in the parietal cortex. This body surface map forms a homunculus—a disproportionate scale of physical body size. Sensoria with keen acuity are represented by spatially larger areas of cortex and have neurons with smaller receptive fields, resulting in cortical maps of the highest precision. Within anthropoid primates, SI can be

divided into four separate regions based on neuronal architecture first revealed by Brodmann and Vogt ((Brodmann, 1909), (Vogt and Vogt, 1919)). Arranged rostrally to caudally, areas 3a, 3b, 1, and 2 each contain a complete body representation but map different classes of receptors. The subregion boundaries can be objectively determined through cytoarchitectural features ((Geyer et al., 1999), (Geyer et al., 2000)), but no clear structural landmarks exist, leading to challenges in defining the boundaries with typical structural MRI techniques. The intersubject variability in neural geometry also adds to the difficulty in accurately indentifying the location of subregions ((Geyer et al., 2001)). Based on their extensive cytoarchitectural and MR studies of human SI, Geyer et al. have put forth guidelines for delineating the boundaries of the four subregions (Figure 1A, (Geyer et al., 2000)). Area 3a is located within the fundus of the CS, area 3b is located at along the posterior bank of the CS, area 1 is located at the crest of the postcentral gyrus, and area 2 is located on the anterior bank of the postcentral sulcus. In the following studies we focus on the representation of digits, and the hand area representation in area 3b can be identified by the omega-shaped folding of the CS and postcentral gyrus in the axial plane ((Moore et al., 2000), (White et al., 1997)). The topographic maps in each of these areas differ in response to different stimuli (i.e. tactile and noxious). For example, areas 3b and 1 are robustly responsive to cutaneous tactile stimuli, and single-cell recordings in monkey cortex have localized nociceptive neurons in area 3a, 3b, and 1, suggesting that these areas are robustly responsive to pain stimuli ((Kenshalo and Isensee, 1983), (Whitsel et al., 2009)). Images acquired at 7 T are able to delineate these structural and functional boundaries. A composite map of touch and pain activation in a single subject (digits 2 and/or 3) was overlaid on the subject's anatomical images in the three canonical planes (sagittal, coronal, and axial) for a three-dimensional affect (Figure 1). A zoomed-in image of the activation clusters illustrates the location of the SI subdivisions, with touch activations restricted to the posterior bank of

the CS (area 3b: yellow) and the crest of the postcentral gyrus (area 1: green) and pain activation within the fundus of the CS (area 3a: red), demonstrating that the SI subdivisions can be delineated with high resolution 7 T imaging (Figure 1C).

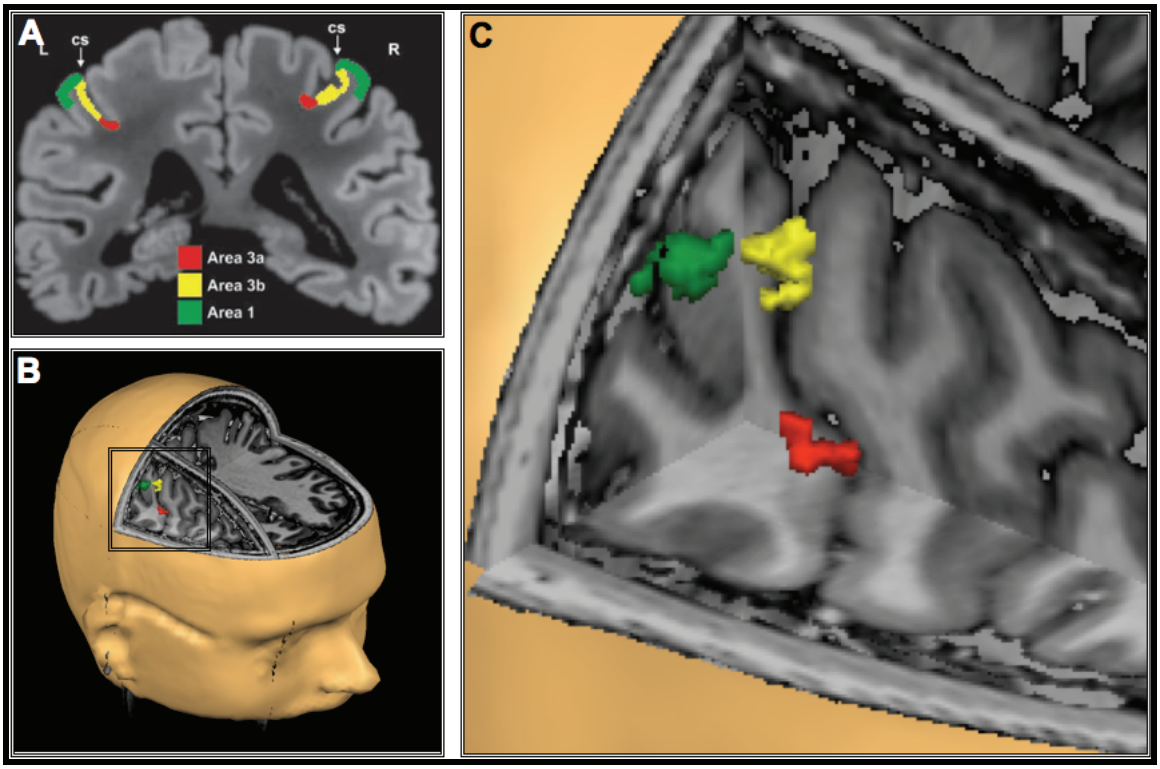

Figure 1. Cytoarchitectural subdivisions with SI. (***A***) Coronal slice of cortex over the central sulcus (CS) illustrating the cytoarchitectonic areas 3a (red), 3b (yellow), and 1 (green), from Geyer et al., 2000. (***B***) A composite image is overlaid on the three cardinal planes, axial, sagittal, and coronal to visulaize localized activations within areas 3a, 3b, and 1 in 3D. The black box indicates the volume of the zoomed-in image. (***C***) The zoomed image indicates the specificity of activations that can be localized to cytoarchitectural subdivisions within SI.

Somatic Sensation

Periphery and Subcortex

Sensory receptors that populate the cutaneous tissue and detect tactile stimuli are known as mechanoreceptors. As stimuli reach and deform the skin, there is a depolarization of mechanoreceptors, triggering an action potential. This transduction of

mechanical energy to electrical signal is the first step in somatosensory processing. Some mechanoreceptors fire rapidly at the onset of a stimulus and grow weaker with continued stimulation, others maintain firing throughout the duration of the stimulus; these receptors are called rapidly (RA) and slowly (SA) adapting receptors due to their ability to adapt (or not) to the applied stimulation. Four types of mechanoreceptors receive and transmit tactile information: Meissner's corpuscles, Pancinian corpuscles, Ruffini's corpuscles, and Merkel's disks. Meissner's corpuscles mainly populate the glabrous skin of the hands and feet and are sensitive to low-frequency (30-50 Hz) vibratory stimuli. Merkel's disks heavily populate the fingertips and are sensitive to even lower frequency (5-15 Hz) vibratory stimuli. Both Pancinian and Ruffini's corpuscles are associated with deep pressure vibration and skin stretching, respectively. The afferents that innervate all four types of mechanoreceptors are large myelinated axons (6-12 μm in diameter), known as Aβ nerve fibers that rapidly transmit tactile information (35-75 m/s) ((Purves, 1997), (Kandel et al., 2000), (Johnson, 2001)).

The Aβ fibers transmit tactile signals from the periphery to the spinal cord where a relay of afferents carry the information to the cortex through a pathway called the dorsal column-medial lemniscus system (Figure 3, (Purves, 1997)). The cell bodies of Aβ axons lie in the dorsal root ganglia and send ipsilateral projections up the dorsal columns of the spinal cord where they synapse in the gracile (lower body) and cuneate (upper body) nuclei of the caudal medulla. The contacting second-order neurons send axons that decussate (cross the midline) and then project up the contralateral medial lemniscus of the brainstem and synapse in the ventral posterior lateral (VPL) nucleus of the thalamus. The VPL sends projections to contralateral SI in a topographically organized manner.

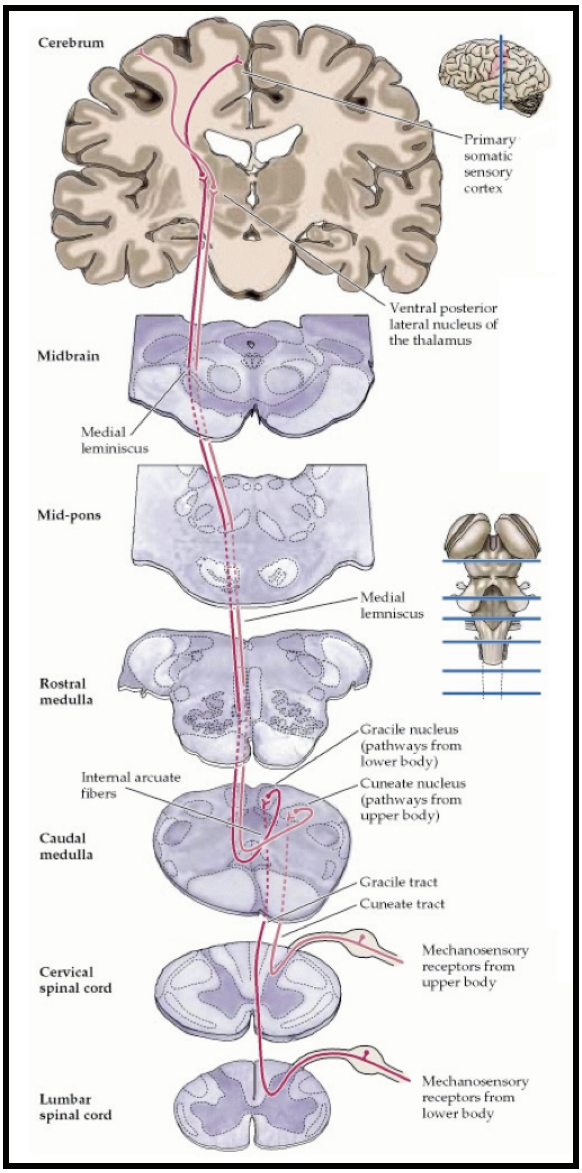

Figure 2. The dorsal columns and medial lemniscus pathway, from Purves, 1997. The blue lines on spinal cord and brainstem diagram to the right indicated the level of the pathway illustrated on the left. The blue line over the cortex indicates the coronal slice of the brain illustrated on the left. The red line demonstrates the path of touch processing through the dorsal column-medial lemniscus pathway.

Cortex

SI is comprised of four regions with unique responses to tactile stimuli. Areas 3a and 2 respond to proprioceptive stimuli, and in addition area 2 responds to some tactile stimuli. Both areas 3b and 1 respond to cutaneous stimuli, with area 3b responding to SA cutaneous mechanoreceptors and both areas 3b and 1 responding to RA cutaneous mechanoreceptors. All four areas contain a separate and complete systematic representation of body surface. While these maps have been well characterized in

nonhuman primates, the degree of agreement among all primates including humans is unknown.

Neurons within SI cortex project to higher-order regions of cortex, specifically secondary somatosensory cortex (SII). The function of SII in somatosensory processing and encoding is poorly understood but is thought to integrate information from multiple areas within SI resulting in a perceptual experience. The hippocampus and amygdala, structures that encode memory and are critical for learning, receive projections from SII, and thus this pathway is hypothesized to be significant for tactile learning. SI also sends projections to motor cortex, playing a critical role in motor planning and feedback ((Kandel et al., 2000), (Purves, 1997)).

Pain

Pain has been described as a silent epidemic because few realize that it is considered by many to be the leading public health problem in America. A significant portion of budgetary funding goes into pain research, yet our understanding of this highly complex system is lacking, evidenced by the millions of Americans that experience pain everyday. Acute cutaneous damage to the periphery results in the perception of pain which is defined as an unpleasant sensory and emotional experience. This experience is a defensive mechanism, a warning relay to prevent present and future injury, crucial for survival. Supraspinal processing of noxious information plays a major role in the integration of the sensory, emotional, cognitive, and motor signaling that comprise a person's subjective perception of and reaction to the painful stimulus. Specific brain structures play a critical part in the representation and modulation of this experience.

Periphery and Subcortex

Pain sensation is not caused by the overstimulation of the somatic sensory receptors. Although there are parallels between somatosensory and pain systems, the pain system has its own class of receptors, pathways, and circuits. Free nerve endings that sit in the epidermal layer of the skin, superficial to sensory receptors, arise from cell bodies within the dorsal root ganglia. Damage to the peripheral tissue is transduced by these nociceptors into potentials that are propagated along the afferent fibers into the spinal cord. The vanilloid subfamily of transient receptor potential ion channels (TRPVs) is activated by hot temperatures, low pH, capsaicin, and other vanilloids. TRPVs are highly expressed on both A-delta and C afferent fibers. A-delta fibers are thin, lightly myelinated axons with conduction velocities raging from 5-35 m/s; C fibers are thin unmyelinated axons with conduction velocities ranging from 0.5-2 m/s. The speed at which these fibers transmit pain signals explain the phenomenon known as first and second pain. First pain (A-delta mediated) is described as immediate, sharp, and concentrated while second pain (C mediated) is delayed, dull, and diffuse ((Torebjork and Hallin, 1973)). A-delta and C afferent fibers enter the spinal cord through the dorsal root ganglia and synapse in the superficial laminae of the dorsal horn. Within the dorsal horn the pain signal is transmitted to second-order projection neurons whose axons cross the midline joining the spinothalamic tract (Figure 4: (Purves, 1997), (Willis et al., 1979)). The fibers ascend through the anterolateral system of the spinal cord. As they enter the brainstem they send projections to the rostral ventromedial medulla and the periaqueductal gray (PAG), areas essential for arousal and analgesia. The tract terminates in the ventral posterior nuclei (ventral posterior lateral, ventral posterior medial, and ventral posterior inferior) of the thalamus which project to SI and SII ((Treede, 2002)). This network has been coined the lateral pain network. The anterolateral projections terminate in several other thalamic nuclei including the

ventromedial posterior, medial dorsal, parafascicular, and centrolateral, which in turn project to the insula and anterior cingulate, comprising the medial pain network ((Purves, 1997), (Hunt and Koltzenburg, 2005), (Kandel et al., 2000)).

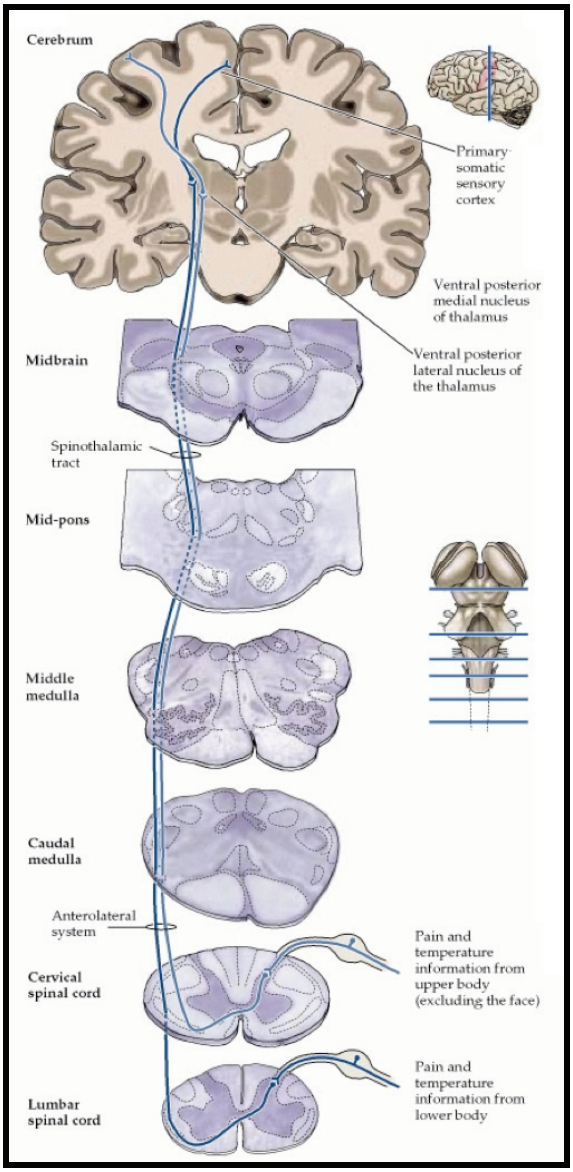

Figure 3. The spinothalamic pathway, from Purves, 1997. The blue lines on spinal cord and brainstem diagram to the right indicated the level of the pathway illustrated on the left. The blue line over the cortex indicates the coronal slice of the brain illustrated on the left. The blue line demonstrates the path of pain processing through the spinothalamic pathway.

Cortex

Integration of the multiple circuits involved in the subjective pain experience occurs in the brain. Anatomical studies show thalamic projections from the ventral

posterior nuclei terminate in SI. Initially the pain center of the cortex was believed to be SI as a submodality of touch. In 1911 Head and Holmes challenged this view when they reported that patients with SI lesions could still feel pain ((Head and Holmes, 1911)). In agreement with the theory of widespread cortical involvement, early imaging studies of neural activity during painful events revealed complex circuitry. This left the field open to find new brain structures associated with pain processing. Although variability exists between reports, imaging studies, regardless of modality, converge on four main areas activated by pain. These are the primary somatosensory cortex (SI), secondary somatosensory cortex (SII), insular cortex (IC), and anterior cingulate cortex (ACC) ((Apkarian et al., 2005)). Presurgical intracranial recordings have confirmed neural activity in S1, S2, IC, and ACC after the onset of painful stimuli ((Lenz et al., 1998), (Kanda et al., 2000), (Vogel et al., 2003)). Additional regions found to be involved in the processing of pain without the same consistency include posterior parietal cortex, supplementary motor cortex (SMA), prefrontal cortex (PFC), thalamus (Th), basal ganglia (BG), amygdala, hippocampus, PAG, and cerebellum ((Apkarian et al., 2005), (Brooks and Tracey, 2005), (Peyron et al., 2000)). Advances in noninvasive imaging technology have made it possible to tease apart the circuits that govern these components of the pain experience. Although there has been inconsistency over the last couple of decades in study findings, there is agreement on the main regions involved in the processing of pain and their functional roles. One finding that is not disputed is the large degree of interindividual variability. With the sensitivity that high field imaging provides, subjects can be analyzed individually without the need for averaging. This approach is advantageous to networks that are highly variable across subjects.

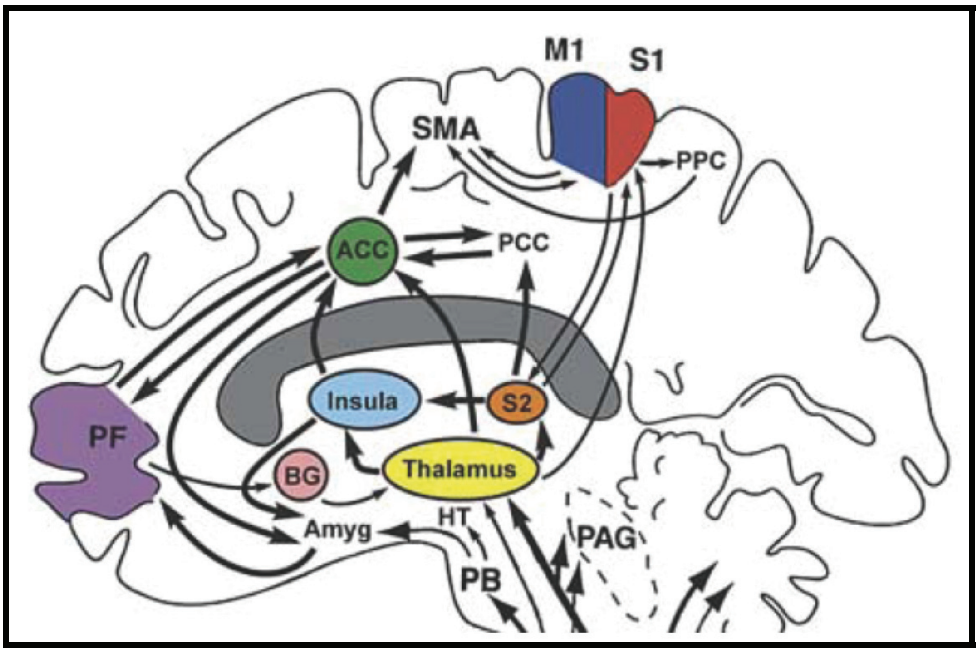

Figure 4. Supraspinal regions involved in the processing of pain, from Apkarian et al., 2005. Connections and circuitry that govern the perception of pain. Brain structures: primary and secondary somatosensory cortices (S1, S2, red and orange); anterior cingulate cortex (ACC, green); insular cortex (blue); thalamus (yellow); prefrontal cortex (PF, purple); primary and supplementary cortices (M1, SMA, dark blue); posterior parietal cortex (PPC); posterior cingulate cortex (PCC); basal ganglia (BG, pink); hypothalamus (HT); amygdala (AMYG); parabrachial nuclei (PB); periaqueductal gray (PAG).

Neuroimaging

Exploration of the human brain fascinates people partly because the organ that controls our thoughts and actions is shrouded in mystery, as if it were an uncharted new continent. Early neuroscientists thought that different functions of the brain could be specifically localized, and that the volume of neural tissue over these specific locations, as measured by protrusions in the skull, was proportionate to one's personality traits and propensities. While phrenology is now considered only a pseudoscience, it proposed the more lasting theory that aspects of brain function can be localized and mapped. Today neuroscientists use a handful of neuroimaging techniques to characterize the structure and function of the human cortex.

Neuroimaging techniques that are commonly used in human studies are noninvasive, including electroencephalography (EEG), positron emission tomography (PET), and functional magnetic resonance imaging (fMRI), each with its own advantages and disadvantages. EEG has the advantage of directly measuring neural electrical activity on the order of milliseconds, while PET and fMRI typically measure correlates of neural activity on the order of seconds to minutes. Centimeters away from the grey matter of cortex, EEG electrodes measure electrical activity originating from the post-synaptic potentials of neurons. While EEG is arguably the safest and least expensive technique, the poor spatial resolution renders it ineffective at answering questions of neural specificity. It can reliably identify neural activity only from the superficial layers of cortex, and the inverse problem makes it mathematically impossible to identify precisely the specific current sources. PET has similar limitations in spatial resolution. During PET, a radioactive tracer isotope (as part of a biologically relevant molecule) is injected into a person, and as the isotope undergoes decay, it emits a positron that will travel up to a millimeter before it interacts with an electron. The encounter annihilates both positron and electron, producing gamma photons that are counted by detectors. Due to detection errors and the inability to precisely identify the location of decay, the spatial resolution available with PET is just under a centimeter. PET has the advantage of imaging a variety of biologically relevant molecules, such as [^{11}C]carefentanil that targets the μ-opioid receptor or [^{18}F]FDG (2-fluoro-2-deoxy-D-glucose) that measures glucose uptake, which is a correlate of neural activity. Similar to PET, fMRI reports changes in the energy demand of active neurons by detecting disruptions in the magnetic field caused by changes in the concentration of deoxygenated hemoglobin (Hgb) during neural activity. Similar to EEG, fMRI is safe for repeated use and most clinical populations. While both EEG and PET have their benefits, neither has the millimeter spatial resolution that fMRI affords.

fMRI Signal

The human body is composed primarily of water (roughly 50-60 % by weight, (Marieb, 1999)), so organs such as the brain have a high molar concentration of hydrogen nuclei. These protons can be detected using nuclear magnetic resonance (NMR) and their NMR signals can be used to produce high quality images via MRI. To gain insight into the anatomy of organs like the brain, a static magnetic (B) field (approximately 140,000 times the strength of the Earth's magnetic field at 7 T) is applied, aligning a majority of the protons along the direction of the B-field to create a macroscopic nuclear magnetization. A radiofrequency (RF) pulse at the resonance frequency of the protons (4-26 MHz/Tesla) is applied, tipping the magnetization away from the equilibrium alignment. As the protons gradually realign with the static B-field, energy is released to the surrounding medium. Moreover, the magnetization experiences a torque that causes it to precess or rotate about the field direction, which induces an electromagnetic signal in a conducting coil around the sample. In order to encode spatial information, gradient coils within the scanner apply a gradation to the static B-field, thereby altering the frequency and/or phase of these induced currents that allow for localization of the signal.

The local magnetic field experienced by water molecules can also be influenced by changes in the amount of oxygen within the vasculature blood supply. In areas of increased neuronal activity, there is increased energy consumption that leads to an enhanced oxygen demand. Oxygen for aerobic metabolism is supplied to neurons via the vasculature so blood flow increases to meet the higher demand. Blood is concentrated with Hgb, an iron-containing molecule that transports oxygen throughout the body. The oxygenated Hgb (oxy-Hgb) molecule is diamagnetic, and has a very similar magnetic susceptibility to tissue, but deoxygenated Hgb (deoxy-Hgb) is

paramagnetic due to unpaired electrons in the iron within the heme group (no longer bound to oxygen atoms), so that it has a strong magnetic moment that disturbs the uniformity of the local B-field and reduces the lifetime of the NMR signal. Contrary to logic, the ratio of deoxy-Hgb to oxy-Hgb decreases in areas of neural activity. The change in blood flow, supplying glucose and oxy-Hgb to areas of energy and oxygen demand, is greater than the increase in oxygen consumption, leading to a local decrease in the concentration of deoxy-Hgb and ultimately an increase in MR signal. This effect is known as the Blood Oxygen Level Dependent effect, or BOLD ((Ogawa et al., 1990)). While the precise relationship between neural activity and BOLD is still debated and heavily researched, the effect is robust and measurable.

fMRI Protocol

Multiple imaging sequences have been developed for functional MRI, some of the most popular of which aim to exploit the BOLD signal. Of these imaging sequences, gradient echo-echo planar imaging (GE-EPI) is one of the most common. In the following work we used a high spatial resolution single-shot EPI, which acquires the data in two-dimensions and multiple slices. For sensitivity to the BOLD signal, the total imaging volume should be acquired in less than 5 s. It is also advantageous to acquire images as rapidly as possible to mitigate the increased signal degradation caused my local field inhomogeneities and subject movement that evolve over long image acquisitions, while still remaining sensitive to the detection of BOLD signal. Here we employed several techniques to improve the quality of the acquired images including shimming, B_0 (static B-field) field correction, parallel imaging, and reduced imaging volume. Static shimming during image acquisition partially corrects for the B_0 inhomgeneities, and post image processing that includes distortion correction based on B_0 field maps provides additional improvements to the image quality. With our 16-channel receive coil, we could employ a

parallel imaging technique, sensitivity encoding or SENSE, permitting us to reconstruct images from undersampled data, acquired in a shorter amount of time. Within the imaging volume, we acquired 16 slices in an interleaved pattern, spanning 32 mm, providing us with images of high spatial resolution, yet limited coverage.

Study Design

A myriad of disciplines has benefited from the development of fMRI, including psychology, neurology, psychiatry, and basic neuroscience. The commonality between fields is a desire to map the function of the human brain by detecting changes in neural activity elicited by specific stimuli or conditions. In order to "pull-out" active areas, scientists have to carefully consider their study design in regards to the population being studied. MRI scanners are known to be uncomfortable. The subject typically lies supine and is asked to remain still for an hour or more while loud noises emanate from the scanner, so imaging scientists aim to acquire images with a maximum amount of signal in the shortest amount of time. This can be accomplished by implementing a standard block design protocol in which a specific stimulus is "on" for a given time interval and "off" (at rest) for a given time interval. By directly comparing these conditions, areas that alter neural state can be readily detected.

For maximum detection of fMRI signals, specific criteria must be met. First, the difference in BOLD signals between conditions must be maximized, so the block interval should be long enough to elicit the largest evoked response. In addition, fMRI-BOLD is a measurement of hemodynamic changes in the brain, and the hemodynamic response function (HRF) is slow to evolve, reaching its maximum amplitude approximately 4-6 s after task onset, supporting the need for longer blocks. Not only does the HRF need time to fully evolve to reach a maximum amplitude, but at the offset of the task, the HRF needs time to return to baseline. If there is not full recovery, there will not be a maximum

difference between conditions. Many parameters must be taken into account to determine the length of a block, but generally, in practice, the time interval of a block is between 20 and 30 s. The second criterion takes into consideration the noise that is always present in functional MR imaging. If the noise within a block is greater than the signal difference between conditions, there is no way to reliably detect a difference between conditions. Repeating blocks multiple times can mitigate this noise so that the signals within each condition can be averaged and compared for maximum detection.

Data Analysis

With a thoughtful and careful study design many challenges can be overcome in order to answer the specific question being asked. Once the images have been acquired, however, there are steps that must be taken to process the data appropriately. These preprocessing steps typically include slice-time correction, motion correction in three dimensions, temporal filtering, and spatial smoothing. The MR scanner acquires the EPI-BOLD images systematically (usually interleaved) in planes (slices). Each plane is collected at a different point in time, leading to temporal discrepancies throughout the larger image volume. Slice-time correction is an attempt to “shift” the planes as if they were collected in unison, usually through temporal interpolation techniques.

As stated previously, fMRI sessions typically last an hour or longer, during which the subject is asked to remain still. While a good subject moves their body minimally, it is impossible to stay absolutely rigid for this length of time. Head motion can be caused by any number of phenomena such as the surprise at the novelty of a stimulus, a motor task, the sensation of falling asleep, and deglutition. A whole subfield of fMRI is dedicated to minimizing the affects of head motion in images through various types of models, typically through rigid registration algorithms that maximize the shared or mutual information of whole volume images. Physiological “noise” can also lead to motion and

other temporal artifacts, and these effects grow at higher B-fields. Respiration and heart rate can be monitored and recorded with ease during an imaging session using a respiratory bellow that fits around the chest and a pulse monitor that attaches to the subject's finger, respectively. These temporal signals can be regressed (filtered) out of the image data using a method known as RETROICOR ((Glover et al., 2000)). Other temporal noise can affect the functional images as well, such as scanner drift. Typically a high-pass filter with a linear trend removal is also applied to the image data to mitigate the temporal noise.

Finally, most fMRI studies investigate a group of subjects in order to make a statistical inference on the population at large. In group studies, the subjects' data are warped into a common stereotactic space and the functional data of each subject are averaged. Since every subject has their own unique cortical geometry and physiology, the overlap of activations across subjects can be minimal. To amplify the activity overlap across subjects, the image data is spatially smoothed. Smoothing kernels between 4 and 12 mm are applied voxel by voxel to smooth and blur the data in order to maximize the detection of activity that is common within a diverse group. In the following chapters, there are no group studies. Enabled by the higher SNR at 7 T each subject is analyzed individually, and no group averaging is calculated, negating the need for spatial smoothing. This assures the precision and specificity of the localization of fMRI signal.

Once the data have been preprocessed, they are analyzed to detect areas of activation. The most widely used technique for extracting information about neural activity is the statistical general linear model (GLM) ((Friston, 1995)), by which the data are represented in the form: $y(t) = \beta_1 \cdot x_1(t) + \beta_2 \cdot x_2(t) + e(t)$, where y(t) is the BOLD time signal of a single voxel, x(t) is one of the conditions or regressors being tested, β (beta-weight) is the measure of how well the regressor fits the data, and e(t) is the

residual error. Any number of conditions can be added to the study design, and thus the same number of regressors is added to the model (x_1, x_2, x_3, etc). fMRI is a measurement of the hemodynamic changes in response to a task, and for this reason the regressors are convolved with the HRF before the model is applied to the data in order to reflect the physiological phenomenon that is being measured. The greater the task specific β-weight at a particular voxel, the more the regressor (or task condition) accounts for the signal variance measured in the specific voxel.

Functional Connectivity

Most fMRI studies take advantage of a stimulus paradigm and stimulus driven detection of fMRI signal. On the other hand, so-called resting state methods do not involve a task but may be used to assess functional connectivity. Functional connectivity assesses "the organization, interrelationship, and integrated performance of different regions ((Rogers et al., 2007))." Functional connectivity can be assed by measuring the correlations in spontaneous BOLD fluctuations across the brain. While many MRI studies evaluate the function and anatomy of individual regions in the brain, functional connectivity is a systems level evaluation of intrinsic networks. This type of analysis has been used to study how disease and disorder affects visual, language, motor, and working memory circuits, with the general finding that patient populations often have disruptions in these resting state networks. For example patients with autism spectrum disorder have a disrupted social and emotional network, but their attentional and goal-directed cognitive network does not differ from normal subjects ((Kennedy and Courchesne, 2008)). This offers promise for the study of chronic pain because autism spectrum disorder, like chronic pain, has a large heterogeneity within the patient population. Resting state functional connectivity could be a useful tool for evaluating chronic pain because it is less subjective, and the diversity and subject variability makes

it hard to attain conclusive results with chronic pain populations. A recent study found that chronic pain patients have a disrupted default mode network ((Baliki et al., 2008)). Before we study the patient population however, we need to understand how the intrinsic pain network functions in normal subjects.

Somatosenation

The transduction and processing of somatosensation has been carefully characterized in nonhuman primate studies. The flow of information from the thalamus to SI, and from SI to SII and motor cortices, and onto other higher-order brain structures is rather straight forward (in comparison to the processing of pain information). Several fMRI studies have confirmed somatotopic organization of body surface in both SI and SII, and in particular the fine-scale topography of digits in SI. These maps, however, lack the spatial specificity and sensitivity necessary for applications where there are dynamic cortical changes in vulnerable patient populations, such as cortical reorganization following stroke or amputation.

Pain

In many sensory systems, we have gained tremendous insight into the processing of the human cortex by studying other parallel mammalian cortices. Pain is a highly subjective experience making it very difficult to interpret findings in animal model studies. Sensory, affective, and cognitive elements are integrated in the brain to form an individual's perception of pain. These three components comprise specific brain structures, some of which overlap. The sensory component of pain, comprising the lateral pain network, discriminates stimulus intensity, location, and modality; this network involves SI, SII, and insular cortex (IC). Neuroelectrical imaging methods (EEG and MEG) have the highest temporal resolution (milliseconds), allowing researchers to

distinguish sensory inputs originating from separate afferent fibers ((Bromm and Treede, 1983), (Arendt-Nielsen et al., 1990), (Bragard et al., 1996), (Opsommer et al., 2001), (Tran et al., 2002), (Ploner et al., 2002), (Iannetti et al., 2003)). Onset of activity can be correlated with stimulus intensity, meaning that areas activated by fast transmitting innocuous signals can be filtered from those activated by slower transmitting noxious signals. These electrical studies along with anatomical studies indicate that SII and posterior IC as primary nociceptive inputs, SII receiving the earliest pain signal in the cortex ((Apkarian and Shi, 1994), (Craig, 2002)). Moreover, the frontal operculum, which comprises SII and IC, is the only cortical region to elicit pain perception in response to electrical stimulation ((Ostrowsky et al., 2002), (Frot and Mauguiere, 2003)). SII and IC are prominent regions involved in pain circuitry but not touch circuitry, yet single unit recordings in monkeys have identified specific nociceptive neurons within SI ((Kenshalo et al., 1988), (Kenshalo and Isensee, 1983)). Hemodynamic imaging methods, like PET and fMRI, have higher spatial resolution than EEG and MEG and agree with the findings that SI, SII, and IC are involved in stimulus intensity discrimination. Graded painful stimuli delivered to subjects resulted in graded increases in neural activation in SI, SII, and IC, reflecting that these regions encode pain intensity ((Coghill et al., 1999), (Craig et al., 2000)). In a study assessing attentional components of pain, subjects were either diverted from the noxious stimulus or were asked to attend to the stimulus. Only SI, SII, and IC were activated regardless of attention task ((Peyron et al., 1999)). When the temporal signal was assessed in an fMRI pain study, time courses in both SI and SII had double peaks that paralleled the increase in intensity rating ((Chen et al., 2002)). While intensity discrimination is mediated by SI, SII, and IC, there is little evidence that SII and IC can discriminate between the locations of painful stimuli. SI is the only cortical region with clear pain topography that is consistent with the sensory-touch homunculus ((Tarkka and Treede, 1993), (Ploner et al., 1999)). In these pain and imaging studies,

various types of stimuli have been used to evoke pain including contact heat/cold, muscular/cutaneous electric shock, hypertonic saline, capsaicin, colonic/rectal/gastric/esophageal distention, ischemia, ascorbic acid, laser heat, and illusion of pain. Some studies have investigated whether different stimulus modalities elicit different neural activation patterns. Most do not report significant differences ((Craig et al., 1996), (Davis et al., 1998), (Kwan et al., 2000), (Tracey et al., 2000)), but of those that do, the PFC is the region consistently implicated in stimulus modality discrimination ((Svensson et al., 1997), (Strigo et al., 2003)).

The affective component of pain, comprising the medial pain network, mediates the fear and anxiety associated with anticipation of pain, and encodes the degree of stimulus unpleasantness; this network involves limbic areas PFC, ACC, IC, hippocampus, and amygdala. Neural activity during anticipation of painful stimulus was evaluated using different colored lights to cue for delivery of nonpainful and painful stimuli. During the time between the cue and stimulus onset, researchers found activation in the anterior IC and medial PFC ((Ploghaus et al., 1999)). The same group looked further into how anxiety during this anticipation period increases perception of pain. They tested whether the increase in pain perception caused by anxiety results in increased neural activation paralleling the increase in activation brought on by increasing in stimulus intensity. There was not uniform increase in activation as was expected except for increases in entorhinal cortex ((Ploghaus et al., 2001)). Temporal data reveal that ACC onset lags other regions', meaning that it is improbable that ACC is part of the sensory pain circuit. The amplitude of activation in this region is more highly correlated with perceived intensity of the stimulus than the actual stimulus strength ((Beydoun et al., 1993)). In a study evaluating empathy, subjects were scanned while undergoing a painful task and while watching a friend in an adjacent room undergoing a painful task. Activation in the anterior IC and the rostral ACC were tightly correlated with the subject's

feelings of empathy for another's pain ((Singer et al., 2004)). Hypnotic suggestions have been used to alter the unpleasantness of the painful stimulus perceived by a subject without changing the intensity of the stimulus. This resulted in an increase in activity solely in the ACC ((Rainville et al., 1997)). The correlation between ACC activation and stimulus unpleasantness has been confirmed by other studies ((Tolle et al., 1999), (Fulbright et al., 2001)).

The cognitive component of pain involves attention, memory, and evaluation; this network engages PFC, ACC, IC, and SMA. It is almost impossible for a subject to attend to stimuli of varying intensities with the same vigilance. The greater the pain, the more the attention the subject pays. This poses a challenge for researchers in separating cognitive-attentional and sensory-intensity networks. Peyron *et al* found that when subjects attended to, as opposed to being distracted from, the noxious stimulus, PFC and ACC were activated ((Peyron et al., 1999)). The memory of pain experienced in the past has been shown to modulate the perception of pain, making it critical to map this network ((Koyama et al., 2005)). Albanese et al. compared activation during a control motor task and a memory task evaluating the intensity and location of the painful stimulus ((Albanese et al., 2007)). Memory specific activation was found in SI and anterior IC. It is likely that SI was activated because the memory task was sensory-discriminate, but more research is required to make this conclusion. When exposed to a noxious stimulus over a period of time, sensitization and habituation modulate the perception of stimulus intensity. Most studies require subject evaluation of pain to control for these changes in perception. SMA, motor and premotor cortices are not consistently reported as part of the pain network. While some hypothesize that they arise from either pain-evoked motion or suppression of motion, data suggests that they could arise from the physical act of evaluating pain ((Moulton et al., 2005)). Evaluation of a noxious

stimulus is dependent on integrating both sensory-discriminative and motivational-affective circuits ((Peyron et al., 2000)).

Specific Aims

The goal of the following studies was to provide insight into how human sensory experiences are processed in subdivisions of SI by taking advantage of ultra-high field imaging at 7 T. Benefits to imaging at higher field strengths include increased SNR and sensitivity to BOLD signal which permit imaging scientists to acquire MR data at a higher spatial resolution, and thus to delineate functional responses that correspond to different anatomical subdivisions. The aims of this dissertation were to a) map digit somatotopy and measure inter-digit distance in areas 3b and 1 of SI, b) detect and characterizes spatial and temporal response differences to innocuous tactile stimulation in area 3b and area 1, and c) identify areas that respond to pain intensity estimation within SI, asses how these areas are functionally integrated in the resting state, and evaluate how the experience of pain alters these interareal relationships.

References

Albanese, M.C., Duerden, E.G., Rainville, P., Duncan, G.H., 2007. Memory traces of pain in human cortex. J Neurosci 27, 4612-4620.

Apkarian, A.V., Bushnell, M.C., Treede, R.D., Zubieta, J.K., 2005. Human brain mechanisms of pain perception and regulation in health and disease. Eur J Pain 9, 463-484.

Apkarian, A.V., Shi, T., 1994. Squirrel monkey lateral thalamus. I. Somatic nociresponsive neurons and their relation to spinothalamic terminals. J Neurosci 14, 6779-6795.

Arendt-Nielsen, L., Zachariae, R., Bjerring, P., 1990. Quantitative evaluation of hypnotically suggested hyperaesthesia and analgesia by painful laser stimulation. Pain 42, 243-251.

Baliki, M.N., Geha, P.Y., Apkarian, A.V., Chialvo, D.R., 2008. Beyond feeling: chronic pain hurts the brain, disrupting the default-mode network dynamics. J Neurosci 28, 1398-1403.

Beydoun, A., Morrow, T.J., Shen, J.F., Casey, K.L., 1993. Variability of laser-evoked potentials: attention, arousal and lateralized differences. Electroencephalogr Clin Neurophysiol 88, 173-181.

Bragard, D., Chen, A.C., Plaghki, L., 1996. Direct isolation of ultra-late (C-fibre) evoked brain potentials by CO2 laser stimulation of tiny cutaneous surface areas in man. Neurosci Lett 209, 81-84.

Brodmann, K., 1909. VergleichendeLocalisationslehre der Gro Hhirnrinde. Barth, Leipzig.

Bromm, B., Treede, R.D., 1983. CO2 laser radiant heat pulses activate C nociceptors in man. Pflugers Arch 399, 155-156.

Brooks, J., Tracey, I., 2005. From nociception to pain perception: imaging the spinal and supraspinal pathways. J Anat 207, 19-33.

Chen, J.I., Ha, B., Bushnell, M.C., Pike, B., Duncan, G.H., 2002. Differentiating noxious- and innocuous-related activation of human somatosensory cortices using temporal analysis of fMRI. J Neurophysiol 88, 464-474.

Coghill, R.C., Sang, C.N., Maisog, J.M., Iadarola, M.J., 1999. Pain intensity processing within the human brain: a bilateral, distributed mechanism. J Neurophysiol 82, 1934-1943.

Craig, A.D., 2002. How do you feel? Interoception: the sense of the physiological condition of the body. Nat Rev Neurosci 3, 655-666.

Craig, A.D., Chen, K., Bandy, D., Reiman, E.M., 2000. Thermosensory activation of insular cortex. Nat Neurosci 3, 184-190.

Craig, A.D., Reiman, E.M., Evans, A., Bushnell, M.C., 1996. Functional imaging of an illusion of pain. Nature 384, 258-260.

Davis, K.D., Kwan, C.L., Crawley, A.P., Mikulis, D.J., 1998. Functional MRI study of thalamic and cortical activations evoked by cutaneous heat, cold, and tactile stimuli. J Neurophysiol 80, 1533-1546.

Friston, K.J., 1995. Commentary and opinion: II. Statistical parametric mapping: ontology and current issues. J Cereb Blood Flow Metab 15, 361-370.

Frot, M., Mauguiere, F., 2003. Dual representation of pain in the operculo-insular cortex in humans. Brain 126, 438-450.

Fulbright, R.K., Troche, C.J., Skudlarski, P., Gore, J.C., Wexler, B.E., 2001. Functional MR imaging of regional brain activation associated with the affective experience of pain. AJR Am J Roentgenol 177, 1205-1210.

Geyer, S., Schleicher, A., Schormann, T., Mohlberg, H., Bodegard, A., Roland, P.E., Zilles, K., 2001. Integration of microstructural and functional aspects of human somatosensory areas 3a, 3b, and 1 on the basis of a computerized brain atlas. Anat Embryol (Berl) 204, 351-366.

Geyer, S., Schleicher, A., Zilles, K., 1999. Areas 3a, 3b, and 1 of human primary somatosensory cortex. Neuroimage 10, 63-83.

Geyer, S., Schormann, T., Mohlberg, H., Zilles, K., 2000. Areas 3a, 3b, and 1 of human primary somatosensory cortex. Part 2. Spatial normalization to standard anatomical space. Neuroimage 11, 684-696.

Glover, G.H., Li, T.Q., Ress, D., 2000. Image-based method for retrospective correction of physiological motion effects in fMRI: RETROICOR. Magn Reson Med 44, 162-167.

Head, H., Holmes, G., 1911. Sensory Disturbances from Cerebral Lesions. Brain 34, 102-254.

Hunt, S., Koltzenburg, M., 2005. The Neurobiology of Pain. Oxford Universtiy Press.

Iannetti, G.D., Truini, A., Romaniello, A., Galeotti, F., Rizzo, C., Manfredi, M., Cruccu, G., 2003. Evidence of a specific spinal pathway for the sense of warmth in humans. J Neurophysiol 89, 562-570.

Kanda, M., Nagamine, T., Ikeda, A., Ohara, S., Kunieda, T., Fujiwara, N., Yazawa, S., Sawamoto, N., Matsumoto, R., Taki, W., Shibasaki, H., 2000. Primary somatosensory cortex is actively involved in pain processing in human. Brain Res 853, 282-289.

Kandel, E., Schwartz, J., Jessell, T., 2000. Principles of Neural Science, 4th ed. McGraw-Hill Medical.

Kennedy, D.P., Courchesne, E., 2008. The intrinsic functional organization of the brain is altered in autism. Neuroimage 39, 1877-1885.

Kenshalo, D.R., Jr., Chudler, E.H., Anton, F., Dubner, R., 1988. SI nociceptive neurons participate in the encoding process by which monkeys perceive the intensity of noxious thermal stimulation. Brain Res 454, 378-382.

Kenshalo, D.R., Jr., Isensee, O., 1983. Responses of primate SI cortical neurons to noxious stimuli. J Neurophysiol 50, 1479-1496.

Koyama, T., McHaffie, J.G., Laurienti, P.J., Coghill, R.C., 2005. The subjective experience of pain: where expectations become reality. Proc Natl Acad Sci U S A 102, 12950-12955.

Kwan, C.L., Crawley, A.P., Mikulis, D.J., Davis, K.D., 2000. An fMRI study of the anterior cingulate cortex and surrounding medial wall activations evoked by noxious cutaneous heat and cold stimuli. Pain 85, 359-374.

Johnson, K.O., 2001. The roles and functions of cutaneous mechanoreceptors. Curr Opin in Neurobiology 11, 455-461.

Lenz, F.A., Rios, M., Chau, D., Krauss, G.L., Zirh, T.A., Lesser, R.P., 1998. Painful stimuli evoke potentials recorded from the parasylvian cortex in humans. J Neurophysiol 80, 2077-2088.

Marieb, E., 1999. Human Anatomy and Physiology, 5th ed. Benjamin Cummings.

Moore, C.I., Stern, C.E., Corkin, S., Fischl, B., Gray, A.C., Rosen, B.R., Dale, A.M., 2000. Segregation of somatosensory activation in the human rolandic cortex using fMRI. J Neurophysiol 84, 558-569.

Moulton, E.A., Keaser, M.L., Gullapalli, R.P., Greenspan, J.D., 2005. Regional intensive and temporal patterns of functional MRI activation distinguishing noxious and innocuous contact heat. J Neurophysiol 93, 2183-2193.

Ogawa, S., Lee, T.M., Nayak, A.S., Glynn, P., 1990. Oxygenation-sensitive contrast in magnetic resonance image of rodent brain at high magnetic fields. Magn Reson Med 14, 68-78.

Opsommer, E., Weiss, T., Plaghki, L., Miltner, W.H., 2001. Dipole analysis of ultralate (C-fibres) evoked potentials after laser stimulation of tiny cutaneous surface areas in humans. Neurosci Lett 298, 41-44.

Ostrowsky, K., Magnin, M., Ryvlin, P., Isnard, J., Guenot, M., Mauguiere, F., 2002. Representation of pain and somatic sensation in the human insula: a study of responses to direct electrical cortical stimulation. Cereb Cortex 12, 376-385.

Peyron, R., Garcia-Larrea, L., Gregoire, M.C., Costes, N., Convers, P., Lavenne, F., Mauguiere, F., Michel, D., Laurent, B., 1999. Haemodynamic brain responses to acute pain in humans: sensory and attentional networks. Brain 122 (Pt 9), 1765-1780.

Peyron, R., Laurent, B., Garcia-Larrea, L., 2000. Functional imaging of brain responses to pain. A review and meta-analysis (2000). Neurophysiol Clin 30, 263-288.

Ploghaus, A., Narain, C., Beckmann, C.F., Clare, S., Bantick, S., Wise, R., Matthews, P.M., Rawlins, J.N., Tracey, I., 2001. Exacerbation of pain by anxiety is associated with activity in a hippocampal network. J Neurosci 21, 9896-9903.

Ploghaus, A., Tracey, I., Gati, J.S., Clare, S., Menon, R.S., Matthews, P.M., Rawlins, J.N., 1999. Dissociating pain from its anticipation in the human brain. Science 284, 1979-1981.

Ploner, M., Gross, J., Timmermann, L., Schnitzler, A., 2002. Cortical representation of first and second pain sensation in humans. Proc Natl Acad Sci U S A 99, 12444-12448.

Ploner, M., Schmitz, F., Freund, H.J., Schnitzler, A., 1999. Parallel activation of primary and secondary somatosensory cortices in human pain processing. J Neurophysiol 81, 3100-3104.

Purves, D., 1997. Neuroscience. Neuroscience, xix+562p.

Rainville, P., Duncan, G.H., Price, D.D., Carrier, B., Bushnell, M.C., 1997. Pain affect encoded in human anterior cingulate but not somatosensory cortex. Science 277, 968-971.

Rogers, B.P., Morgan, V.L., Newton, A.T., Gore, J.C., 2007. Assessing functional connectivity in the human brain by fMRI. Magn Reson Imaging 25, 1347-1357.

Singer, T., Seymour, B., O'Doherty, J., Kaube, H., Dolan, R.J., Frith, C.D., 2004. Empathy for pain involves the affective but not sensory components of pain. Science 303, 1157-1162.

Strigo, I.A., Duncan, G.H., Boivin, M., Bushnell, M.C., 2003. Differentiation of visceral and cutaneous pain in the human brain. J Neurophysiol 89, 3294-3303.

Svensson, P., Minoshima, S., Beydoun, A., Morrow, T.J., Casey, K.L., 1997. Cerebral processing of acute skin and muscle pain in humans. J Neurophysiol 78, 450-460.

Tarkka, I.M., Treede, R.D., 1993. Equivalent electrical source analysis of pain-related somatosensory evoked potentials elicited by a CO2 laser. J Clin Neurophysiol 10, 513-519.

Tolle, T.R., Kaufmann, T., Siessmeier, T., Lautenbacher, S., Berthele, A., Munz, F., Zieglgansberger, W., Willoch, F., Schwaiger, M., Conrad, B., Bartenstein, P., 1999. Region-specific encoding of sensory and affective components of pain in the human brain: a positron emission tomography correlation analysis. Ann Neurol 45, 40-47.

Torebjork, H.E., Hallin, R.G., 1973. Perceptual changes accompanying controlled preferential blocking of A and C fibre responses in intact human skin. Exper Brain Res 16, 321-332.

Tracey, I., Becerra, L., Chang, I., Breiter, H., Jenkins, L., Borsook, D., Gonzalez, R.G., 2000. Noxious hot and cold stimulation produce common patterns of brain activation in humans: a functional magnetic resonance imaging study. Neurosci Lett 288, 159-162.

Tran, T.D., Inui, K., Hoshiyama, M., Lam, K., Qiu, Y., Kakigi, R., 2002. Cerebral activation by the signals ascending through unmyelinated C-fibers in humans: a magnetoencephalographic study. Neuroscience 113, 375-386.

Treede, R.D., 2002. Spinathalamic and thalamocortical nociceptive pathways. J Pain 3, 109-112.

Vogel, H., Port, J.D., Lenz, F.A., Solaiyappan, M., Krauss, G., Treede, R.D., 2003. Dipole source analysis of laser-evoked subdural potentials recorded from parasylvian cortex in humans. J Neurophysiol 89, 3051-3060.

Vogt, C., Vogt, O., 1919. Allgemeiner Ergebnisse unserer Hinforschung. Journal Psychology and Neurology 25, 279-462.

White, L.E., Andrews, T.J., Hulette, C., Richards, A., Groelle, M., Paydarfar, J., Purves, D., 1997. Structure of the human sensorimotor system .1. Morphology and cytoarchitecture of the central sulcus. Cerebral Cortex 7, 18-30.

Whitsel, B.L., Favorov, O.V., Li, Y.B., Quibrera, M., Tommerdahl, M., 2009. Area 3a Neuron Response to Skin Nociceptor Afferent Drive. Cerebral Cortex 19, 349-366.

Willis, W.D., Kenshalo, D.R., Leonard, R.B., 1979. The cells of origin of the primate spinothalamic tract. T Comp Neurol 188, 543-573.

CHAPTER II

DIFFERENTIATION OF SOMATOSENSORY CORTICES BY HIGH-RESOLUTION FMRI AT 7 T

Abstract

This study aimed to evaluate the ability of BOLD signals at high MRI field (7 Tesla (T)) to map fine-scale single-digit activations in subdivisions (areas 3b and 1) of the human primary somatosensory cortex (SI) in individual subjects. We acquired BOLD fMRI data from cortical areas around the central sulcus in six healthy human subjects while stimulating individual finger pads with 2-Hz air puffs. Discrete, single-digit responses were identified in an area along the posterior bank of the central sulcus corresponding to area 3b and in an area along the crest of the postcentral gyrus corresponding to area 1. In single subjects, activations of digits 1 to 4 in both areas 3b and 1 were organized in a somatotopic manner. The separation of digit representations was measured for adjacent digits and was approximately 1.6 times greater in area 3b than in area 1. Within individual subjects, the cortical responses to single-digit stimulations and the magnitude of the BOLD signals were reproducible across imaging runs and were comparable across subjects. Our findings demonstrate that BOLD fMRI at 7 T is capable of revealing the somatotopic organization of single-digit activations with good within-subject reliability and reproducibility, and activation maps can be acquired

within a reasonably short time window, which are essential characteristics for several neurological applications within patient populations.

Introduction

Functional magnetic resonance imaging (fMRI) based on measuring changes in blood oxygen level-dependent (BOLD) signals has been used extensively to study the functional architecture of somatosensory and other cortices in humans ((Fox, 2009), (Kayser et al., 2005), (Moore et al., 2000), (Nelson and Chen, 2008), (Sasaki et al., 2005), (Schweizer et al., 2008), (Silver and Kastner, 2009), (Tootell et al., 2008)). Such studies provide important insights into not only the normal organization of sensory cortices but also potentially into how neural systems are affected by disease or damage and how they may change over time during remodeling and with interventions ((Borsook et al., 1998), (Fox, 2009), (Schaechter et al., 2006)). fMRI is uniquely suited to address such questions because it is non-invasive and relatively easy to implement, but for ultimate success it is essential that the spatial resolution and sensitivity of fMRI data are adequate for recording fine details in single subjects with adequate within-subject reliability and reproducibility in reasonably short acquisition times (Harel et al., 2006). To date, these criteria have not been satisfied, where previous studies typically have reported findings with insufficient spatial resolution, or have used average maps from multiple subjects, reflecting the practical current limits on sensitivity and image contrast to noise ratio (Francis et al., 2000; Gelnar et al., 1998; Krause et al., 2001; Kurth et al., 2000; Maldjian et al., 1999; Nelson and Chen, 2008). Theoretically, the use of ultra-high

fields (7 T or above) for fMRI promises to provide greater sensitivity for detecting functional activations and to permit the use of higher spatial resolution acquisitions ((Bandettini, 2009)). Thus, the advent of commercial ultra-high field MRI systems operating at 7 T provides an opportunity to push the limits of performance of fMRI to examine anew whether single-subject high-resolution functional maps can be acquired in reasonable times in order to be useful for a variety of applications. In general, throughout the history of MRI, each substantive increase in field strength has in time led to dramatic improvements in the quality of images obtainable, but each major increase in field has also introduced new technical challenges and problems ((Bandettini, 2009)).

Image quality in MRI is always limited by the relative strengths of the available signal and the "noise"—those random fluctuations in images that are unavoidable but which obscure details and make the detection of small signal differences more difficult. In principle, the strength of MRI signals increase quadratically with field strength but in practice other factors are also important and affect the achieved signal to noise ratio (SNR). However, experiences to date have demonstrated that SNR increases when moving from 1.5 T or 3 T to 7 T, and the higher SNR can be used to make images with finer spatial resolution, or in less time, or in which small signal differences are easier to detect ((Haacke et al., 1999), Stark and Bradley, 1999)). In addition, differences in signal induced by functional activation via the BOLD effect will also be magnified at higher fields and therefore should be detected with greater sensitivity ((Dula et al., 2010), (Gati et al., 1997), (Ogawa et al., 1993), (van der Zwaag et al., 2009)). To date, however, there have been few convincing demonstrations that fMRI at 7 T offers significant advantages over lower fields and few illustrations of where the higher spatial resolution provides additional information.

In 1937, Penfield and colleagues, using invasive electrophysiological techniques, successfully mapped body surface representations in the human primary somatosensory

cortex, establishing the existence of a somatotopic map or homunculus of the body surface in the human brain ((Penfield and Boldrey, 1937)). In the subsequent 60 years, with the lack of non-invasive imaging techniques, little advancement was made in the understanding of somatosensory organization in human cortex. Following the first development of BOLD fMRI ((Ogawa et al., 1990)), human somatotopy has been studied extensively at varying field strengths (1.5, 3, and 4 T) ((Blankenburg et al., 2003), (Eickhoff et al., 2006), (Francis et al., 2000), (Gelnar et al., 1998), (Hinkley et al., 2007), (Kurth et al., 2000, 1998), (Maldjian et al., 1999), (Overduin and Servos, 2004), (Ruben et al., 2006), (Schweizer et al., 2008), (Weibull et al., 2008)). Studies have revealed a topographical organization of digits in area 3b ((Gelnar et al., 1998), (Jack et al., 1994), (Maldjian et al., 1999), (Schweizer et al., 2008)). In a major step forward, Nelson and Chen (2008) elegantly demonstrated the existences of topographically organized digit maps in both area 3b and area 1, findings that complement those found by other techniques in non-human primates ((Chen et al., 2005, 2007), (Friedman et al., 2008), (Nelson and Chen, 2008), (Sur et al., 1982)). Taken together, the existing knowledge on the digit representation within the primary somatosensory cortex provides an excellent model for the evaluation of the performance of BOLD at ultra-high field (7 T). Specifically, in this study, we assess (1) whether fMRI at 7 T can reliably resolve the separation of adjacent single digits, (2) the across-run reproducibility of single-digit activation, and (3) the across-subject variation of digit separation in subregions of SI (areas 3b and 1). We demonstrate that fMRI at 7 T can provide millimeter-scale depictions of the fine-detail organization of SI in individual subjects reliably and with good reproducibility of activation and signal magnitude. The robustness of single-trial BOLD activation significantly reduces imaging acquisition duration, an advantage that is desirable for fine-scale mapping studies particularly in patients when only limited scan

time is possible. Additionally, the fine-scale mapping capability of 7 T appears to be well suited for studies of differences between subjects and across time.

Methods

Stimulation Protocol

Six healthy human subjects (5 men, 1 woman) gave informed consented for this study in accordance with a protocol approved by the Vanderbilt University Institutional Review Board. A hand and finger cast was connected to an air pressure generator via plastic tubing. Stretchable fabric was fitted across each opening in the cast, allowing for restricted skin displacement in response to an air puff. Air puffs were delivered to the glabrous skin of selected distal finger pads (Fig. 1B). The digits (D) were stimulated at 2 Hz in a block design of 24 s on and 24 s off (Fig. 1C). The “on” blocks alternated between digits. Each run consisted of 2 or 3 blocks for each digit being studied. Each subject performed multiple runs so as to acquire 6 to 12 stimulation “on” blocks per individual digit. To map the digit somatotopy and evaluate the reproducibility of single-digit activation, we mapped digit responses by stimulating nonadjacent digits (D2 and D4 in Subjects 1 and 2), adjacent digits (D2 and D3 in Subjects 3 and 4), and four digits (D1, D2, D3, and D4 in Subjects 5 and 6).

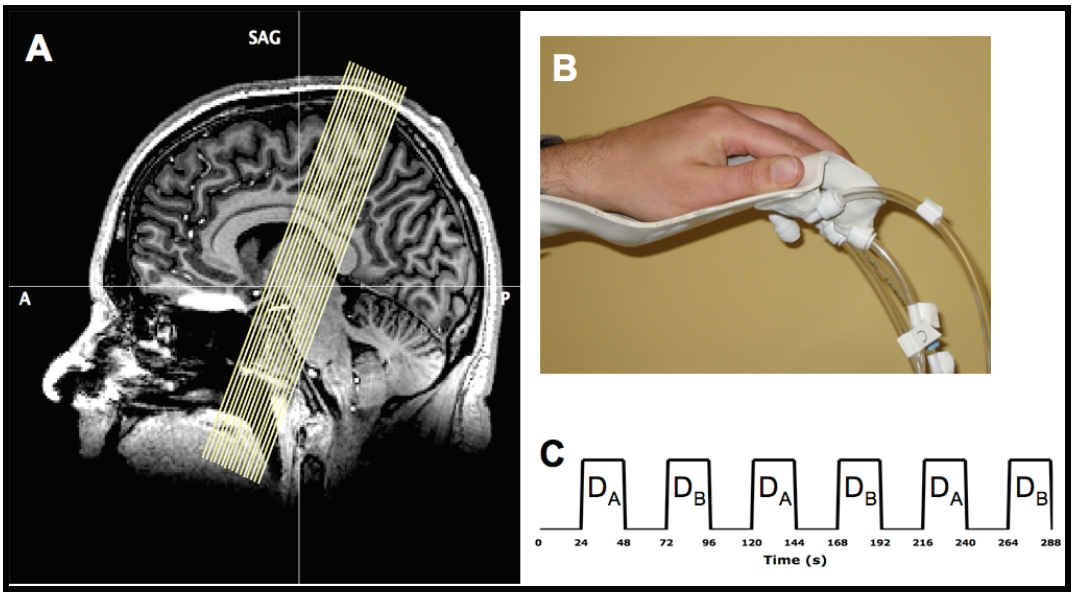

Figure 1. Experimental setup. (***A***) The yellow lines over the sagittal structural image indicate the slice prescription for the functional images. The imaging volume covers SI, SII, posterior insula, and the thalamus. (***B***) A hand cast was constructed to deliver air puffs to individual digits through plastic tubing. (***C***) Two digits were stimulated separately in a 24-s on and 24-s off blocks design. A single run lasted 288 s (4 min 48 s).

MRI Data Acquisition

Subjects were scanned on a 7-T Philips Achieva magnet with a 16-channel NOVA head coil. Structural imageswere collected using a three dimensional fast field echo (3D-FFE) sequence, TR=3.7 ms, TE=1.8 ms, and TI=1300ms, with a 1×1×1-mm^3 voxel resolution. Functional images were acquired using a gradient-echo echo-planar imaging (GE-EPI) sequence, TR=2000ms, TE=25ms, flip angle=80°, and a 192×192 field of view (FOV). The voxel resolution was 1×1×2mm^3. Sixteen oblique coronal slices (0mm gap thickness) were acquired covering cortical regions around the central sulcus—primary somatosensory cortex (SI) region, posterior part of the lateral sulcus, and thalamus (Figure 1A). A SENSE acceleration factor of 3, and volume selective second- or third-order shimming using a pencil-beam method were employed. All EPI images were distortion corrected using a B_0 field-map obtained at the start of scanning

using two gradient-echo scans ((Jezzard and Balaban, 1995)). All preprocessing and imaging analysis was implemented in BrainVoyager QX following a standard pipeline. Preprocessing included slice scan time correction using a cubic spline, motion correction in three dimensions, and slice alignment using an intra-session registration.

fMRI Data Analysis

BOLD signals were temporally filtered with a 0.007-Hz high-pass filter, including a linear trend removal. The functional images were interpolated into 1×1×1 mm^3 voxels for visualization. To preserve the high spatial resolution, warping into stereotactic space was not performed and spatial smoothing of the functional images was not applied. A general linear model (GLM) was fitted to the data and t-maps were created. Single–condition activity maps (DA–Rest) and contrast maps (DA–DB) were examined. Individual subject maps were thresholded at q (FDR) < 0.001 with 4 voxels minimum per cluster. To reveal single-run activation, maps were thresholded at q (FDR) < 0.05 with 4 voxels minimum per cluster. Single–condition activity maps were used to define regions of interest (ROIs). Composite maps of cortical digit representation were created to visualize digit topography in SI (area 3b and area 1). Surface volume renderings of the single-digit ROI clusters were also created to visualize the somatotopy. For all subjects, the functional maps are presented in their native space with native coordinates reported. These coordinates do not correlate with Talairach nor MNI space. We did not create and do not report any group activation maps.

Identification of Cortical Activations in Areas 3b and 1

The primary somatosensory cortex (SI) lies directly posterior to the central sulcus (CS) and can be identified by the omega-shaped folding in the axial plane ((Moore et al., 2000), (White et al., 1997)). SI cortex was divided into three cytoarchitecturally distinct

subregions by Brodmann (1909) and further subdivided into four subregions a decade later ((Vogt and Vogt, 1919)). The subregion boundaries can be objectively determined through histological methods ((Geyer et al., 1999), (Geyer et al., 2000)), but no clear anatomical landmarks exist, leading to challenges in defining the boundaries with typical structural MRI techniques. Additionally, the intersubject variability in neural geometry adds to the difficultly in accurately indentifying the location of subregions ((Geyer et al., 2001)). We therefore use the guidelines put forth by Geyer et al. (2000) to delineate the boundaries between subregions within SI. Area 3a is located within the fundus of the CS, area 3b is located along the posterior bank of the CS, area 1 is located at the crest of the postcentral gyrus, and area 2 is located on the anterior bank of the postcentral sulcus (medial) ((Geyer et al., 2000), (Krause et al., 2001), (Kurth et al., 2000), (Nelson and Chen, 2008)). These operational definitions are applied throughout the paper when areas 3b and 1 are referenced.

Measure of Interdigit Distance

When measuring interdigit distances in three dimensions, two approaches were taken. We denote the two methods as “Surface” and “Euclidian.” From each single–condition activity map (DA–Rest; thresholded at q (FDR) < 0.001), we defined ROIs for each of the digit clusters in both areas 3b and 1. We then determined the three-dimensional coordinates for the peak (highest t-value) voxel within each ROI. In the Surface approach to determine interdigit distance, we traced the three-dimensional path, voxel by voxel, between the peak voxels of neighboring digit responses along the folds of the postcentral gyrus (e.g., 3D distance between D2 and D3 in area 3b). We then calculated the length of the path based on the voxel dimension, 1×1×1 mm^3. For the

Euclidian approach we measured the distance between peak voxels according to the Euclidian formula: $\sqrt{(x_{DA} - x_{DB})^2 + (y_{DA} - y_{DB})^2 + (z_{DA} - z_{DB})^2}$.

Cortical Response Displacement across Runs

We tested the spatial reproducibility of cortical responses to finger pad stimulation by calculating peak voxel and center of mass (COM) displacement. We defined ROIs from single–condition activity maps (DA–Rest; thresholded at q (FDR) < 0.05) for each individual run. We determined the peak voxel and calculated the COM for each of these digit-specific ROIs and recorded the 3D coordinates. Additionally, we defined ROIs from the mean single–condition activity maps (DA–Rest; thresholded at q (FDR) < 0.001) across all runs. We recorded the peak voxel and the COM coordinates for each digit-specific ROI. To measure the ROI displacement for each run, we calculated the distance between the mean multi-run peak voxel and the individual run peak voxel; we made the same displacement calculations for the ROI COM measurements. The displacement between ROI coordinates (peak voxel and COM) was calculated using the Euclidian formula.

Magnitude of BOLD Signal

We tested the temporal reproducibility of the BOLD signal magnitude by comparing the area under the curve from single-run BOLD signal time courses. The area under the curve encompasses several metrics such as the maximum change in BOLD, time to onset, time to offset, and shape of the curve. We created single–condition activity maps (DA–Rest; thresholded at q (FDR) < 0.05) for each run of a single subject and defined ROIs for each of the digit clusters in both areas 3b and 1. The BOLD signal time courses from the five peak voxels in each ROI were averaged for each single–condition

block (DA) and across blocks, resulting in one mean BOLD signal time course per run. Based on inspection of the time courses and prior knowledge of the hemodynamic response function, we used a trapezoidal approximation to calculate the area under the curve from4 s after the stimulus onset to 2 s after the stimulus ended. An ANOVA was performed on the BOLD signal magnitude to test whether the variance across runs was greater than the variance across ROIs.

Results

In individual subjects (n=6), we detected single-digit activations in subregions (areas 3b and 1) of the primary somatosensory cortex (SI). Single-digit activation was robust in single runs, and the activation maps were reproducible across runs. Digit activations were organized topographically in areas 3b and 1 with apparent intersubject variation.

Digit Somatotopy in Area 3b and Area 1 in Individual Subjects

Digit Separation within Area 3b

We first examined the cortical responses to tactile stimulation of nonadjacent distal finger pads. In digit contrast maps (digit A condition minus digit B condition, Figure 2A) of Subject 1, we observed distinct and focal cortical activations along the posterior bank of the central sulcus (CS), corresponding to area 3b. Where nonadjacent digits 2 and 4 were stimulated separately in subject 1, two separate activation clusters (thresholded at q (FDR) < 0.001; D2 (blue/green) and D4 (orange/yellow)) were observed in three sequential lateral (x=44) to medial (x=46) sagittal slices (insets in Figure 2A). The pink box over the large whole head sagittal image indicates the zoomed-in region around CS as displayed in the left most inset (x=44). In this particular case, due

to the great sinuosity of the CS, when viewing in the sagittal plane, the CS of Subject 1 extended from the anterior to the posterior part of the inset window; thus, we used two arrows to indicate the location of the CS. D2 activation was located anterior and inferior to D4 activation in area 3b. In 3D space, the spatial extent (in the x medial to lateral direction) of D2 activation also extended both laterally and medially to D4 activation. In this case, we observed visibly discrete separation between cortical responses to nonadjacent neighboring digits D2 and D4.

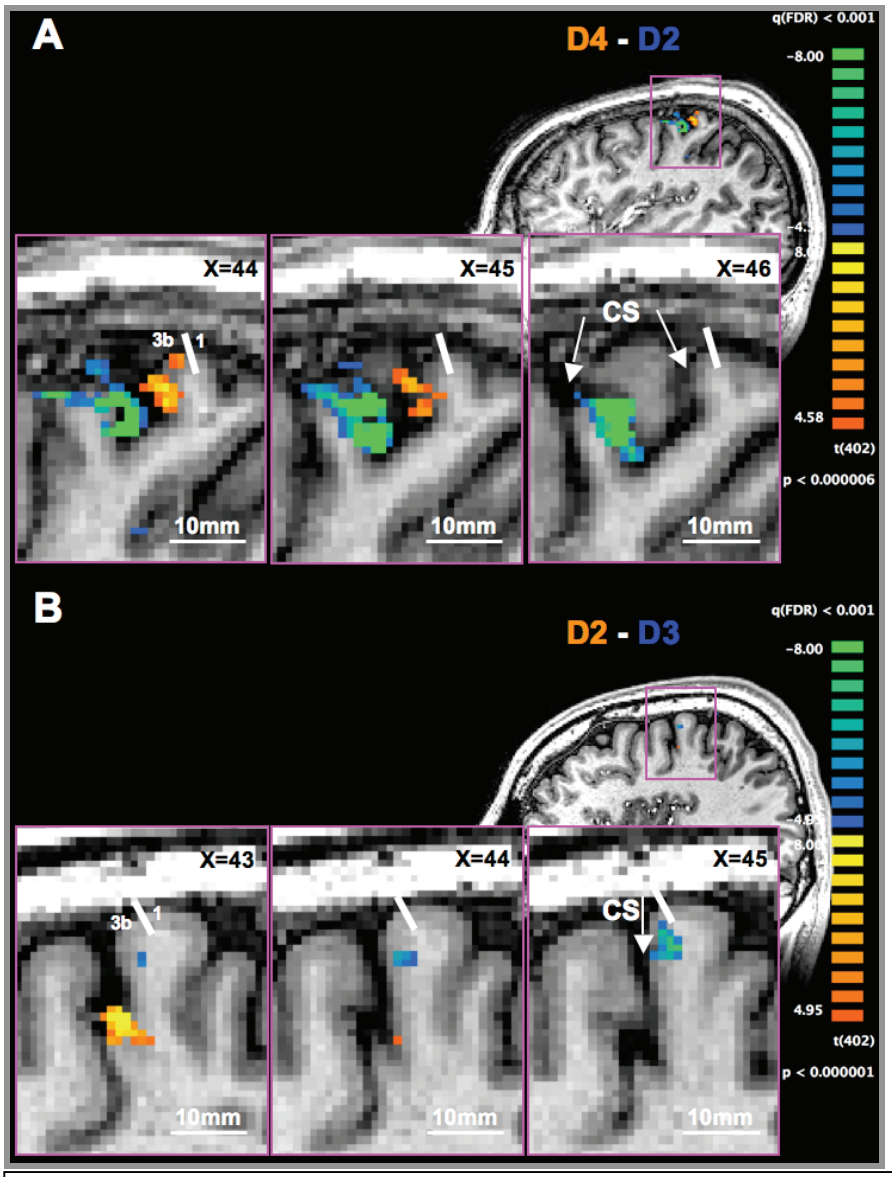

Figure 2. Contrast maps from two subjects. (***A***) A contrast map (D4–D2) from Subject 1 is overlaid on the subject's structural image in the sagittal plane and in radiological orientation, thresholded q (FDR) < 0.001. The pink box indicates the area displayed in the left most increased field of view inset. The inset windows are arranged lateral (x=44) to medial (x=46). The x-coordinate is in the subject's native space. There is a clear separation of digit responses along the posterior bank of the central sulcus (area 3b), with D4 response (orange/yellow) located posterior and superior to D2 response (blue/green) in the contralateral cortex. The white arrows indicate the location of the central sulcus (CS), and the white line indicates the area 3b/area 1 boundary. (***B***) A contrast map (D2–D3) from Subject 3 is overlaid on the subject's structural image in the sagittal plane and in radiological orientation, thresholded q (FDR) < 0.001. The pink box indicates the area displayed in the center increased field of view inset. The inset windows are arranged lateral (x=43) to medial (x=45). The x-coordinates are in the subject's native space. There is a clear separation of digit responses along the posterior bank of the central sulcus (area 3b), with D3 response (blue/green) located superior to D2 response (orange/yellow) in the contralateral cortex. The white arrows indicate the location of the CS, and the white line indicates the area 3b/area 1 boundary.

We next examined whether we could detect activation separations in adjacent digits. Figure 2B shows cortical responses to D2 (orange/yellow) and D3 (blue/green) stimulation in Subject 3 (thresholded at q (FDR) < 0.001). Similar to the observation in Subject 1, D2 activation is located anterior, inferior, and lateral to D3 activation along the posterior bank of the central sulcus in area 3b. There is a sizeable spatial separation between D2 and D3 clusters, which is emphasized in the zoomed-in insets centered over the CS and arranged lateral (x=43) to medial (x=45). While the separation of D2 and D3 responses is modest in the x and y planes, there is considerable separation along the z plane, even greater than the separation of nonadjacent digits observed in Subject 1. In general, the cortical responses to single-digit stimulation are unique for each individual subject. Together, the discrete cortical responses to nonadjacent digit stimulation in Subject 1 and adjacent digit stimulation in Subject 3 illustrate that individual digit representations in area 3b are distinct and separable, which suggest minimal overlap across adjacent digits.

Digit Topography

We further examined whether the spatially distinct cortical BOLD activations in response to stimulating individual finger pads were organized in a topographic manner in both areas 3b and1. The finger pad somatotopies of two subjects (Subjects 5 and 6) as displayed in Figure 3 provided evidence for two separate digit maps. The surface volume renderings of Subject 5 (Figures 3A and B) and Subject 6 (Figures 3C and D) revealed subject-specific organization of D1 (red), D2 (blue), D3 (yellow), and D4 (green) in three orientations (axial plane along the blue axis, coronal plane along the green axis, and sagittal plane along the red axis). Two separate digit maps were established. The zoomed-in images (Figures 3B and D) illustrate that digit activations in area 3b (rostral clusters) were located anterior and medial to area 1 (caudal clusters), and that the

spatial expanse of digit responses are greater in area 3b than in area 1. A similar activation pattern was observed in Subject 6 (Figures 3C and D) and the majority of the cases. Within these maps (areas 3b and 1), the digit-specific cortical activations were topographically organized from D1 to D4 in a lateral to medial, anterior to posterior, and inferior to superior pattern.

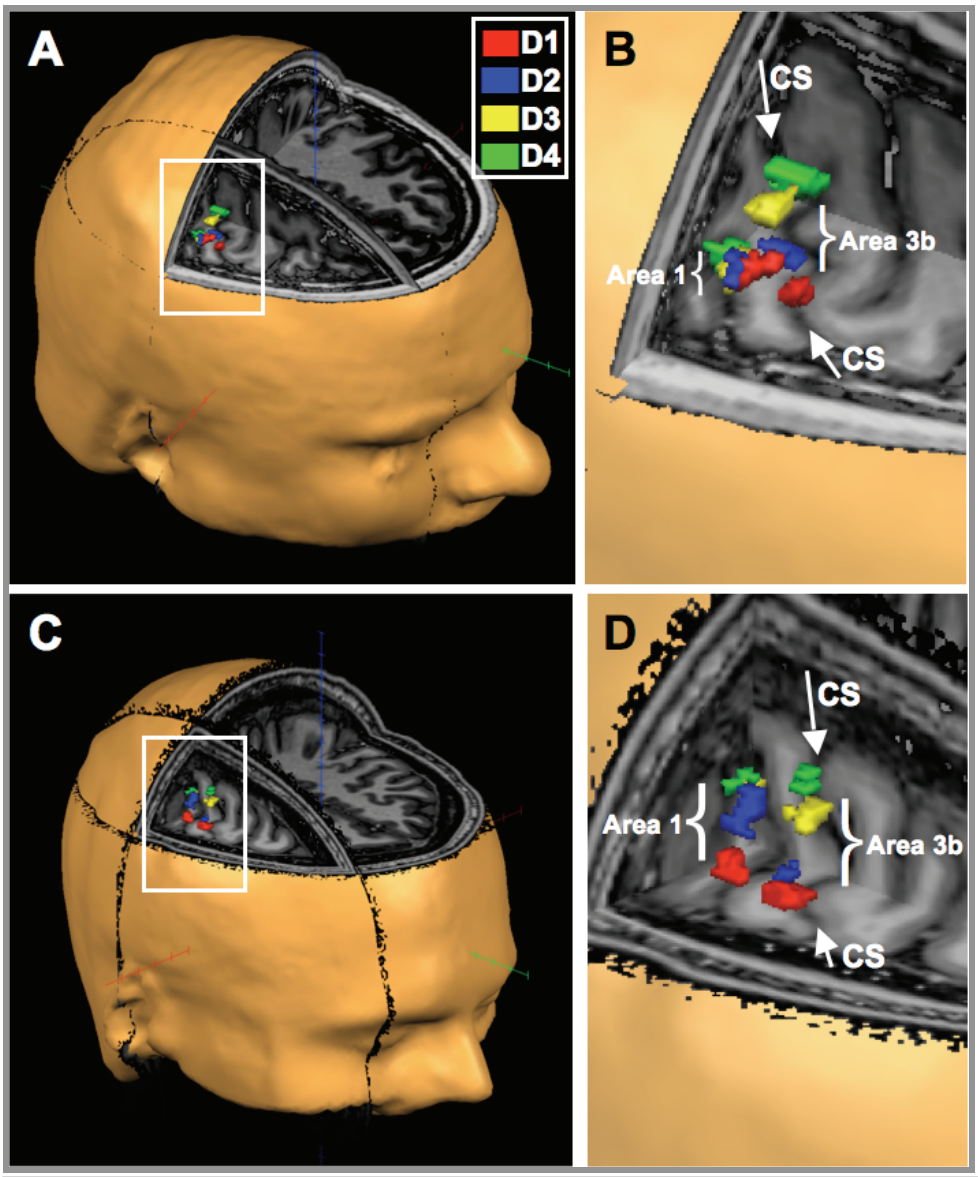

Figure 3. Surface composite maps of digit topography in two subjects. (***A***) Subject 5 and (***C***) Subject 6 are depicted in surface renderings in the neurological orientation. Part of the facial surface is cut away to expose the T1-weighted structural images of each subject in three orientations, axial (blue axis), coronal (green axis), and sagittal (red axis). The white boxes indicate the volumes displayed in the increased field of view windows. The cortical digit representations in the contralateral cortex are displayed in 3D for (***B***) Subject 5 and (***D***) Subject 6. The CS is highlighted by the white arrows. Digit representations are organized topographically in two distinct maps, one along the posterior bank of the CS (area 3b), and along the crest of the postcentral gyrus (area 1). Cortical response to D1 stimulation is illustrated in red, D2 blue, D3 yellow, and D4 green.

Intersubject variability was apparent, and a topographical exception was observed in Subject 5 where a reversal of digit organization in the axial plane in area 1

was present. Single-digit cortical responses from D1 to D4 followed the standard lateral to medial and anterior to posterior pattern, yet an anomalous superior to inferior pattern (Figure 3B). In contrast, digit activations in area 3b followed a typical organization. By virtue of the unique geometry of an individual brain, there were significant variations in the localization of digit representations across subjects. However, each subject revealed a clear topographical organization of the finger pad representations. In sum, while a standard digit topography was observed in the majority of subjects, subtle differences in digit somatotopy were apparent, especially in area 1 in one subject.

Differential Spatial Separation of Finger Pads in Area 3b and Area 1

Due to the observed differences in digit organization, we further quantified the separation between digit representations in areas 3b and 1. Of primary interest was the quantifiable separation between adjacent digits (D2 and D3), leading us to exclude the two subjects that were D3 separation ranged from 11 mm to 14 mm (mean±standard deviation (SD): 12±1.41mm) measured by the surface method and from 5.39 mm to 9.17mm (mean±SD: 7.25±0.96mm) calculated by the Euclidean method. Within area 1, D2 and D3 separation ranged from 6 mm to 8 mm (mean±SD: 7.46±1.61mm) measured by the Surface method and from 3.74 mm to 5.83mm (mean±SD: 4.68±0.86mm) calculated by the Euclidean method. The separation of cortical responses to stimulation of adjacent digits was 1.6 times greater in area 3b than in area 1 across subjects.

Reproducibility within a Single-Subject across Multiple Runs

Spatial Reproducibility in Areas 3b and 1

To evaluate the spatial reproducibility of single-digit activation across runs, we collected multiple functional runs per imaging session (3–6). Figure 4 illustrates the spatial overlap of the cortical activations to stimulation of D2 and D4 in the axial image

plane between runs (Run 1 in blue, Run 2 in red, Run 3 in yellow, and Run 4 in green) in Subject 2. The four panels present the two conditions in both areas 3b and 1: D2–Rest in area 3b (top panel), D2–Rest in area 1 (second panel), D4–Rest in area 3b (third panel), and D4–Rest in area 1 (bottom panel). The enlarged field of view in Figure 4B illustrates that the spatial variability in across-run responses is minimal.

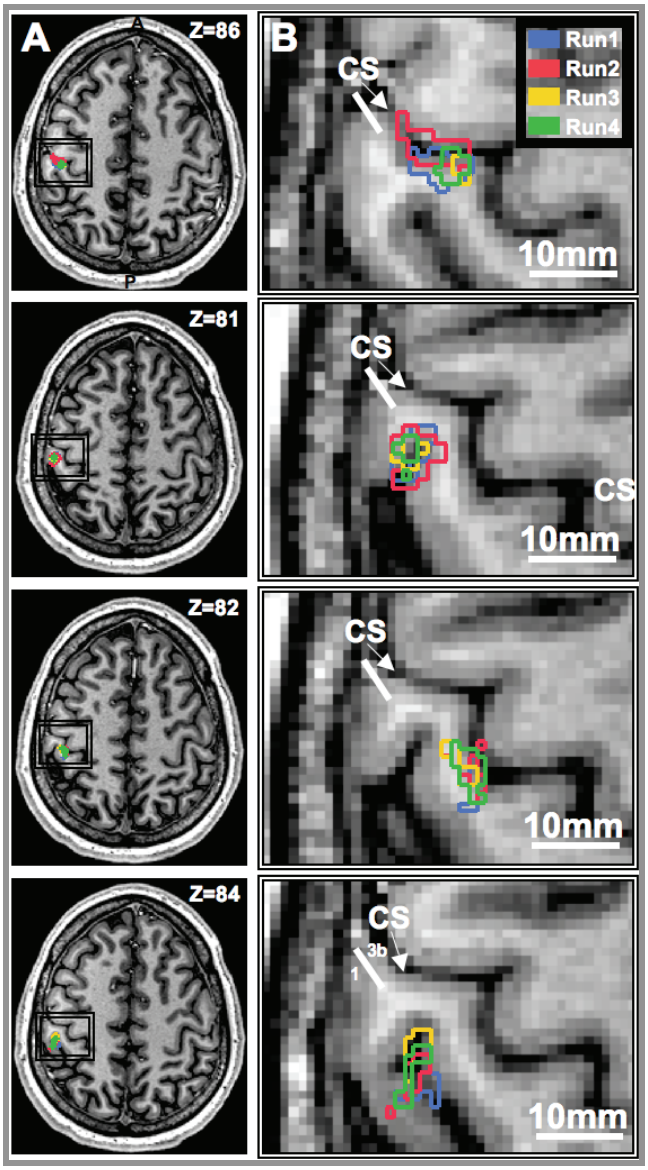

Figure 4. Spatial reproducibility of BOLD signals. (***A***) Single-run composite maps of activation clusters are overlaid on the axial plane of the structural images in the radiological orientation for an individual subject, q (FDR) < 0.005. The first and second rows represent activation during stimulation of D2 in area 3b and area 1, respectively. The third and forth rows represent activation during stimulation of D4 in area 3b and area 1, respectively. (***B***) The zoomed images illustrate a high degree of spatial agreement between ROIs across 4 runs. The ROIs for Run 1 are outlined in blue, Run 2 red, Run 3 yellow, and Run 4 green. Z-coordinates displayed are in subject's native space. The white line highlights the boundary between area 3b and area 1, and the white arrow indicates the CS.

We quantified the extent of spatial reproducibility by calculating the displacement of each ROI's peak voxel and center of mass (COM) for each of the individual digits. Figure 5 illustrates the calculated COM displacement for all digit-specific ROIs in each run: Run 1 (blue), Run 2 (red), Run 3 (yellow), and Run 4 (green), with the grey bar indicating the displacement of one voxel length. The mean peak voxel and COM displacements are 1.84±0.33 mm and 1.45±0.15 mm, respectively. The maximum displacements were 4.12mm for the peak voxel and 2.45mm for the COM.

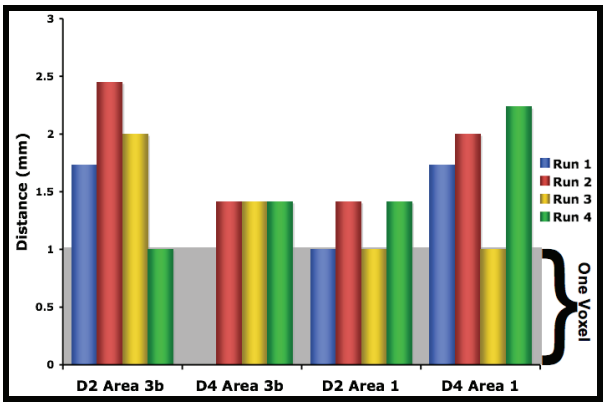

Figure 5. Center of mass displacement across runs. The center of mass (COM) for each ROI was determined for a single run (as displayed in Figure 4) and for the mean. The displacement of single-run COM from the mean COM was calculated. The grey shading represents the displacement by one voxel, 1 mm. The COM displacement was less than 2.5 mm for all runs within an ROI. Run 1 blue, Run 2 red, Run 3 yellow, and Run 4 green.

Temporal Reproducibility in Areas 3b and 1

To evaluate the cross-run temporal reproducibility of BOLD signals, we compared the magnitude of the BOLD signal by calculating the area under the curve for each run of the digit-specific ROIs defined in Figure 4. An ANOVA was performed on the BOLD signal magnitudes to test whether the variance across runs was greater than the variance across ROIs. The ANOVA showed no main effect of run ($F(1, 3)=0.44$, $p<0.73$), suggesting a high degree of temporal reproducibility of the BOLD signal.

Discussion

Differentiability of BOLD Signal at Ultra-High Field (7 T)

The differentiability of BOLD signals is constrained by the imaging resolution employed in fMRI experiments. Typical functional imaging studies use "snapshot" imaging techniques of which echo-planar imaging (EPI) is a prime example, in which complete cross sectional images that are sensitive to BOLD effects are obtained in very short times, substantially less than one second. These functional images are of lower resolution than more conventional anatomic MR images, so that activation maps are typically acquired with voxels on the order of $3\times3\times3mm^3$ (>20 mm^3). At this spatial resolution, differentiation between neighboring regions, such as area 3b and 1, or neighboring digits, is uncertain. High-resolution studies (e.g. $1\times1\times2$ mm^3) have been employed to reveal fine-scale functional structures in cortex ((Harel et al., 2006), (Sanchez-Panchuelo et al., 2010), (Schweizer et al., 2008)), such as ocular dominance columns in visual cortex and digit somatotopic maps within subregions of SI cortex. In these studies, multiple blocks or runs were combined to compensate for the signal drop resulting from smaller voxel sizes ((Schweizer et al., 2008)). High-resolution mapping at higher fields benefits from an increased SNR and there is less need to average over as many acquisitions.

In this study, single-run BOLD activations (acquired as 3 blocks each of 12 images with and without the stimulus) were robust and spatially reproducible across runs. The clear separation of adjacent digits within areas 3b and 1 in individual subjects support the differentiability of BOLD signals at 7 T. A direct comparison with lower fields was not attempted here so we cannot quantify the specific benefits of conducting a BOLD fMRI experiment at 7 T in this study. However, our experience at 3 T and the existent literature supports our observation that the reliability at 7 T is substantially better

than at lower fields and that individual results at higher resolution are obtainable with significantly fewer acquisitions and runs than are commonly achieved ((van der Zwaag et al., 2009)).

The present study has demonstrated that BOLD signals at high field can be focal and spatially specific such as for individual digit representations in area 3b. This observation is consistent with our findings obtained with an identical approach in anesthetized monkeys at high field (9.4 T). In area 3b of monkeys, BOLD activation maps (obtained with 0.625×0.625 mm^2 in plane resolution) correlate well with maps identified by the receptive fields of neurons ((Chen et al., 2007)). Our observations in humans and monkeys seem to be inconsistent with previous reports (e.g., (Kim et al., 2004)) where BOLD signals appeared to be less focal and had a poor correlation with underlying electrical activity. We believe that the stimulus and model systems (visual versus somatosensory) contribute to the discrepancy between their study and our studies. In our present study, natural and subtle vibrotactile stimulation of a single distal finger pad was used. In this condition, only a small piece of cortex was activated (~ 1 mm^2 in New World primates and ~10mm^2 in human area 3b), and the vascular response may be much more constrained for such a subtle stimulus.

Technical Challenges of High-Field BOLD Mapping

Ultra-high field fMRI faces several challenges. The first is related to macroscopic field variations caused by increased inhomogeneities of magnetic susceptibility, which can introduce image distortion. Secondly, the performance of radiofrequency (RF) coils is also affected at higher fields, and it is more difficult to create uniform RF fields within large objects (i.e. the human brain). To meet these challenges, we employed the use of parallel array coils (16 channels) for data acquisition, reduced the imaging volume to partial brain coverage, and applied B0 distortion correction in data preprocessing.

Additionally, we took extra efforts in defining the shim volume for each subject. With these approaches, the susceptibility problems in SI areas around the CS appear minimal. There is, however, some degree of signal drop in brain regions near air-tissue interfaces, specifically the inferior temporal lobes. Other techniques such as dynamic shimming during functional scans for high-resolution fMRI studies are currently under development in our laboratory ((Sengupta et al., 2009)). The data presented in this paper highlight the current potential 7 T BOLD imaging can provide in the understanding of brain function.

Functional Imaging of Individual Subject

While many previous studies of digit topography in SI have relied on group analysis ((Gelnar et al., 1998), (Maldjian et al., 1999), (Weibull et al., 2008)), less than a handful have successfully achieved single-subject analysis ((Nelson and Chen, 2008), (Sanchez-Panchuelo et al., 2010), (Schweizer et al., 2008)). Nelson and Chen identified the somatotopic organization of all five digits in both area 3b and area 1 of SI, where the thumb (D1) was represented most laterally, anteriorly, and inferiorly in both areas, similar to our findings, but their spatial resolution was limited to 2.08×2.08×2.4 mm^3 (>10 mm^3) voxel size ((Nelson and Chen, 2008)). Similarly, Schweizer et al. (2008) achieved a single-subject analysis of the topography of all five digits in SI area 3b. Their voxel resolution was 1×1×2 mm^3, but also employed a 0.4-mm gap thickness, decreasing the effective sampling of the cortical tissue. In addition, while fine-scale somatotopic maps were obtained, the overall imaging time required to achieve these was considerably longer. Two imaging sessions were conducted in order to complete the study. Each digit required approximately 12 min 18 s to scan, and with 5 digits the total functional scan time was 61 min 30 s. In our study, the functional scan time varied between subjects, but on average the scan time per digit was 7 min 12 s.

Single-subject somatotopic maps are achievable at 3 T ((Nelson and Chen, 2008), (Schweizer et al., 2008)), but Sanchez-Panchuelo et al. (2010) demonstrated how the increase in CNR at 7 T can be utilized in order to increase spatial resolution (1 mm^3) and decrease the total scan time necessary to achieve topographic maps of digit topography ((Sanchez-Panchuelo et al., 2010)). In their study, however, the employed stimulus paradigm consisting of a "traveling wave" and the data analysis generating a "digit-phase correspondence" do not allow for mapping of discrete digit representations. Instead the authors present a spectrum of continuous distal finger pad representations along SI cortex. Here we were able to measure and delineate digit representations in both areas 3b and 1 of SI cortex.

Although individual subject analysis can be accomplished at lower MRI field strengths ((Nelson and Chen, 2008), (Schweizer et al., 2008)), the greater signal sensitivity at 7 T could provide extra benefits. For instance, reliable BOLD signal in a single subject can be acquired in as little as 2 min 30 s per stimulus, given that our reproducibility analysis indicates that a scan time of only 2 min 24 s is necessary to accurately map a single-digit response. This improvement could negate the need for more across-run averaging, ultimately reducing the total scan time to collect functional data. The across-run temporal reproducibility implies 7 T imaging has a potential application in examining dynamic cortical changes within one imaging session in an individual subject, such as immediate plastic changes following a manipulation of the stimulus. Measurements of the variability of the magnitude of the BOLD response provide another quantification for characterizing the cortical response strength at a specific cortical region (e.g., areas 3b and 1). Finally, the detection of subtle variations of digit representation could have significant potential for detecting small cortical changes in disease conditions such as plastic changes following spinal cord injury.

Cortical Magnification: Interdigit Distance

It has been suggested that the cortical magnification factor (M) of the cortex is proportional to sensory acuity ((Cowey and Rolls, 1974), (Duncan and Boynton, 2003)). There have only been a few studies that have examined the somatosensory cortical magnification factor in human or non-human primates ((Nelson et al., 1980), (Schwartz et al., 2004), (Sur et al., 1982)). In primates, area 3b has a greater M factor than area 1, implying an important role of area 3b on the representation of tactile acuity ((Friedman et al., 2008), (Sur et al., 1982)). Our data along with other studies suggest that the same rule also exists in human SI cortex ((Kurth et al., 2000), (Nelson and Chen, 2008)). A greater digit separation in area 3b than in area 1was observed, with a ratio of 1.6. Specifically in our study, the measured interdigit distance was 12mm (Surface) and 7.46mm (Euclidian) in area 3b, and 7.25 mm (Surface) and 4.68 mm (Euclidian) in area 1. These observations are comparable to previous data, where the reported cortical distance between D1 and D5 varied from 16.05 to 17.09 mm in area 3b and varied from 14.26 to 14.9 mm in area 1 ((Kurth et al., 2000), (Nelson and Chen, 2008)). Our data suggest that calculating digit distance based on the Euclidian formula underestimates cortical distance measurements that could affect the interpretations of digital distance measurements.

The degree of intersubject variability was large, a finding consistent within the literature ((Francis et al., 2000), (Kurth et al., 2000), (Nelson and Chen, 2008)). Our decision to analyze subjects in their native space may have added to the degree of variability; however, we found that the use of the “Surface” method for calculating digit separation did not decrease the intersubject variability. Thus the inconsistency in digit distance measurements across subjects is at least partially due to a unique somatotopic representation of each subject. This observation stresses the need for analyzing subjects on an individual level in their native space.

Conclusion

This study demonstrates that ultra-high field BOLD fMRI at 7 T is capable of resolving fine-scale digit topography within areas 3b and 1 of SI cortex. These maps are comparable to nonhuman primate somatotopic maps derived from high-resolution electrophysiological and intrinsic optical methods and are in agreement with human digit somatotopic maps derived from fMRI and intraoperative imaging studies. BOLD activation is robust and reproducible across runs, highlighting its potential application in mapping cortical dynamic changes in individual subjects.

References

Bandettini, P.A., 2009. What's new in neuroimaging methods? Ann. NY Acad. Sci. 1156, 260–293.

Blankenburg, F., Ruben, J., Meyer, R., Schwiemann, J., Villringer, A., 2003. Evidence for a rostral-to-caudal somatotopic organization in human primary somatosensory cortex with mirror-reversal in areas 3b and 1. Cereb. Cortex 13, 987–993.

Borsook, D., Becerra, L., Fishman, S., Edwards, A., Jennings, C.L., Stojanovic, M., Papinicolas, L., Ramachandran, V.S., Gonzalez, R.G., Breiter, H., 1998. Acute plasticity in the human somatosensory cortex following amputation. NeuroReport 9, 1013–1017.

Brodmann, K., 1909. VergleichendeLocalisationslehre der Gro Hhirnrinde. Barth, Leipzig.

Chen, L.M., Friedman, R.M., Roe, A.W., 2005. Optical imaging of SI topography in anesthetized and awake squirrel monkeys. J. Neurosci. 25, 7648–7659.

Chen, L.M., Turner, G.H., Friedman, R.M., Zhang, N., Gore, J.C., Roe, A.W., Avison, M.J., 2007. High-resolution maps of real and illusory tactile activation in primary somatosensory cortex in individual monkeys with functional magnetic resonance imaging and optical imaging. J. Neurosci. 27, 9181–9191.

Cowey, A., Rolls, E.T., 1974. Human cortical magnification factor and its relation to visual acuity. Exp. Brain Res. 21, 447–454.

Dula, A., Welch, E., Creasy, J., Gatenby, J., Stringer, E., Chen, L., Anderson, A., Avison, M., Gore, J., 2010. New Frontiers in Biomedical Engineering. Proceedings of the 3rd International Conference on the Development of BME in Vietnam. Springer and IFMBE, Ho Chi Minh City, Vietnam.

Duncan, R.O., Boynton, G.M., 2003. Cortical magnification within human primary visual cortex correlates with acuity thresholds. Neuron 38, 659–671.

Eickhoff, S.B., Lotze, M., Wietek, B., Amunts, K., Enck, P., Zilles, K., 2006. Segregation of visceral and somatosensory afferents: an fMRI and cytoarchitectonic mapping study. Neuroimage 31, 1004–1014.

Fox, K., 2009. Experience-dependent plasticity mechanisms for neural rehabilitation in somatosensory cortex. Philos. Trans. R. Soc. Lond. B Biol. Sci. 364, 369–381.

Francis, S.T., Kelly, E.F., Bowtell, R., Dunseath, W.J., Folger, S.E., McGlone, F., 2000. fMRI of the responses to vibratory stimulation of digit tips. Neuroimage 11, 188–202.

Friedman, R.M., Chen, L.M., Roe, A.W., 2008. Responses of areas 3b and 1 in anesthetized squirrel monkeys to single- and dual-site stimulation of the digits. J. Neurophysiol. 100, 3185–3196.

Gati, J.S., Menon, R.S., Ugurbil, K., Rutt, B.K., 1997. Experimental determination of the BOLD field strength dependence in vessels and tissue. Magn. Reson. Med. 38, 296–302.

Gelnar, P.A., Krauss, B.R., Szeverenyi, N.M., Apkarian, A.V., 1998. Fingertip representation in the human somatosensory cortex: an fMRI study. Neuroimage 7, 261–283.

Geyer, S., Schleicher, A., Zilles, K., 1999. Areas 3a, 3b, and 1 of human primary somatosensory cortex. Neuroimage 10, 63–83.

Geyer, S., Schormann, T., Mohlberg, H., Zilles, K., 2000. Areas 3a, 3b, and 1 of human primary somatosensory cortex. Part 2. Spatial normalization to standard anatomical space. Neuroimage 11, 684–696.

Geyer, S., Schleicher, A., Schormann, T., Mohlberg, H., Bodegard, A., Roland, P.E., Zilles, K., 2001. Integration of microstructural and functional aspects of human somatosensory areas 3a, 3b, and 1 on the basis of a computerized brain atlas. Anat. Embryol. (Berl.) 204, 351–366.

Haacke, E.M., Brown, R.W., Thompson, M.R., Venkatesan, R., 1999. Magnetic Resonance Imaging: Physical Principles and Sequence Design. Wiley-Liss, New York.

Harel, N., Ugurbil, K., Uludag, K., Yacoub, E., 2006. Frontiers of brain mapping using MRI. J. Magn. Reson. Imaging 23, 945–957.

Hinkley, L.B., Krubitzer, L.A., Nagarajan, S.S., Disbrow, E.A., 2007. Sensorimotor integration in S2, PV, and parietal rostroventral areas of the human sylvian fissure. J. Neurophysiol. 97, 1288–1297.

Jack Jr., C.R., Thompson, R.M., Butts, R.K., Sharbrough, F.W., Kelly, P.J., Hanson, D.P., Riederer, S.J., Ehman, R.L., Hangiandreou, N.J., Cascino, G.D., 1994. Sensory motor cortex: correlation of presurgical mapping with functional MR imaging and invasive cortical mapping. Radiology 190, 85–92.

Jezzard, P., Balaban, R.S., 1995. Correction for geometric distortion in echo planar images from B0 field variations. Magn. Reson. Med. 34, 65–73.

Kayser, C., Petkov, C.I., Augath, M., Logothetis, N.K., 2005. Integration of touch and sound in auditory cortex. Neuron 48, 373–384.

Kim, D.S., Ronen, I., Olman, C., Kim, S.G., Ugurbil, K., Toth, L.J., 2004. Spatial relationship between neuronal activity and BOLD functional MRI. Neuroimage 21, 876–885.

Krause, T., Kurth, R., Ruben, J., Schwiemann, J., Villringer, K., Deuchert, M., Moosmann, M., Brandt, S., Wolf, K., Curio, G., Villringer, A., 2001. Representational overlap of adjacent fingers in multiple areas of human primary somatosensory cortex depends on electrical stimulus intensity: an fMRI study. Brain Res. 899, 36–46.

Kurth, R., Villringer, K., Mackert, B.M., Schwiemann, J., Braun, J., Curio, G., Villringer, A., Wolf, K.J., 1998. fMRI assessment of somatotopy in human Brodmann area 3b by electrical finger stimulation. NeuroReport 9, 207–212.

Kurth, R., Villringer, K., Curio, G., Wolf, K.J., Krause, T., Repenthin, J., Schwiemann, J., Deuchert, M., Villringer, A., 2000. fMRI shows multiple somatotopic digit representations in human primary somatosensory cortex. NeuroReport 11, 1487–1491.

Maldjian, J.A., Gottschalk, A., Patel, R.S., Detre, J.A., Alsop, D.C., 1999. The sensory somatotopicmap of the human hand demonstrated at 4 Tesla.Neuroimage 10, 55–62.

Moore, C.I., Stern, C.E., Corkin, S., Fischl, B., Gray, A.C., Rosen, B.R., Dale, A.M., 2000. Segregation of somatosensory activation in the human rolandic cortex using fMRI. J. Neurophysiol. 84, 558–569.

Nelson, A.J., Chen, R., 2008. Digit somatotopy within cortical areas of the postcentral gyrus in humans. Cereb. Cortex 18, 2341–2351.

Nelson, R.J., Sur, M., Felleman, D.J., Kaas, J.H., 1980. Representations of the body surface in postcentral parietal cortex of Macaca fascicularis. J. Comp. Neurol. 192, 611–643.

Ogawa, S., Lee, T.M., Nayak, A.S., Glynn, P., 1990. Oxygenation-sensitive contrast in magnetic resonance image of rodent brain at high magnetic fields. Magn. Reson. Med. 14, 68–78.

Ogawa, S., Menon, R.S., Tank, D.W., Kim, S.G., Merkle, H., Ellermann, J.M., Ugurbil, K., 1993. Functional brain mapping by blood oxygenation level-dependent contrast magnetic resonance imaging. A comparison of signal characteristics with a biophysical model. Biophys. J. 64, 803–812.

Overduin, S.A., Servos, P., 2004. Distributed digit somatotopy in primary somatosensory cortex. Neuroimage 23, 462–472.

Penfield, W., Boldrey, E., 1937. Somatic motor and sensory representations in the cerebral cortex of man as studied by electrical stimulation. Brain 60, 389–443.

Ruben, J., Krause, T., Taskin, B., Blankenburg, F., Moosmann, M., Villringer, A., 2006. Subarea-specific suppressive interaction in the BOLD responses to simultaneous finger stimulation in human primary somatosensory cortex: evidence for increasing rostral-to caudal convergence. Cereb. Cortex 16, 819–826.

Sanchez-Panchuelo, R.M., Francis, S., Bowtell, R., Schluppeck, D., 2010. Mapping human somatosensory cortex in individual subjects with 7 T functional MRI. J Neurophysiol 103, 2544–2556.

Sasaki, Y., Vanduffel, W., Knutsen, T., Tyler, C., Tootell, R., 2005. Symmetry activates extrastriate visual cortex in human and nonhuman primates. Proc. Natl Acad. Sci. USA 102, 3159–3163.

Schaechter, J.D., Moore, C.I., Connell, B.D., Rosen, B.R., Dijkhuizen, R.M., 2006. Structural and functional plasticity in the somatosensory cortex of chronic stroke patients. Brain 129, 2722–2733.

Schwartz, T.H., Chen, L.M., Friedman, R.M., Spencer, D.D., Roe, A.W., 2004. Intraoperative optical imaging of human face cortical topography: a case study. NeuroReport 15, 1527–1531.

Schweizer, R., Voit, D., Frahm, J., 2008. Finger representations in human primary somatosensory cortex as revealed by high-resolution functional MRI of tactile stimulation. Neuroimage 42, 28–35.

Sengupta, S.,Welch, E., Zhao, Y., Foxall, D., Starewicz, P., Anderson, A., Gore, J., Avison, M., 2009. Dynamic B0 Shimming at 7 Tesla. Proceedings of the 17th Annual Meeting, International Society for Magnetic Resonance in Medicine, Hawaii, USA, p. 777.

Silver, M.A., Kastner, S., 2009. Topographic maps in human frontal and parietal cortex. Trends Cogn. Sci. 13, 488–495.

Stark, D.D., Bradley, W.G., 1999. Magnetic Resonance Imaging. C. V. Mosby.

Sur, M., Nelson, R.J., Kaas, J.H., 1982. Representations of the body surface in cortical areas 3b and 1 of squirrel monkeys: comparisons with other primates. J. Comp. Neurol. 211, 177–192.

Tootell, R.B., Devaney, K.J., Young, J.C., Postelnicu, G., Rajimehr, R., Ungerleider, L.G., 2008. fMRI mapping of a morphed continuum of 3D shapes within inferior temporal cortex. Proc. Natl Acad. Sci. USA 105, 3605–3609.

van der Zwaag, W., Francis, S., Head, K., Peters, A., Gowland, P., Morris, P., Bowtell, R., 2009. fMRI at 1.5, 3 and 7 T: characterising BOLD signal changes. Neuroimage 47, 1425–1434.

Vogt, C., Vogt, O., 1919. Allgemeiner Ergebnisse unserer Hinforschung. J. Psychol. Neurol. 25, 279–462.

Weibull, A., Bjorkman, A., Hall, H., Rosen, B., Lundborg, G., Svensson, J., 2008. Optimizing the mapping of finger areas in primary somatosensory cortex using functional MRI. Magn. Reson. Imaging 26, 1342–1351.

White, L.E., Andrews, T.J., Hulette, C., Richards, A., Groelle, M., Paydarfar, J., Purves, D., 1997. Structure of the human sensorimotor system. I: morphology and cytoarchitecture of the central sulcus. Cereb. Cortex 7, 18–30.

CHAPTER III

DISTINCTIVE CORTICAL RESPONSES TO TACTION IN SUBREGIONS OF PRIMARY SOMATOSENSORY CORTEX

Abstract

Little is known in humans about the functional differences of Brodmann areas 3b and 1 of primary somatosensory cortex (SI). With MRI at 7 T, we examined in individual subjects BOLD responses in SI to vibrotactile stimuli presented on individual distal finger pads. In all subjects we observed activation foci along the posterior bank of central sulcus and crown of postcentral gyrus, corresponding to areas 3b and 1. In two subjects, focal activations also were detected in areas 3a and 2 of SI. Responses to different digit stimulation (D1 to D4) were organized somatotopically in an inferior/lateral to superior/medial manner in both areas 3b and 1. Inter-digit distances between activation centers were greater in areas 3b than area 1. BOLD signal time courses from voxels located on a path crossing the distal finger pad representations demonstrated that the responses in area 3b were more digit-selective than in area 1. The temporal profile of the BOLD signal in area 3b showed sustained response throughout the duration of stimulation, while the time course in area 1 had a greater initial transient phase followed by a weaker sustained phase. The surface area of cortex that responded to stimulation of a finger were similar in size in areas 3b and 1, suggesting that the overlap of digit responses in area 1 is the result of smaller cortical allotment, rather than larger response fields. In sum, the different response properties of areas 3b and 1 suggest that these areas play different roles in touch perception.

Introduction

Somatosensory cortices vary greatly across mammals, but despite inter-species differences, all mammals possess a systematic representation of contralateral cutaneous mechanoreceptors known as the primary somatosensory cortex (SI). Studies in both new world and old world monkeys indicate a clear separation of adjacent body sensorium, most particularly the hand area. Tactile search and manipulation of tangible objects by the hands and fingers is vital to the survival of all primates, and thus the acuity of the hand map reflects the functional specialization of the primate's digits. Myelin stains in area 3b of nonhuman primate SI detect myelin dense septa that not only separate the lower and upper extremities, but facial features and individual digits as well ((Jain et al., 1998), (Jain et al., 2001), (Qi and Kaas, 2004), (Qi et al., 2008)). Such septa might be present in area 3b of ape and human SI, however, these studies have not yet been performed. Similar septa and separation patterns of body representations have never been demonstrated in area 1.

In nonhuman primates, electrophysiological recordings from SI cortex may reflect these anatomical divisions. Receptive fields of neurons within area 3b of the owl monkey are restricted in size, to half a single distal finger pad, while neurons in area 1 can respond to stimulation of an entire distal finger pad, or to an entire finger, or to multiple fingers ((Sur et al., 1980)). The receptive fields of neurons are consistently larger in area 1 than area 3b, and demonstrate there is significant overlap in the digit representation in area 1 ((Sur et al., 1980), (Costanzo and Gardner, 1980), (Iwamura, 1998), (Iwamura et al., 1985b), (Iwamura et al., 1985a), (Iwamura et al., 1993)). Such electrophysiological studies have not been performed in human subjects. These invasive techniques of

measuring cortical activation give us insight into the cortex of the primate order, but are not appropriate for testing agreement with human SI.

A question that still plagues the field is the precision of the somatotopic maps in areas 3b and 1 in humans. Some SI studies report finely organized maps without overlap, while others have found evidence of significant overlap of body surface ((Allison et al., 1989a), (Allison et al., 1989b), (Allison et al., 1991), (Woolsey et al., 1979)). Human studies, some intraoperative, have provided evidence for greater overlap in area 1 than in area 3b. Intraoperative intrinsic optical imaging in human cortex revealed significant overlap of nonadjacent digits in area 1, but the study was limited by technique and could not investigate area 3b ((Cannestra et al., 1998)). Noninvasive imaging techniques have begun to target these questions of cortical overlap and precision of body surface maps.

Functional imaging techniques, such as positron emission topography (PET) and fMRI, have been used to map the sensory cortices in humans for decades ((Blankenburg et al., 2003), (Francis et al., 2000), (Gelnar et al., 1998), (Krause et al., 2001), (Kurth et al., 2000), (Maldjian et al., 1999), (Sanchez-Panchuelo et al., 2010), (Schweizer et al., 2008), (Weibull et al., 2008)). Initially these studies were conducted at low resolutions and were only able to confirm somatotopy across the full body surface, and could not identify topography of individual digits ((Fox et al., 1987)). The first study to target digit representation in human SI was not able to consistently detect activations in both areas 3b and 1 ((Gelnar et al., 1998)). Kurth and colleagues were the first to reliably separate digit maps between areas 3b and 1, detecting a mildly larger spread between digit representations in area 3b than area 1 ((Kurth et al., 2000)). FMRI studies have shown pronounced overlap in both areas, with greater overlap in area 1 and more distinct somatotopic maps in area 3b than area 1 ((Hansson and Brismar, 1999), (Maldjian et al., 1999), (Francis et al., 2000), (Kurth et al., 1998), (Kurth et al., 2000), (Krause et al.,

2001), (Ruben et al., 2006)). No studies, however, have been able to demonstrate consistent evidence for the lack of overlap across digit representations in area 3b. With the recent advances in MR signal strength due to ever increasing magnet size, it might be possible with the recent spatial resolutions available to distinguish topographic overlap differences in areas 3b and 1 ((Stringer et al., 2010a)).

In this study we investigate the spatial profile of single digit responses in areas 3b and 1. We use BOLD signal time course analysis to determine the overlap of digit representations in SI. Our study shows distinct somatotopic maps in areas 3b and 1, with greater overlap of digit representations in area 3b than area 1. We also found that the size of the digit response fields in areas 3b and 1 is the same in human cortex.

Methods

Stimulation Protocol

Six healthy human subjects (5 men, 1 woman, ages: 22 to 40 years, average: 31 years) gave informed consent for this study in accordance with a protocol approved by the Vanderbilt University Institutional Review Board. Air puffs were delivered to the glabrous skin of selected distal finger pads by a hand and finger cast connected via plastic tubing to an air pressure generator. Stretchable fabric was fitted across each opening in the cast, allowing for focal skin displacement in response to an air puff. The digits (D1, D2, D3 or D4) were stimulated at 2 Hz in a block design of 24 s on and 24 s off, with “on” blocks alternating between two digits in each run. Within one imaging session, multiple runs were acquired to obtain 6 to 12 repeats per individual digit. We mapped digit responses by stimulating nonadjacent digits (D2 and D4 in Subjects 1 and 2), adjacent digits (D2 and D3 in Subjects 3 and 4), and four digits (D1, D2, D3, and D4

in Subjects 5 and 6). Across subjects, a total of 16 digits were mapped.

MRI Data Acquisition

Subjects were scanned on a 7 T Philips Achieva magnet with a 16-channel NOVA head coil. Structural images were collected using a three-dimensional fast field echo (3D-FFE) sequence, TR/TE/TI = 3.7/1.8/1300 ms, with a 1 x 1 x 1-mm^3 voxel resolution. Functional images were acquired using a gradient-echo echo-planar imaging (GE-EPI) sequence, TR/TE = 2000/25 ms, flip angle = 80°, and a 192 x 192 field of view (FOV), with a voxel resolution of 1 x 1 x 2 mm^3. Sixteen oblique coronal slices (0 mm gap thickness) were acquired covering cortical regions: the primary somatosensory cortex (SI) region posterior to central suclus, posterior part of the lateral sulcus, and thalamus. We used a SENSE acceleration factor of 3, and volume selective 2^{nd} or 3^{rd} order shimming using a pencil-beam method.

fMRI Data Analysis

EPI images were corrected for distortion using a B_0 field-map (Jezzard and Balaban, 1995) in Matlab prior to inputting data into BrainVoyager QX for standard preprocessing and statistical analysis. Preprocessing included slice scan time correction using a cubic spline, motion correction in three dimensions, slice alignment using an intra-session registration, and temporal filter using a 7-mHz high-pass filter and linear trend removal. A general linear model (GLM) was fitted to the time series of BOLD signals and t-maps (indicating the correlation strength between the model and signal) were created. Single condition activity maps (Single digit – Rest) were examined in each individual subject. Activation maps of contralateral hemisphere were thresholded at q (FDR) < 0.001 with 4 voxels minimum per cluster. Activation maps were interpolated into 1x1 x1 mm^3 voxels for visualization. To preserve the high spatial resolution, spatial

smoothing of the functional EPI images was not applied. For all subjects the activation maps are presented in their native space with native coordinates reported. These coordinates do not correlate with Talariach or MNI space. Composite maps of individual digit activation were created to visualize digit topography in SI (area 3b and area 1). In order to compare activation coordinates across subjects and with previous studies of digit somatotopy, the data were transformed into Talariach space. These normalized coordinates of activated clusters were presented in the clustering plot. Single-condition activity maps were used to define regions of interest (ROIs) for time course analysis.

Identification of Subregions of SI cortex

According to literature, we classified digit activations into four distinct cytoarchitectural subregions of SI cortex, Brodmann Areas 3a, 3b, 1, and 2 ((Brodmann, 1909),(Vogt and Vogt, 1919)). The location of the SI hand region is identified by the omega-shaped folding (visible in the axial plane) of the postcentral gyrus ((Moore et al., 2000), (White et al., 1997)). We used the SI subregions maps (areas 3a, 3b, 1, and 2) as being cytoarchitectonically defined by Geyer *et al* and Grefkes *et al* to locate the activation foci detected ((Geyer et al., 2000), (Grefkes et al., 2001)). According to their maps, Area 3a is located within the fundus of the CS, area 3b is located along the posterior bank of the CS, area 1 is located at the crest of the postcentral gyrus, and area 2 is located at the caudal part of the postcentral gyrus or on the anterior bank of the postcentral sulcus ((Geyer et al., 2000), (Grefkes et al., 2001), (Kurth et al., 2000), (Krause et al., 2001), (Nelson and Chen, 2008)).

Voxel by Voxel BOLD Signal Time Course Profile

To reveal the spatial profile of single-digit activation, we plotted the BOLD signal time course at selected single voxels along digit responses in both areas 3b and 1. From

each single-condition activity map, we determined the 3D (x, y, z) coordinates for the peak (highest t-value) voxel responding single-digit stimulation in both areas 3b and 1. We first traced the 3D path, voxel by voxel, between the peak voxels of neighboring digit responses along the folds of the postcentral gyrus (e.g., 3D distance between D2 and D3 in area 3b), and then extracted the BOLD signal time course from each digit's peak voxel and intermediate voxels along the traced path, ten in total for both area 3b and 1. The time courses of single-condition blocks (D_A, D_B, etc) were averaged within runs and across runs.

Calculation of Mean BOLD Signal Time Course

We calculated the average time course of the BOLD signal in areas 3b and 1 separately. At each single-digit activation center in each of areas (3b or 1), we first selected the peak five voxels (highest t-values) and then averaged their time courses for each condition within a run, across runs, and across subjects. The voxel size is quite small in our study (1x1x1 mm^3), so the five peak voxels used for time course calculation typically did not overlap across digits and area. One exception is in Subject 5 where there was one overlap voxel for D3 and D4 time course calculation in area 1. To compare the mean signal time course in area 3b versus area 1, the time courses from all digits were included (Figure 7A). In order to compare the BOLD signal time courses of adjacent digits in both areas 3b and 1, the time courses of both D_A (e.g. D2) and D_B (e.g. D3) were averaged within a run, across runs, and across subjects. Data from four subjects (Subjects 3 – 6) were used for the adjacent digits time course quantification (Figure 7B and 7C).

The statistical difference between mean time courses in area 3b and area 1 was compared using a multivariate permutation paired t-test ((Karniski et al., 1994), (Blackford, 2002), (Salomon et al., 2005)). This analysis was performed using the R

Statistical Computing Environment, a free statistical analysis software package (R 1.8.1, 2003). A statistical threshold of $p < 0.05$ (uncontrolled for multiple comparisons) was used.

Spatial Decay of Single-Digit BOLD Response in Areas 3b and 1

We used a normalized single-digit BOLD response to evaluate the spatial extents of digit response fields in areas 3b and 1. To identify voxels responsive to single-digit stimulation, we used an ROI defining threshold of $q(FDR) < 0.05$. The BOLD response for each voxel within each ROI was estimated using the regression parameters from the GLM (i.e. D_A-Rest) and was normalized to the peak voxels in areas 3b and 1. Using the Euclidian formula, we also calculated each voxel's distance away from the peak voxel. For each given distance, we averaged the normalized BOLD response to give a single point at each distance resulting in a BOLD response vs. distance curve. We averaged the curves across subjects and plotted the normalized BOLD response as a function of cortical distance from the peak voxel for each digit (D1, D2, D3, and D4) in both areas 3b and 1. We then calculated the average curve (combing all digits) for area 3b and area 1.

Results

Functional Organization of Single-Digit Tactile Responses in Areas 3b and 1

All single-digit stimulation evoked focal and robust BOLD responses in cortical areas areas 3b and 1. To reveal the location and spatial characterization of single-digit activation, the D2 activation maps (D2 – Rest, thresholded at $q (FDR) < 0.001$) were displayed in the three cardinal planes (i; sagittal, ii: coronal, iii: axial) for each subject (Figures 1&2, A Subject 1, B Subject 2, C Subject 3, D Subject 4, E Subject 5, and F

Subject 6). Based on the local anatomical features around the central sulcus (CS), we located D2 activations in area 3b (Figure 1) and area 1 (Figure 2) in all six subjects. The white cross-hairs indicate the peak (highest t-value) cortical responses in both areas 3b and 1 to D2 stimulation. Additionally, in many of the subjects activations were also observed in other cortical areas such as areas along the postcentral sulcus, the lateral sulcus. The focus of this paper is on contralateral SI cortex, so only activations within SI cortex were described and illustrated.

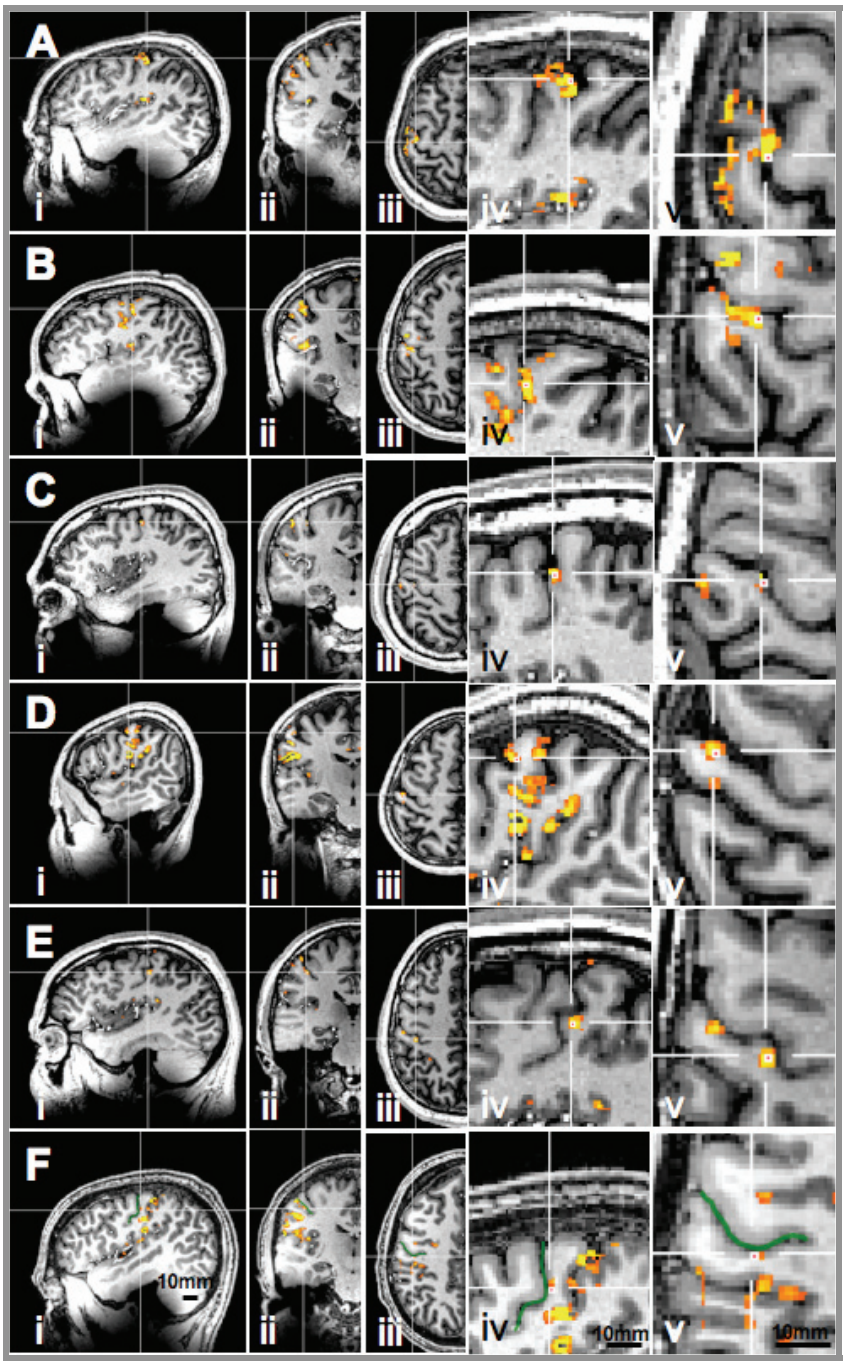

Figure 1. D2 activation maps in area 3b in all subjects (***A-F***). Single condition (stimulus-rest) activations to stimulation of D2 distal finger pad showed in the three large sagittal (***i***), coronal (***ii***), and axial (***iii***) planes, and in two zoomed-in sagittal (***iv***) and axial (***v***) views. Activation maps are thresholded at q (FDR) < 0.001 with cluster threshold of 4 voxels. Green lines highlight the location of the central sulcus and the black scale bars indicate a 10 mm distance in the bottom panel.

Anatomically, Brodmann area 3b subdivision of SI cortex locates at the posterior bank of the CS, which is bested viewed on sagittal and axial plan images as shown in Figure 1. The hand region in area 3b is located near the omega-shaped hook of the CS, which is best viewed on the axial plan images. Across all subjects, while robust

activations were present in appropriate hand regions in areas 3b, some variations in peak location and spatial distribution of activation were also present (Figure 1). For example, Subject 3 had a small activation along the upper bank of CS, rendering localization of D2 cortical response in area 3b simple (Figure 1C). In Subject 2, D2 activations appeared to be stronger, and formed one big cluster along the posterior bank of the CS (Figure 1B).

Brodmann Area 1 lies at the crest of the postcentral gyrus, a location that is superior and caudal to areas 3b. We observed activations to D2 stimulation in areas 1 in all subjects (Figure 2). Similarly to area 3b, while somatotopically appropriate activation retained across subjects, close examination of signal subject activation revealed apparent variations in activation location and strength. Subject 3 had a small activation rendering the localization of digit response in area 1 simple (Figure 2C). In this subject, the D2 activation in area 1 can be easily localized in the axial plane by its superficial location near the dermis. In the sagittal plane the hump of the postcentral gyrus is evident, with the CS anteriorly and the postercentral sulcus posteriorly defining the hump. Area 1 is located from the top of the hump to the top posterior part of the hump, where activations were detected in all subjects. In sum, while robust and focal activations were detected in areas 3b and 1 in all six subjects, apparent variations in response location, spatial pattern and strength were also present.

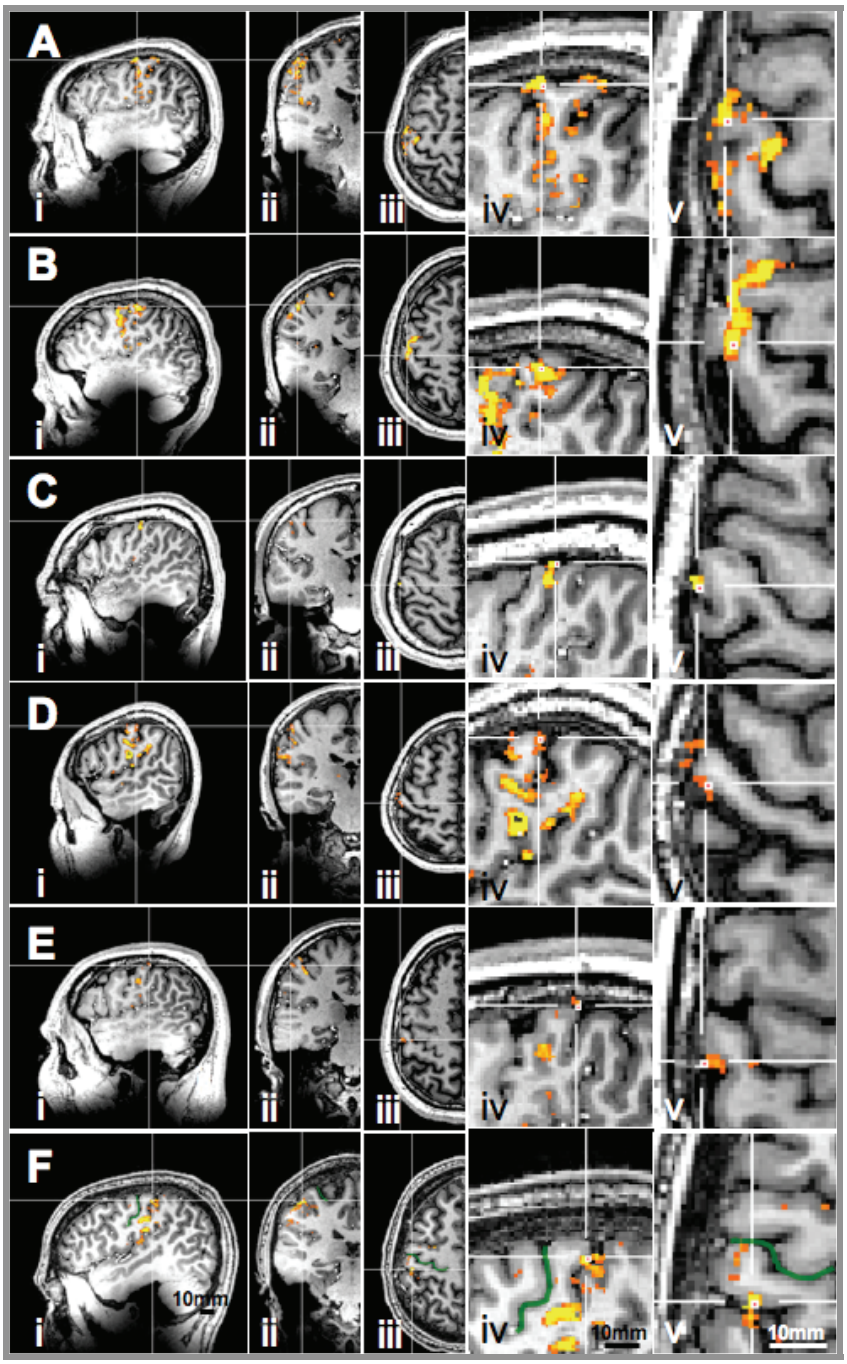

Figure 2. D2 activation maps in area 1 in all subjects (***A***-***F***). Single condition (stimulus-rest) activations to stimulation of D2 distal finger pad showed in the three large sagittal (***i***), coronal (***ii***), and axial (***iii***) planes, and in two zoom-in sagittal (***iv***) and axial (***v***) views. Activation maps are thresholded at q (FDR) < 0.001 with cluster threshold of 4 voxels. Green lines highlight the location of the central sulcus and the black/white scale bars indicate a 10 mm distance in the bottom panel.

In addition to activations observed in areas 3b and 1, in two subjects, we also detected activations in areas corresponding to areas 3a and 2. To illustrate the digit activations in subregions of areas 3b, 3a, 1 and 1 in a common space, and to compare with SI tactile activations reported in previous studies, we normalized activation in each

subject to Talariach space, and plotted the average digit activation coordinates in Figure 3. Digit activations in area 3b (solid black circle), area 1 (solid black diamond) and area 2 (solid black triangle) distributed nicely in an anterior to posterior order on sagittal plan whereas activation in area 3b (solid black square) located in a more superior and medial position (Figure 3A). The spatial extent of area activation ranged in a very small spatial scale: 6 mm in A-P dimension (-21 to -27), 6 mm in S-I dimension (43 to 48), and 19 mm in L-M dimension (30 to 49).

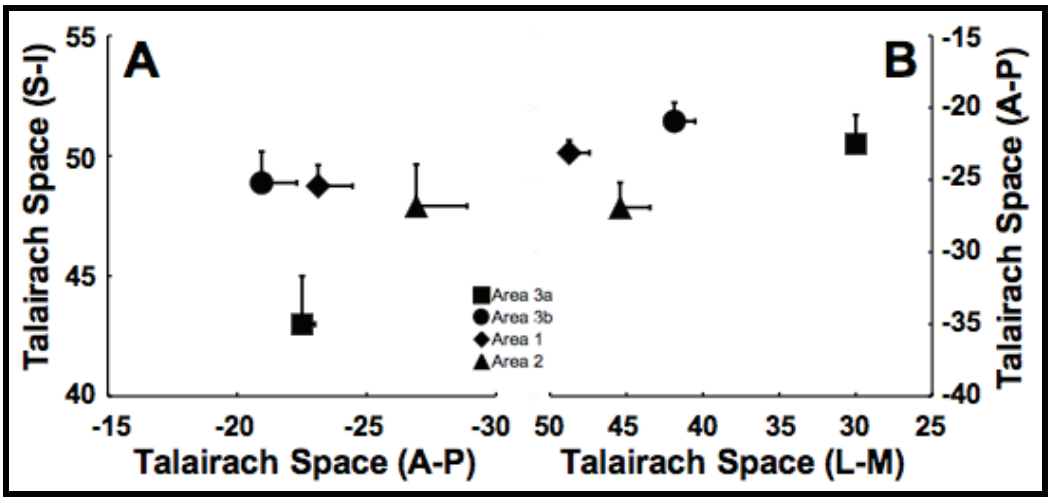

Figure 3. Coordinate plot of digit activations in Talairach space. The spatial distribution of the mean coordinates of digit activations in areas of 3a, 3b, 1 and 2 in (***A***) sagittal and (***B***) axial planes. Area 1, diamonds; Area 3b, circles; Area 3a, squares; Area 2, triangles. S: superior; I: inferior; A: anterior; P: posterior; L: lateral; M: medal.

Somatotopic Organization of Single-Digit Activation in Areas 3b and 1

To evaluate the somatotopic organization of digit representation within areas 3b and 1, we stimulated multiple digits independently in each subject. Figure 4 illustrated sample data in Subject 5 where tactile activations of four digits (D1-D4) were mapped. On the series of zoom-in axial images (Figure 4B), focal activation clusters were present in areas along the postcentral gyrus (blue lines in A and the first image of the top row in B indicate the central sulcus) during D1 (top row in B), D2 (the second row in B), D3 (the

third row in B), and D4 (the fourth row in B) stimulation. Each activation cluster was showing in different images slices, therefore, the color arrows were used to indicate the centers (highest t value) of digit activation in area 3b (light blue arrows) and area 1 (light green arrows). For example in axial slice Z = 71 (third column) there is a peak cortical response to the stimulation of D3 in both areas 3b and 1. The blue arrow indicates the activation cluster located at the posterior bank of the CS that corresponds to area 3b. The green arrow indicates the activation cluster at the crest of postcentral gyrus that corresponds to area 1. From D1 to D4 (top to bottom rows in B), activation centers shifted from anterior to posterior locations in both areas 3b and 1 as indicated by the color arrow positions.

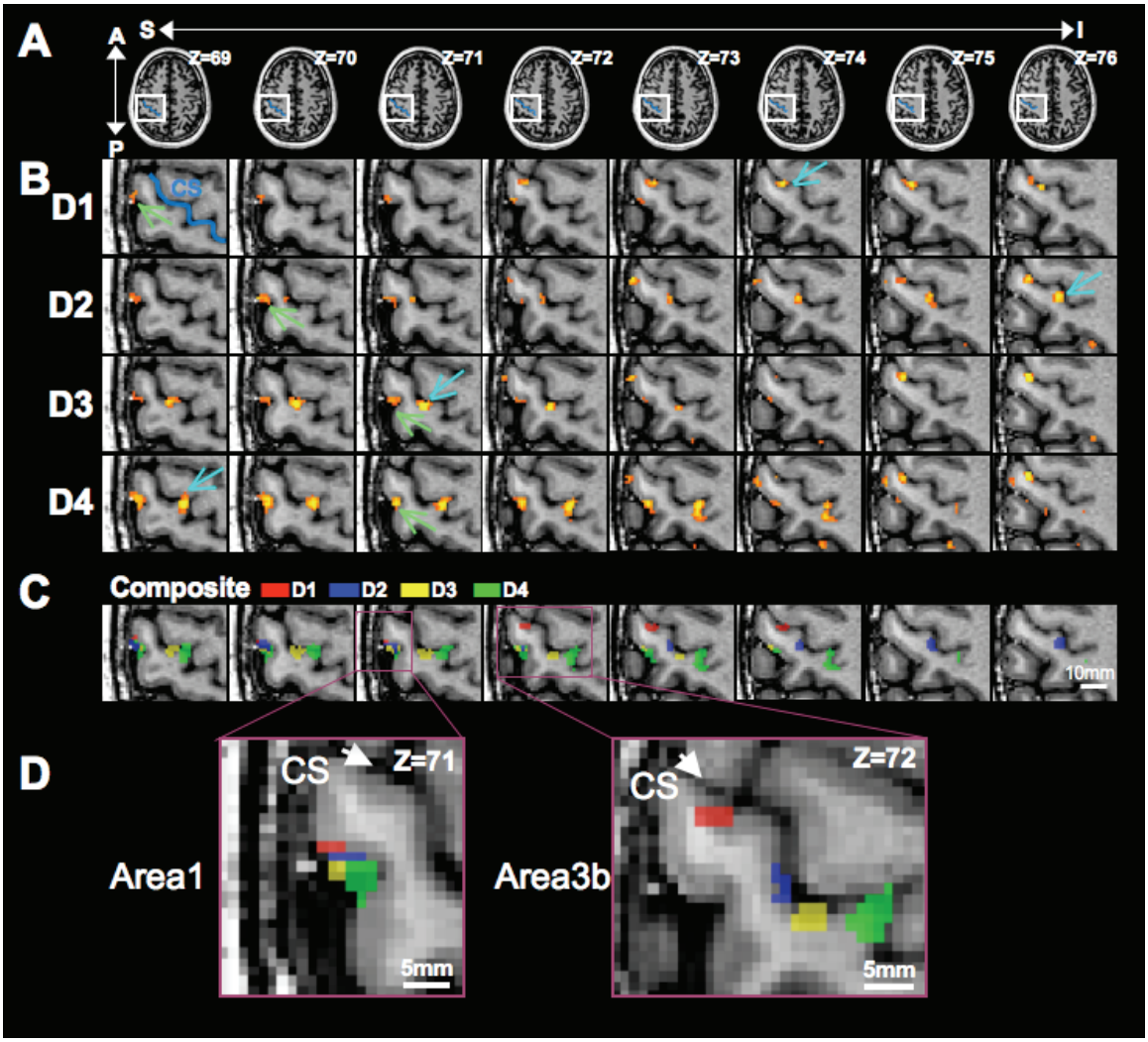

Figure 4. Somatotopic organization of individual digit activations (D1 to D4) in areas 3b and 1 in one representative subject. (***B***) Single digit activity maps are shown in the (***A***) axial plane, displayed in 1 mm increments from superior (left) to inferior (right). The blue lines in ***A*** and the first image in the top row of B indicate the location of the central sulcus (CS). (***B***) and (***C***) display the zoomed-in images corresponding to the region of interest (white line boxes in ***A***). Activity maps (Digit - Rest) for D1, D2, D3, and D4 are displayed in the four rows in ***B***, respectively. The light blue arrows point to the peak activation locus (voxel with the highest t-value) in area 3b; the light green arrows point to the peak activation in area 1. Activation maps are displayed at q (FDR) < 0.001 with a cluster threshold of 4 voxels. (***C***) The composite map illustrates the representation of all digits in each image plane with D1 in red, D2 blue, D3 yellow, and D4 green. The white scale bar in the last image of ***C*** indicates 10 mm (for both ***B*** and ***C***). (***D***) The magnified views are displayed for two selected regions (green line boxes in C) in area 1 (left) and area 3b (right), respectively.

To examine the spatial relationship of different digit activations, we combined all four digit activations into one image series (Figure 4C) showing the color-coded activation of

all the digits (D1 red, D2 blue, D3 yellow, and D4 green). In area 3b digit topography of D1 (37, 151, 74) to D4 (50, 160, 68) progressed from lateral to medial, anterior to posterior, and inferior to superior (illustrated on the right image in Figure 4D), but with two exceptions (displayed in subject's native space). D2 representation (Z = 76) was observed inferior to D1 representation (Z = 74), and following along the folds of the central sulcus, D3 representation (Y = 161) was observed posterior to D4 representation (Y = 160). In area 1, digit topography of D1 (33, 154, 68) to D4 (35, 160, 71) progressed from lateral to medical, anterior to posterior, and superior to inferior (illustrated on the left image in Figure 4D), but with an exception of D2 representation (X = 31) observed lateral to D1 representation (X = 33). In comparing the functional organization of four digit activations in areas 3b and 1 (Figure 4D), one feature was apparent. Digit representations in area 3b occupied a larger cortical area (more spatial distributed) than that in area 1. At this given threshold, the amount of overlap between digit representations was greater for area 1 than for area 3b, and a finding observed in all subjects. In sum, we observed a superior to inferior and anterior to posterior orderly progression of the digit representations in both areas 3b and 1 with slight variations in inter-digit spatial relationship in their specific 3D space.

In addition to the digit-specific activation foci in areas 3b and 1, we also observed one common activation at the inferior and lateral most part of area 3b (Figure 2B, Z=76). This region of cortex responded robustly to stimulation of all digits (similar location in D1-D4 rows in B) in this particular subject. Analysis of the BOLD signal time course in this ROI confirmed a non-differential response to individual digit stimulation, with an average BOLD signal amplitude of 1.92 ± 0.07 %. This common-digit activation was not detected in other subjects.

3D Plot of Digit Representations across Subjects in Talairach Space

To evaluate the spatial distribution of individual digit representation in four subregions (areas 3b, 1, 3a and 2) across subjects, we transformed activation maps into Talairach space. Figure 5 displays plots of mean coordinates of peak activations of individual digits in different areas (areas 3b and 1 in A & B and areas 3b and 1 in C & D) with error bars indicating the variability in spatial location across subjects on the sagittal (Figure 5A&5C) and axial planes (Figure 5B&5D). From D1 (red symbols), to D2 (blue symbols), to D3 (yellow symbols), and to D4 there were systematic coordinates shift in both areas 3b (solid circles in A and C) and 1 (solid diamonds in A and C) in all three dimensions. In the sagittal plane (Figure 5A) there was an orderly progression along an inferior/anterior to superior/posterior trajectory of D1 to D4 digit activations in Talairach space. D1 activations (red circles and diamonds) located in the most anterior, lateral and inferior position whereas D4 activations (green circles and diamonds) located in the most posterior, medial, and superior positions in both areas 3b and 1 (Figure 5A&5C). D2 (blue circles and diamonds) and D3 (yellow circles and diamonds) activations located at positions in between D1 and D4. Similarly, in the axial plane (Fig 3D) the activations of D1 to D4 progressed along the medial/anterior to lateral/posterior trajectories. In Talairach space the mean coordinate values for D1 to D4 in area 3b were X = 46.5, Y= -17, Z = 42.5 for D1, 42.7, -19.5, 46.2 for D2, 41.5, -19.5, 52.5 for D3, and 38.78, -26.5, 52.5 for D4, respectively. Digit activation in area 1 (color diamonds) appeared to shift approximately 10 mm laterally and 2 mm anteriorally to area 3b digits representation (color circles). The mean Talairach coordinates for D1, D2, D3 and D4 in area 1 were D1: (51.5, -18.5, 45), D2: (49.8, -22, 49.7), D3: (47.5, -22.8, 49.5), and D4: (45.6, -27.5, 48.5) in x, y, and z, respectively.

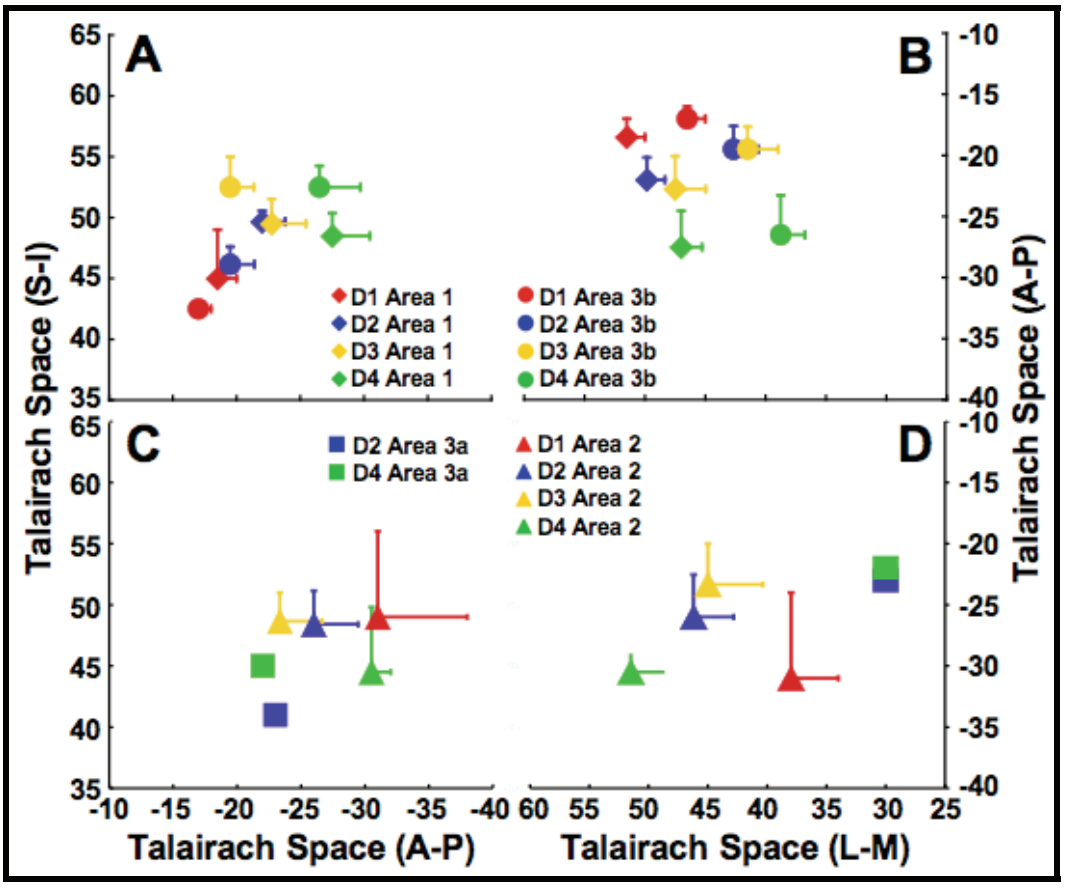

Figure 5. Cluster plots of individual subjects' digit responses in contralateral SI cortex with the coordinates displayed in Talairach space (mm). (***A***) The distribution of digit responses viewed in the sagittal plane, (***B***) and in the axial plane. The large solid diamonds and circles represent the mean coordinates across subjects in areas 1 and 3b, respectively. The insets display the mean coordinates to illustrate the topography in these two subregions. L, lateral; M, medial; A, anterior; P, posterior; Area 1, diamonds; Area 3b, circles; Area 3a, squares; Area 2, triangles; D1, red; D2, blue; D3, yellow; D4, green.

Activation in areas 3a and 2 were observed in two and four subjects, respectively (Figure 5 C&D). In contrast, spatial organization of D1 to D4 activations in areas 3a (solid squares in B and D) and 2 (solid triangles in B and D) appeared not as orderly as corresponding digit activations in areas 3b and 1. In sum, across subjects, orderly representations of D1 to D4 were present in areas 3b and 1, but not in areas 3a and 2.

Selectivity of BOLD Signals in Areas 3b and 1

Given the larger cortical distance of digit representation in area 3b than area 1, we further examined the temporal and magnitude differences of BOLD signal changes to non-adjacent digits (e.g. D2 and D4) stimulation in areas 3b and 1 (Figure 6). In one representative subject, D2 stimulation evoked activations (D2 – Rest) in both areas 3b and 1 as indicated by green arrows in Figure 6A. At D2 location of area 1, D2 stimulation (blue blocks) evoked robust BOLD signal increase (black line in C) starting a few seconds after stimulus presentation. Interestingly, at this D2 location, D4 stimulation (green blocks in C) also evoked BOLD signal increase but in a lower amplitude (~50%). This observation shows that D2 representation region in area 1 responded to both D2 and D4 stimulation, but with a greater response to D2. In contrast, at D2 location of area 3b, D2 stimulation (blue blocks in D) evoked robust BOLD signal increases whereas D4 stimulation (green blocks in D) resulted no signal changes (black lines during green blocks). This finding illustrates that D2 representation region in area 3b only responds to D2 stimulation, but not non-adjacent D4 stimulation.

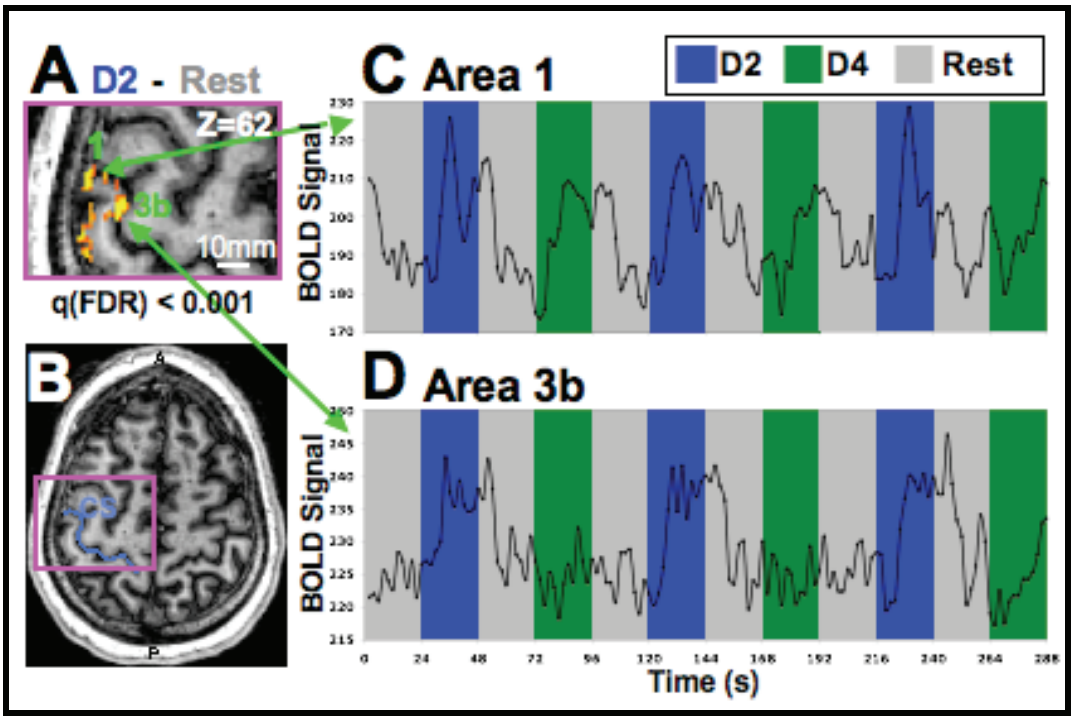

Figure 6. Activity map and time course of digit responses in areas 1 and 3b. (***A***) The activity map (D2 - Rest) is displayed in the increase field of view image, with distinct representations in areas 1 and 3b. (***B***) The axial slice of the anatomical image is displayed with the central sulcus (CS) highlighted in blue and the pink box indicating the area displayed in ***A***. The time course of BOLD signal change from (***C***) area 1 and (***D***) area 3b were extracted from the peak five voxels within each ROI (area 3b and 1) and displayed in the time course plots for a single run; Rest grey, D2 blue, D4 green.

To compare the temporal profile of the average BOLD response in areas 3b and 1, we averaged BOLD signal time courses of all subjects across all runs (Figure 7). The mean time courses highlighted a number of differences between BOLD signal profiles in area 3b and area 1. Firstly, in response to single-digit stimulation, area 1 response (red curve in Figure 7A) was greater than area 3b response (purple curve). The peak BOLD signal change was 4.56 % in area 1 (red curve) compared to a 2.92 % peak signal change in area 3b (purple curve). Secondly, similar to the observations obtained in the subject as showing in Figure 6, during a 24 s stimulus block (grey bars in Figure 7 A-C) signal change in area 1 had an initial strong and transient phase (6-14 sec) and then

followed by a sustained component that was smaller in magnitude. BOLD signal decayed immediately after stimulus offset. In contrast, the BOLD signal change in area 3b showed a sustained response profile that roughly maintained its magnitude, throughout the entire duration of the stimulus. Using multivariate permutation analysis, we determined that there was a statistical difference (p (uncorrected) < 0.05) between the time courses from 6 – 14 s, with the greatest difference at 8 s (t = 3.33).

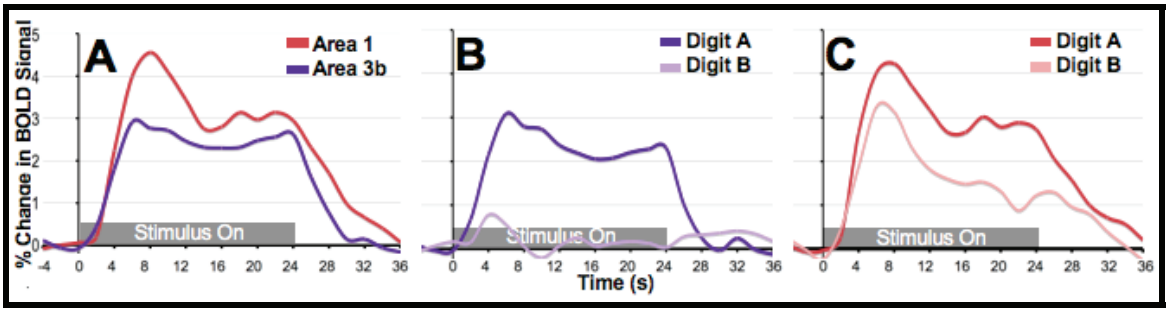

Figure 7. The mean percent BOLD signal change across subjects. (***A***) The BOLD signal response from the peak five voxels in area 3b (red) and area 1 (purple) were averaged across all digits and all subjects (n=6) and the time courses displayed. The mean BOLD signal response from adjacent digits was also extracted (n=4). (***B***) The BOLD signal response from adjacent digits, D_A and D_B, were extracted from the digit A ROI and the time courses for digit A (purple) and digit B (light purple) were displayed for area 3b. (***C***) The BOLD signal response from adjacent digits, D_A and D_B, were extracted from the digit A ROI and the time courses for digit A (red) and digit B (light red) were displayed for area 1. The grey box indicates the stimulus duration, 24 s.

Finally, to evaluate the selectivity of BOLD responses, we further compared the mean time courses at one digit location (e.g. D2) evoked by alternated adjacent digit (D_A and D_B, n = 4) stimulation in area 3b (Figure 7B) and area 1 (Figure 7C). While a single digit stimulation (e.g. D2) evoked a 3.09 % BOLD signal change at each particular digit location (e.g. D2) in area 3b (purple curve in Figure 7B), the average response to stimulation of an adjacent digit D_B (e.g. D3, light purple curve in Figure 7B) was every weak (0.78 %) and short (< 4s). Conversely, in area 1 (Fig 7C), the average response to

single-digit stimulation (D_A) was only slightly larger (4.23 %, red curve) than the response to stimulation of the adjacent digit (3.25 %, pink curve). Temporally, while the response to the adjacent digit was robust, it decayed rapidly during stimulation period, whereas the response to the homologous digit (D_A) was maintained after the initial impulse until stimulus offset.

In summary, the temporal profiles of BOLD responses in area 3b and 1 demonstrate that tactile response in area 1 is stronger than that in area 3b. Response in area 1 contains an initial transit component and a later sustained component whereas response in area 3b sustained during the stimulation period. BOLD signals at single digit location of area 3b are very selective whereas signals in area 1 have more response overlap across digits.

Spatial Profiles of BOLD Signal Changes along the Digit Response Line in Areas 3b and 1

To confirm the distinct fingertip topography (observed in spatial distribution of the BOLD signal time courses along the trajectory path from D1 to D4), we plotted the voxels along the trajectory path that responded significantly to digit stimulation in area 3b (Figure 8) and area 1 (Figure 9). Significantly increased signal noise ratio at high MRI field allowed us to quantitatively evaluate the spatial profiles of BOLD signal changes at a voxel-to-voxel bases along the digits representation line in both areas 3b and 1. We traced the 3-dimensional path between peak responses of D1 to D4 (Euclidian distance 16.9 mm) along the gray matter of the posterior bank of the central sulcus (area 3b) and along the gray matter of the crest of the post central gyrus (area 1, Euclidian distance 6.5 mm), and extracted the BOLD signal time course from 10 selected voxels along this path in the subject's native 3D coordinate system (Figure 8A for area 3b and Figure 9A

for area 1). In area 3b, voxels 1 (37, 151, 74), 4 (44, 156, 76), 7 (45, 161, 71), and 10 (50, 160, 68) are the peak voxels of D1, D2, D3, and D4 activation, respectively and were color-coded for each digit (D1 - 1, red; D2 - 4, blue; D3 – 7, yellow; D4 – 10, green) in Figure 8. Time courses derived from each single voxels (1 to 10) were chosen to best illustrate the selectivity of BOLD signal changes to different digit stimulation (D1 to D4) at each digit center (1, 4, 7, and 10 in Figure 8B) and intermediate locations (2, 3, 5, 6, 8, 9 in Figure 8B). For example, voxel 1 (D1 center) had the largest response to D1 stimulation (red curve in B) than to stimulation of neighboring digits. The responses (blue, green and yellow curves in B) to neighboring digit stimulation (D2 to D4) were minimal. Along the trajectory path to D2 (voxel 5) the response to D1 stimulation gradually waned, while the response to D2 stimulation (blue curves), very weak at voxels 2 and 3, began to rise at voxel 4 and peaked at voxel 5. Along the digit path to D4, even though voxels 6 (45, 161, 73) and 8 (48, 161, 70) were on the trajectory path between D2 and D4 there was no response (flat curves) to digit stimulation (D1 - D4) at these intermediary voxels. The digit selectivity of BOLD signal at each digit location was also illustrated in Figure 8C, where only the peak BOLD signal was plotted and compared. Significantly stronger and selective signals (color bars) were present at each digit center locations (color arrows). Together, these observations demonstrated that BOLD signal at each digit region of area 3b was selective, and the region was spatially restrained, showing little overlap of the digit responses to adjacent digit stimulation.

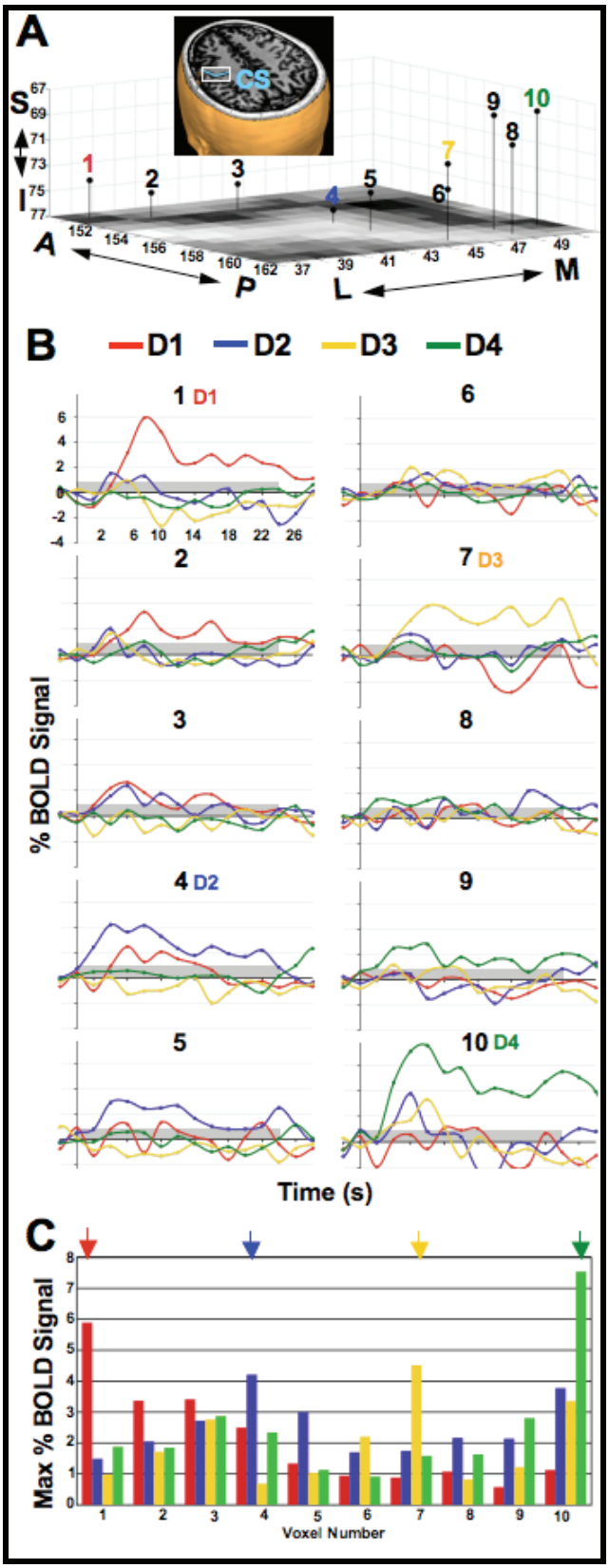

Figure 8. Voxel by voxel time courses along the posterior bank of the central sulcus (area 3b). (***A***) The plot displays the coordinates of the individual voxels from which the time courses were extracted. The structural image in the axial plane (Z=77) is displayed for reference along the central sulcus. The inset displays the brain of the subject in the same orientation, where the white box indicates the section of cortex displayed at the bottom of the stem-plot. (***B***) The time courses extracted from individual voxels describe how individual voxels respond to individual digit stimulation; D1 red, D2 blue, D3 yellow, and D4 green. The time courses show the temporal evolution of the BOLD response as one steps through space. (***C***) A summation of the maximum amplitude in BOLD signal within each voxel for individual digits. The colored arrows indicate the amplitude at peak voxels.

Different spatial distribution of the BOLD signal time courses was observed in area 1 for Subject 5. Ten voxels along the trajectory path from D1 to D4 (Figure 9A) were selected (Euclidian distance 3.6 mm). Voxel 1 (34, 155, 67), voxel 5 (31, 157, 70), voxel 7 (33, 159, 71), and voxel 9 (35, 160, 71) were the peak voxels for D1, D2, D3, and D4, respectively (Figure 9A). In contrast to area 3b the timecourses of individual digit responses suggest an extensive response overlap across digit locations in area 1. For example voxel 9 (35, 160, 71) had a greater response to D4 stimulation (green curve in Figure 9B) than stimulation of neighboring digits, but the responses to D2 (blue curve) and D3 (yellow curve) stimulation were also quite strong, with only a slight difference in maximum BOLD signal amplitude between D4 and D3. At the intermediate voxels locations along the digit path (2, 3, 4, 6, 8, 10), BOLD signals were weak but apparent during neighboring digit stimulations. Another example of time course from voxel 6 (32, 158, 70 in Figure 9B) demonstrates that at this coordinate the cortex responds robustly to stimulation of D1 through D4, with the weakest response to D1, but that is still approximately 4 %. Even though there was a large degree of digit response overlap in the time courses, there was a clear progression of the BOLD signal amplitudes across this path that paralleled and supported the topographic organization observed in the t-activity maps. Max BOLD signal plot as a function of voxels along the digit path further illustrated the observation of a extensive BOLD response overlap across digits (Figure 9C). The lateral and anterior most voxel (voxel 1) responded robustly the D1 stimulation (red bar at the voxel 1 location in C), and the medial and posterior voxel of D4 responded strongly to D4 stimulation (green bar at voxel 10 location in C).

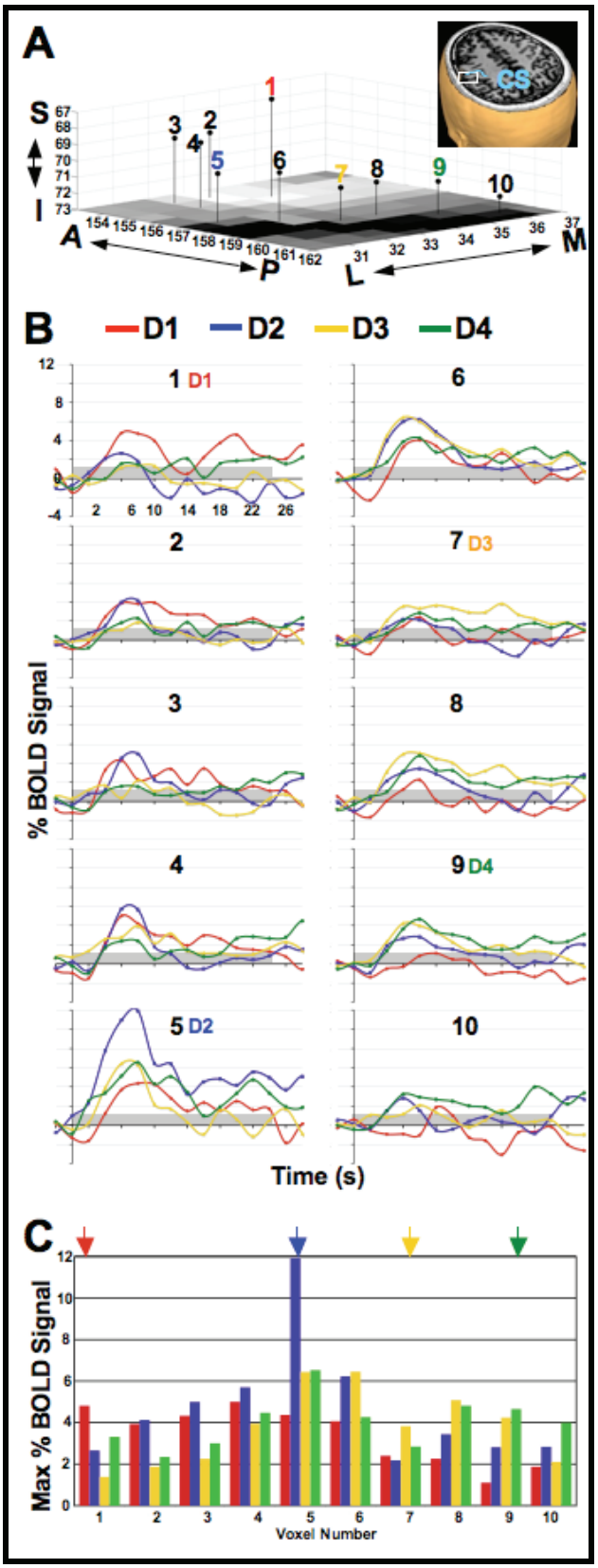

Figure 9. Voxel by voxel time courses along the crest of the postcentral gyrus (area 1). (***A***) The plot displays the coordinates of the individual voxels from which the time courses were extracted. The structural image in the axial plane (Z=73) is displayed for reference along the central sulcus. The inset displays the brain of the subject in the same orientation, where the white box indicates the section of cortex displayed at the bottom of the stem-plot. (***B***) The time courses extracted from individual voxels describe how individual voxels respond to individual digit stimulation; D1 red, D2 blue, D3 yellow, and D4 green. The time courses show the temporal evolution of the BOLD response as one steps through space. (***C***) A summation of the maximum amplitude in BOLD signal within each voxel for individual digits. The colored arrows indicate the amplitude at peak voxels.

Size of Response Field of the Fingertips

Greater overlap in the fingertip representation in area 1 versus area 3b was a finding repeatedly observed in measures taken from the fMRI BOLD signal. We further determine whether the greater overlap of digit response in area 1 versus area 3b paralleled the differences in the size of the response fields of individual digits. Within ROIs as defined from a q(FDR) <0.05 threshold in areas 3b and 1, we calculated the BOLD response of each voxel (estimated from the regressor parameter of the GLM), normalized them to the peak voxel, and then plotted the normalized BOLD response as a function of the Euclidean distance away from the peak voxel (Figure 10). The plot of normalized BOLD responses for a single digit, D1 in this case, showed similar decreasing trends for both areas 3b (green dots) and 1 (blue diamonds) when the voxels were further away from the peak voxel for areas 3b and 1 (Figure 10A). The normalized BOLD response, used as a measure of the response field of a digit, in both areas 3b (green) and 1 (blue) fall off sharply over the first 3 mm away from the peak voxel within the D1 cluster, and continue to slowly fall off at even greater distances (Figure 10A). Of note was that the relationship between normalized BOLD response and the distance away from the peak voxel were similar for areas 3b (green circles) and 1 (blue diamonds), suggesting comparable response fields for the fingertips in areas 3b and 1.

Measures of normalized BOLD response as a function of the distance away from the peak voxel averaged for all the digits confirmed similarly sized response fields were present in areas 3b and 1 (Figure 10B). If a normalized BOLD response of 0.5 was used as a half max threshold level, then a response field of about 5 mm in width was observed for fingertip stimulation. In comparison to the plot for D1, the plot of all digits

was more scattered, suggesting a great variability across digits. For instance, around 4 mm distance from the peak voxel, there is an increase in the BOLD response in area 1 that corresponds to the distance (~4 mm) between distal finger pad cortical representations, likewise at approximately 7 mm from the peak voxel, there is an increase in the BOLD response in area 3b that corresponds to cortical digit response distance (~7 mm).

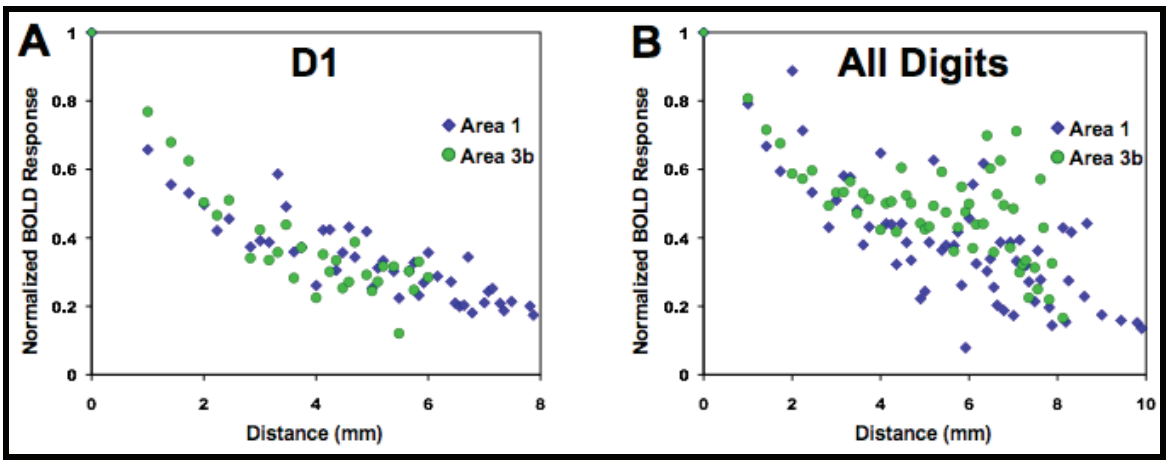

Figure 10. Digit response fields in areas 3b and 1. (***A***) The response field of D1 stimulation is displayed for areas 3b (green circles) and 1 (blue diamonds). The normalized BOLD signal response is plotted as a function of distance from the peak voxel. (***B***) The mean response field for all digits is displayed for areas 3b (green circles) and 1 (blue diamonds).

Discussion

Anthropoid primates have four distinct areas (3a, 3b, 1, and 2) within SI, each possessing their own body surface maps. Area 3b responds to cutaneous mechanoreceptors and is homologous to SI in other mammals, as it is the location for the first synapse of somatic sensation in the cortex. Area 1 also responds to cutaneous receptors and is considered to be an evolutionarily new area, associated with the expertise of hand use in higher order primates by integrating information from primary

somatosensory processing ((Krubitzer and Disbrow, 2008)). Both cortical areas receive somatotopically-organized projections from the ventral posterior nucleus of the thalamus (VP), with denser input into area 3b ((Nelson and Kaas, 1981)). Anatomical studies in areas 3b and 1 of both new and old world monkeys have revealed septa separating sensoria within area 3b, in particular individual digits ((Jain et al., 1998), (Jain et al., 2001), (Qi et al., 2008), (Qi and Kaas, 2004)). These septa provide clear divisions between digit representations in area 3b that are not present within area 1. Although the studies have never been performed, similar septa might be present in human area 3b cortex. This suggests that digit maps with finer detail can be found in area 3b and that restricted representations are not expected in area 1 of human cortex.

Tactile Responses in SI

We observed cortical responses to air puff stimulation of digits 1-4 in all four subdivisions of SI. All subjects showed response in areas 3b and 1, while responses in area 2 were less common, and only twice were responses detected in area 3a. Digit representations in areas 3b, 1, and 2 have been consistently reported in multiple fMRI studies ((Gelnar et al., 1998), (Maldjian et al., 1999), (Francis et al., 2000), (Krause et al., 2001), (Kurth et al., 2000), (Nelson and Chen, 2008)). While cortical responses were unexpected due to afferent inputs into area 3a, we are not the first to report rare observance of activation in area 3a in response to tactile stimulation ((Francis et al., 2000), (Krause et al., 2001), (Kurth et al., 2000)). The lack of consistent response in area 2 in contrast to other studies could be explained by the air puff stimulation versus a vibrotactile or electrical stimulus, which are commonly employed for such studies, that activates deep subdermal mechanoreceptors ((Nelson and Chen, 2008), (Kurth et al., 2000)).

In addition to the consistent activation clusters in areas 3b and 1, we also observed one common activation cluster regardless of the digit stimulated. In Figure 3 slice Z=76 (the second right column), a common cluster along the lateral posterior bank of the central sulcus was observed for all four digits (activation foci anterior and lateral to D2 activation indicated by light blue arrow). This finding is similar to the observation described by Nelson and Chen ((Nelson and Chen, 2008)), where they reported two observed regions of activity in area 1 which they defined as 1_s and 1_i, superior and inferior sub-divisions of area 1. In sub-region 1_s they detected clear topography of digits, while they detected a clustering of digit representation in sub-region 1_i without distinguishable digit topography. Based on the anatomical locations and the digit specific (and non-specific) responses of these sub-regions defined by Nelson and Chen, the sub-region 1_s likely corresponds with what we define as area 1, and sub-region 1_i likely corresponds with the cluster we observe at the lateral most part of area 3b.

Somatotopy and Cortical Magnification in Areas 3b and 1

For decades noninvasive imaging techniques have been used to try to confirm many of the nonhuman primate SI findings in human cortex. Many of the early neuroimaging studies lacked the spatial resolution to determine more than the medial to lateral representation of face, hand, and foot. Gelnar *et al* were the first to report the topographic organization of digits, D1 to D5, medial to lateral, that has now been repeated by a number studies ((Gelnar et al., 1998), (Maldjian et al., 1999), Gelnar 1998, (Stringer et al., 2010b)). The authors, however, did not observe separate maps for both areas 3b and 1. It was not until 2000 that Kurth and colleagues first observed clear and separable somatotopic maps of digit representations in both area 3b and 1, allowing the possibility to compare across SI subdivisions ((Kurth et al., 2000)). Overlap was

observed in both areas, with larger overlap seen in adjacent digits than nonadjacent digits, and greater overlap in area 1 than 3b. In a later study, the same group observed overlap in 7 out of 10 subjects in area 3b, yet all 10 subjects showed overlap in area 1. When comparing overlap by cortical volume, they found 23 % overlap in area 3b and 43 % in area 1 ((Krause et al., 2001)). While not all studies have investigated overlap directly, most have found larger digit separation in area 3b than area 1, suggesting varying degrees of overlap between subdivisions ((Ruben et al., 2006), (Nelson and Chen, 2008)). Slight discrepancies between studies exist, such as findings from anatomical studies showing a 27 % greater cortical volume in area 3b than 1((Geyer et al., 2000)), Overduin *et al* observed larger maps in area 1 than area 3b to a modest degree ((Overduin and Servos, 2004)).

Sensoria with a high degree of acuity are represented within a larger volume of cortex and have neurons with smaller receptive fields ((Chen et al., 2009)). In nonhuman primates the digit tips are especially sensitive and have greater cortical magnification than other parts of the body. In single electrode studies in owl monkeys the cortical magnification in the hand representation is approximately twice as large in area 3b as area 1. Within the digits, cortical magnification is greater moving from the proximal to the distal phalanges, and the difference in magnification between areas 3b and 1 is even more exaggerated at the distal finger pads ((Sur et al., 1980)). Intrinsic optical imaging experiments have shown that the cortical magnification in digit tip representation is 2.5 times greater in area 3b than area 1 in squirrel monkey SI ((Friedman et al., 2008)). In a previous study in humans, we found that the distance between cortical representations of adjacent digits was roughly 1.5 times larger in area 3b than area 1, in agreement with the cortical magnification in the owl and squirrel monkey ((Stringer et al., 2010b)).

We observed a more discrete digit map with a larger cortical span in area 3b than area 1. While some individual subjects in previous studies lacked overlap of digit representations in area 3b, the lack of overlap was not repeatable across subjects. Here, we not only show punctate digit maps in area 3b (Figure 1), we also demonstrate the lack of BOLD signal in individual voxels separating digit representations in area 3b (Figure 4: time course 6 and 8). The mean signal time course across subjects illustrates the digit selectivity in area 3b (Figure 7B).

Distinct Temporal Patterns of BOLD Signal in Areas 3b and 1

Although rare, we are not the first to report time course differences between areas 3b and 1. Krause *et al* report the mean BOLD signal time courses across subjects in area 3b and 1 ((Krause et al., 2001)). Their low intensity stimulus is most comparable to our saliently weak air puff stimulus. The maximum change in BOLD signal in response to low intensity innocuous electric shock is greater in area 1 than area 3b by approximately 0.3 %. We report that the maximum change in BOLD signal is approximately 4.5 % in area 1 and 3 % in area 3b, a difference of 1.5 %. The shape of the BOLD signal response over time is also strikingly different in areas 3b and 1. We observed an initial transient component with a later sustained component in area 1, while area 3b has a sustained response throughout the duration of the stimulus (Figure 7A). The shapes of the time courses presented by Krause *et al* are quite similar to our own. The BOLD signal response in area 3b is sustained throughout the duration of the stimulus, and in area 1 there is a modest initial transient component lasting for roughly the first 15 s of stimulus delivery followed by a sustained component. The similarities are evident between these sets of BOLD signal time courses.

One explanation for the temporal differences between areas 3b and 1 could be the response properties to different classes of receptors. Areas 3b and 1 both respond robustly to rapidly adapting (RA) cutaneous mechanoreceptors, but only area 3b has neurons with receptive field properties similar to neural input provided by the slowly adapting (SA) cutaneous mechanoreceptors. The initial transient component of the area 1 time course could reflect the response property differences between these areas. The neural response to such events, however, is on a much smaller time scale (< ms) than would be reflected in the slow hemodynamic response of the BOLD signal. The present study design makes it impossible to determine the origin to the time course differences; studies such as event-related design are better suited to evaluate temporal differences in BOLD signal response.

Response Fields in Area 3b and 1

Primate electrophysiological studies have found that the receptive fields are larger in area 1 than area 3b, where area 1 has receptive fields that respond to stimulation of the entire digit tip, area 3b typically show receptive areas smaller than the surface of the digit tip. Similar to the cortical magnification decreasing from distal to proximal phalanges, the receptive field size increases from tip to base ((Sur et al., 1980)). Studies from other species of primates have comparable findings and suggest overlap only in area 1 ((Costanzo and Gardner, 1980), (Iwamura, 1998), (Iwamura et al., 1993), (Iwamura et al., 1980)). Our data support the findings in nonhuman primates of smaller cortical magnification and greater overlap of representation in area 1. The somatotopic maps from area 3b show punctate representation of digit finger pads that have no overlap, while the maps from area 1 show a high degree of digit overlap (Figure 3). Moreover, the single voxel time courses in area 3b show areas of cortex in between digit representations that do not respond to stimulation of any digits (Figure 8: voxels time

courses 3, 6, and 8), whereas the time course from area 1 show robust overlap with no voxels that are unresponsive to digit stimulation (Figure 9). The time courses from individual voxels are a direct way of measuring signal in the cortex, negating the strategy of comparing overlap at various arbitrary statistical thresholds. Possible explanations other than the extent of the response fields are that the stimulus did not stimulate the full range or mechanoreceptors within the entire width of the distal finger pad, that the air-puff stimulus does not stimulate the full range of mechanoreceptors that have representations in area 3b, or that the differences are due to differing patterns of lateral inhibition in areas 3b and 1.

While the activation maps and time courses revealed differences in overlap, we did not see a difference in the size of the response fields between areas 3b and 1 (Figure 10). To determine the size of response fields, we calculated a normalized beta-value as our metric for response magnitude. The response amplitude was greater in area 1 than area 3b for all subjects, so comparing a normalized value could have mitigated the size of area 1's response. While invasive studies in nonhuman primates have the advantage of high spatial resolution, down to individual neurons, they are not appropriate for human experiments.

Conclusion

This study demonstrates that distinct systematic maps of digits can be constantly measured through fMRI in human SI cortex. We also provide evidence for the lack of overlap in digit responses in area 3b and significant overlap in area 1. Spatial activation maps and analysis of the BOLD signal in voxel neighboring the peak cortical representation of individual digits demonstrate the differences in overlap between these

areas. By calculating the digit response field in each area, we posit that the overlap is not due to a large response field in area 1, but rather due to the smaller size of cortex represented by area 1.

References

Allison, T., McCarthy, G., Wood, C.C., Darcey, T.M., Spencer, D.D., Williamson, P.D., 1989a. Human cortical potentials evoked by stimulation of the median nerve. I. Cytoarchitectonic areas generating short-latency activity. J Neurophysiol 62, 694-710.

Allison, T., McCarthy, G., Wood, C.C., Williamson, P.D., Spencer, D.D., 1989b. Human cortical potentials evoked by stimulation of the median nerve. II. Cytoarchitectonic areas generating long-latency activity. J Neurophysiol 62, 711-722.

Allison, T., Wood, C.C., McCarthy, G., Spencer, D.D., 1991. Cortical somatosensory evoked potentials. II. Effects of excision of somatosensory or motor cortex in humans and monkeys. J Neurophysiol 66, 64-82.

Blackford, J., 2002. Multivariate Permutation Testing for Paired t-Tests. Vanderbilt Kennedy Center for Research in Human Development, Nashville, TN.

Blankenburg, F., Ruben, J., Meyer, R., Schwiemann, J., Villringer, A., 2003. Evidence for a rostral-to-caudal somatotopic organization in human primary somatosensory cortex with mirror-reversal in areas 3b and 1. Cereb Cortex 13, 987-993.

Brodmann, K., 1909. VergleichendeLocalisationslehre der Gro Hhirnrinde. Barth, Leipzig.

Cannestra, A.F., Black, K.L., Martin, N.A., Cloughesy, T., Burton, J.S., Rubinstein, E., Woods, R.P., Toga, A.W., 1998. Topographical and temporal specificity of human intraoperative optical intrinsic signals. Neuroreport 9, 2557-2563.

Chen, L.M., Friedman, R.M., Roe, A.W., 2009. Area-specific representation of mechanical nociceptive stimuli within SI cortex of squirrel monkeys. Pain 141, 258-268.

Costanzo, R.M., Gardner, E.P., 1980. A quantitative analysis of responses of direction-sensitive neurons in somatosensory cortex of awake monkeys. J Neurophysiol 43, 1319-1341.

Fox, P.T., Burton, H., Raichle, M.E., 1987. Mapping human somatosensory cortex with positron emission tomography. J Neurosurg 67, 34-43.

Francis, S.T., Kelly, E.F., Bowtell, R., Dunseath, W.J., Folger, S.E., McGlone, F., 2000. fMRI of the responses to vibratory stimulation of digit tips. Neuroimage 11, 188-202.

Friedman, R.M., Chen, L.M., Roe, A.W., 2008. Responses of areas 3b and 1 in anesthetized squirrel monkeys to single- and dual-site stimulation of the digits. J Neurophysiol 100, 3185-3196.

Gelnar, P.A., Krauss, B.R., Szeverenyi, N.M., Apkarian, A.V., 1998. Fingertip representation in the human somatosensory cortex: an fMRI study. Neuroimage 7, 261-283.

Geyer, S., Schormann, T., Mohlberg, H., Zilles, K., 2000. Areas 3a, 3b, and 1 of human primary somatosensory cortex. Part 2. Spatial normalization to standard anatomical space. Neuroimage 11, 684-696.

Grefkes, C., Geyer, S., Schormann, T., Roland, P., Zilles, K., 2001. Human somatosensory area 2: observer-independent cytoarchitectonic mapping, interindividual variability, and population map. Neuroimage 14, 617-631.

Hansson, T., Brismar, T., 1999. Tactile stimulation of the hand causes bilateral cortical activation: a functional magnetic resonance study in humans. Neurosci Lett 271, 29-32.

Iwamura, Y., 1998. Hierarchical somatosensory processing. Curr Opin Neurobiol 8, 522-528.

Iwamura, Y., Tanaka, M., Hikosaka, O., 1980. Overlapping representation of fingers in the somatosensory cortex (area 2) of the conscious monkey. Brain Res 197, 516-520.

Iwamura, Y., Tanaka, M., Sakamoto, M., Hikosaka, O., 1985a. Diversity in receptive field properties of vertical neuronal arrays in the crown of the postcentral gyrus of the conscious monkey. Exp Brain Res 58, 400-411.

Iwamura, Y., Tanaka, M., Sakamoto, M., Hikosaka, O., 1985b. Vertical neuronal arrays in the postcentral gyrus signaling active touch: a receptive field study in the conscious monkey. Exp Brain Res 58, 412-420.

Iwamura, Y., Tanaka, M., Sakamoto, M., Hikosaka, O., 1993. Rostrocaudal gradients in the neuronal receptive field complexity in the finger region of the alert monkey's postcentral gyrus. Exp Brain Res 92, 360-368.

Jain, N., Catania, K.C., Kaas, J.H., 1998. A histologically visible representation of the fingers and palm in primate area 3b and its immutability following long-term deafferentations. Cereb Cortex 8, 227-236.

Jain, N., Qi, H.X., Catania, K.C., Kaas, J.H., 2001. Anatomic correlates of the face and oral cavity representations in the somatosensory cortical area 3b of monkeys. J Comp Neurol 429, 455-468.

Jezzard, P., Balaban, R.S., 1995. Correction for geometric distortion in echo planar images from B0 field variations. Magn Reson Med 34, 65-73.

Karniski, W., Blair, R.C., Snider, A.D., 1994. An exact statistical method for comparing topographic maps, with any number of subjects and electrodes. Brain Topogr 6, 203-210.

Krause, T., Kurth, R., Ruben, J., Schwiemann, J., Villringer, K., Deuchert, M., Moosmann, M., Brandt, S., Wolf, K., Curio, G., Villringer, A., 2001. Representational overlap of adjacent fingers in multiple areas of human primary somatosensory cortex depends on electrical stimulus intensity: an fMRI study. Brain Res 899, 36-46.

Krubitzer, L., Disbrow, E., 2008. The Evolution of Parietal Areas Involved in Hand Use in Primates. In: Gardner, E., Kaas, J. (Eds.), The Senses: A Comprehensive Reference. Academic Press, San Diego, pp. 183-214.

Kurth, R., Villringer, K., Curio, G., Wolf, K.J., Krause, T., Repenthin, J., Schwiemann, J., Deuchert, M., Villringer, A., 2000. fMRI shows multiple somatotopic digit representations in human primary somatosensory cortex. Neuroreport 11, 1487-1491.

Kurth, R., Villringer, K., Mackert, B.M., Schwiemann, J., Braun, J., Curio, G., Villringer, A., Wolf, K.J., 1998. fMRI assessment of somatotopy in human Brodmann area 3b by electrical finger stimulation. Neuroreport 9, 207-212.

Maldjian, J.A., Gottschalk, A., Patel, R.S., Detre, J.A., Alsop, D.C., 1999. The sensory somatotopic map of the human hand demonstrated at 4 Tesla. Neuroimage 10, 55-62.

Moore, C.I., Stern, C.E., Corkin, S., Fischl, B., Gray, A.C., Rosen, B.R., Dale, A.M., 2000. Segregation of somatosensory activation in the human rolandic cortex using fMRI. J Neurophysiol 84, 558-569.

Nelson, A.J., Chen, R., 2008. Digit somatotopy within cortical areas of the postcentral gyrus in humans. Cereb Cortex 18, 2341-2351.

Nelson, R.J., Kaas, J.H., 1981. Connections of the ventroposterior nucleus of the thalamus with the body surface representations in cortical areas 3b and 1 of the cynomolgus macaque, (Macaca fascicularis). J Comp Neurol 199, 29-64.

Overduin, S.A., Servos, P., 2004. Distributed digit somatotopy in primary somatosensory cortex. Neuroimage 23, 462-472.

Qi, H., Preuss, T., Kaas, J., 2008. Somatosensation. The Senses: A Comprehensive Reference 6, 143-170.

Qi, H.X., Kaas, J.H., 2004. Myelin stains reveal an anatomical framework for the representation of the digits in somatosensory area 3b of macaque monkeys. J Comp Neurol 477, 172-187.

Ruben, J., Krause, T., Taskin, B., Blankenburg, F., Moosmann, M., Villringer, A., 2006. Sub-area-specific Suppressive Interaction in the BOLD responses to simultaneous finger stimulation in human primary somatosensory cortex: evidence for increasing rostral-to-caudal convergence. Cereb Cortex 16, 819-826.

Salomon, R.M., Kennedy, J.S., Johnson, B.W., Urbano Blackford, J., Schmidt, D.E., Kwentus, J., Gwirtsman, H.E., Gouda, J.F., Shiavi, R.G., 2005. Treatment enhances ultradian rhythms of CSF monoamine metabolites in patients with major depressive episodes. Neuropsychopharmacology 30, 2082-2091.

Sanchez-Panchuelo, R.M., Francis, S., Bowtell, R., Schluppeck, D., 2010. Mapping human somatosensory cortex in individual subjects with 7T functional MRI. J Neurophysiol 103, 2544-2556.

Schweizer, R., Voit, D., Frahm, J., 2008. Finger representations in human primary somatosensory cortex as revealed by high-resolution functional MRI of tactile stimulation. Neuroimage 42, 28-35.

Stringer, E., Chen, L., Friedman, R., Gatenby, J., Gore, J., 2010a. The ability of fMRI at 7T to detect functional differences between areas 1 and 3b of primary somatosensory cortex. In: Processdings of the 19th Annual Meeting of ISMRM, Stockholm, Sweden. Abstract #3470.

Stringer, E.A., Chen, L.M., Friedman, R.M., Gatenby, C., Gore, J.C., 2010b. Differentiation of somatosensory cortices by high-resolution fMRI at 7T. Neuroimage.

Sur, M., Merzenich, M.M., Kaas, J.H., 1980. Magnification, receptive-field area, and "hypercolumn" size in areas 3b and 1 of somatosensory cortex in owl monkeys. J Neurophysiol 44, 295-311.

Vogt, C., Vogt, O., 1919. Allgemeiner Ergebnisse unserer Hinforschung. Journal Psychology and Neurology 25, 279-462.

Weibull, A., Bjorkman, A., Hall, H., Rosen, B., Lundborg, G., Svensson, J., 2008. Optimizing the mapping of finger areas in primary somatosensory cortex using functional MRI. Magn Reson Imaging 26, 1342-1351.

White, L.E., Andrews, T.J., Hulette, C., Richards, A., Groelle, M., Paydarfar, J., Purves, D., 1997. Structure of the human sensorimotor system .1. Morphology and cytoarchitecture of the central sulcus. Cerebral Cortex 7, 18-30.

Woolsey, C.N., Erickson, T.C., Gilson, W.E., 1979. Localization in somatic sensory and motor areas of human cerebral cortex as determined by direct recording of evoked potentials and electrical stimulation. J Neurosurg 51, 476-506.

CHAPTER IV

IDENTIFICATION AND MODULATION OF RESTING STATE FUNCTIONAL CONNECTIVITY IN THE LATERAL PAIN NETWORK

Abstract

There are a myriad of methodologies in neuroscience available to investigate the central and peripheral nervous system at different spatial and temporal scales, from single synapses in a pyramidal neuron to functional imaging methods that map regional responses of cortex to a specific stimulus. Functional connectivity between regions can be obtained by suitable fMRI techniques that attempt to map and measure the relationships between individual regions within neural circuits on a systems level. One approach to measuring functional connectivity uses “resting state” acquisitions (rs-fc) that examine these circuits in the absence of specific stimulation, and thus provide insight into the basal state of the human brain. Using an rs-fc analysis we explore the lateral (sensory) pain network and how multiple areas of cortex related to pain processing work together as a system. We have identified activation clusters within subdivisions of postcentral gyrus (SI) and along the lateral sulcus (parietal operculum and insular cortex) that are responsive to intensity estimation of pain, both contralateral and ispilateral to a thermal noxious stimulus. From these regions of interest, we measured the rs-fc, or interregional correlation coefficients of low frequency BOLD signal fluctuations, and found that these correlations are positive, significant, and invariant before the perception of pain by the thermal stimulus. We also investigated whether these inter-areal correlations were modulated by the perception of pain at multiple time points, by comparing the functional connectivity within the defined pain network before

the pain stimulus, directly after the pain stimulus (40 s after the last pain stimulus offset), approximately five minutes following pain stimulus offset, and approximately eight and a half minutes following pain stimulus offset. The inter-areal correlations in BOLD signals (fc) changed significantly and dynamically following the perception of pain. The painful experience generally reduced the strength of the inter-areal fc within regions of the lateral pain network. Measuring rs-fc provides a tool for evaluating intrinsic neural networks in different neural states such as before and after sensory perception or between healthy and disease populations. Moreover, the functional networks involved show temporal dynamic changes that may indicate secondary aspects of the response to pain.

Introduction

Most functional magnetic resonance imaging (fMRI) studies rely on a task or stimulation paradigm for detecting regions of neural activity that are engaged in task-specific performance or response to specific stimuli. On the other hand, so-called "resting state" methods do not involve a task but record signals over time without extrinsic stimuli and may be used to assess functional connectivity between regions. Functional connectivity can be evaluated by measuring the correlations in spontaneous fluctuations of BOLD signals from different regions across the brain. While many neuroimaging studies use MRI to examine the anatomy and function of individual regions of cortex, functional connectivity measurements provide a systems level evaluation of the integration of individual regions within an intrinsic neural network. Resting state functional connectivity acquisitions and analyses (rs-fc) by MRI provide information about innate neural circuitry within the basal state of an individual's brain.

Little is known about the state of intrinsic neural networks of those suffering from chronic pain, despite the hypothesis that pain perception is processed in the brain, integrating sensory, affective, and cognitive networks. Like the majority of fMRI studies, most pain and imaging studies have relied on specific task designs to detect regions within the brain that are active under specific conditions. Acute pain, however, is not a good model for chronic pain. In addition, chronic pain is not a task condition that can be turned on and off, but rather a steady state (or long time constant) process, so functional connectivity analyses in a resting state could provide useful and objective information on how underlying pain networks are altered in chronic pain patients. Functional connectivity analyses have been implemented previously for the study of how diseases and disorders affect the visual, language, motor, and working memory circuits, with the general finding that functional connectivity in patient populations is altered ((Rogers et al., 2007)). For example, patients with autism spectrum disorder have a disrupted social and emotional network, but their attentional and goal-directed cognitive network does not differ from normal subjects ((Kennedy and Courchesne, 2008)). This offers promise for the study of chronic pain because autism spectrum disorder, like chronic pain, has a large heterogeneity within its patient population.

Multiple functional connectivity studies of various brain circuits have been carried out in chronic pain patients. Patients with lower back pain and neuropathic pain show reduced functional connectivity in distributed corticocortical and thalamocortical networks compared to controls, as well as opiate prescription-dependent patients ((Baliki et al., 2008), (Cauda et al., 2010), (Tagliazucchi et al., 2010), (Upadhyay et al., 2010)). Fibromyalgia patients demonstrated increased functional connectivity versus controls, and the strength of the connectivity was proportional to the degree of spontaneous pain experience during the scan time ((Napadow et al., 2010)). Other studies are less clear, such as in cluster headache patients whose functional connectivity compared to controls

both increased and decreased depending on the network examined and the analysis method implemented ((Rocca et al., 2010)). While these studies have explored the functional connectivity within various neural networks (i.e. affective, attentional, and default mode), none have evaluated functional connectivity within the pain network.

The aim of this study was to measure the functional connectivity in the resting state between focal areas that were activated in a pain task in a healthy population. We also assessed whether this intrinsic pain network was constant or modulated over time, and assessed its dynamical properties by repeating measurement of connectivity before and after a painful experience. A hallmark of pain is a high degree of variability of across subjects, so we assessed each subject individually.

Methods

Stimulation Protocol

Four healthy, right-handed male human subjects gave informed consented for this study in accordance with a protocol approved by the Vanderbilt University Institutional Review Board. All experimentation was performed in a single session with a pre-testing component and an imaging component. Pre-testing was implemented to introduce subjects to the thermal stimulus and to determine the subjects' thermal thresholds used in the imaging session. A Medoc Pathway Pain and Sensory Evaluation System was used to drive an MR-compatible Medoc CHEPS (Contact Heat-Evoked Potential Stimulator) probe, measuring 27 mm in diameter, which was fixed with medical tape to digits (D) 2 and 3 of the left hand of each subject (Medoc Ltd. Ramat Yishai, Israel).

To introduce subjects to the thermal heat sensation produced by the CHEPS probe, a baseline temperature of 35 °C was delivered for 10 s followed by a slow ramp

of 0.1 °C/s for 30 s to the innocuous target temperature 38 °C. Once the target temperature was reached a fast ramp down of 40 °C/s back to baseline (35 °C) was executed. After each testing stimulus was delivered, the subject was asked to rate his peak pain sensation (not the temperature of the stimulus) on a scale of 0 to 10, with 0 corresponding to no sensation of pain and 10 corresponding to strongest imaginable sensation of pain. The first stimulus was followed by a stimulus with a 42 °C target temperature. The probe delivered a 10 s 35 °C baseline followed by a fast ramp of 70 °C/s to 39 C (3 °C below the target temperature). A slow ramp of 0.1 °C/s was employed to reach the target temperature (42 °C), followed by a fast ramp of 40 °C/s back to the 35 °C baseline, resulting in a 30 s noxious thermal pain stimulus. This trapezoidal-shaped thermal pain stimulus was modeled after Hashmi and Davis's dynamic heat pain stimulus in order to more linearly integrate the inputs from Aδ and C fibers ((Hashmi and Davis, 2008)). After the delivery of the thermal pain stimulus, the subject was then asked to rate his peak pain sensation. This procedure was repeated with the target temperature adjusted for each new stimulus until the subject rated the stimulus as a 5/6 and a 7/8 on the 10-point pain scale. These target temperatures were then used for each individual subject in their imaging session.

The stimulus paradigm during the imaging session was implemented in a 30-s "on" and 30-s "off" block design. Two blocks each of three different thermal temperatures were delivered sequentially, resulting in six thermal heat blocks. The protocol consisted of two warm blocks (38 °C), two moderate pain blocks (5/6 on a 10-point pain scale; ~ 46 °C), and two high pain (7/8 on a 10-point pain scale; ~ 47 °C) (Figure 1: pink trace). The four pain blocks were delivered in a trapezoidal temperature waveform as described above. As in the preimaging session, the CHEPS probe was attached to D2 and D3 of the subject's left hand, and an MR filter was connected at the base of the probe near the

Pathway System to decrease the scanner noise interfering with the maintenance of the precisely targeted probe temperature.

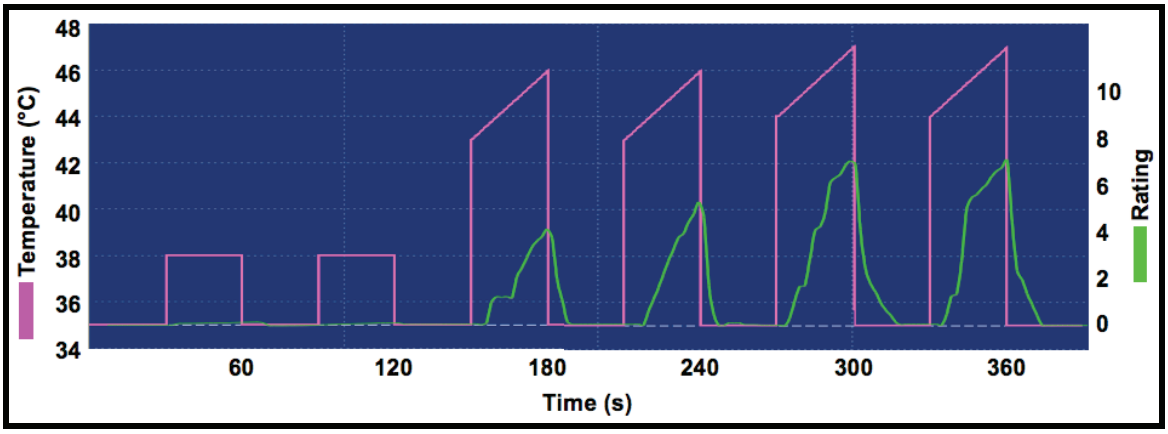

Figure 1. Stimulus protocol and subject rating. The thermal stimulus protocol (pink trace) comprised two blocks each of a warm (38°C), moderately painful (5/6 on 10-point pain scale), and highly painful (7/8 on 10-point pain scale). The painful stimuli were trapezoidal in shape in order to more linearly elicit Aδ and C afferent fibers. The VAS (0 to 10) pain rating from a sample subject in response to the delivery of thermal stimulation is illustrated by the green trace.

Subject's Pain Rating

Subjects were directed to rate their level of pain sensation continuously during the pain runs of the imaging session. The rating device, consisting of a mouse shell fixed to a vertical metal rod with a potentiometer, was strapped around the subject's hips and place on the subject's right thigh so that his right hand lay ergonomically atop the mouse. A LabVIEW programming environment (LabVIEW 2008) was developed to read the voltage output and translate it into a spatial position along a visual analogue scale (VAS) oriented vertically. The subject received real-time feedback of the VAS via an MR compatible projector system. The scale flanked by end markers of "No Sensation of Pain" corresponding to a rating of 0 on a 10-point pain scale and "Strongest Imaginable Sensation of Pain" corresponding to a rating of 10 on a 10-point pain scale. The subject slid the mouse along the potentiometer rod to match his precise pain sensation in real-

time. The temporal variability in subjective pain perception has been well established ((Torebjork, 1985), (Price et al., 1977)), thus for quality assurance the subject was also prompted at the end of each run to rate, on a scale of 0 to 10, the most intense pain sensation perceived during that run. If there was a significant change to the perception of the target temperatures determined in the pre-imaging session, the temperatures were modified accordingly. For example, if the subject indicated that his pain sensation had reached a rating of 9, the target temperatures were slightly decreased, or if the subject rated the most intense pain sensation a 4, the target temperatures were slightly increased based on the ratings acquired during the pre-scanning session.

MRI Data Acquisition

Subjects were scanned on a 7-T Philips Achieva magnet with a 16-channel NOVA head coil. Structural images were collected using a three-dimensional fast field echo (3D-FFE) sequence, TR/TE/TI = 3.7/1.8/1300 ms, with a 1x1x1 mm^3 voxel resolution. Functional images were acquired using a gradient-echo echo-planar imaging (GE-EPI) sequence, TR/TE = 2000/25 ms, flip angle = 80°, and a 192 x 192 field of view (FOV), with a voxel resolution of 1x1x2 mm^3. Sixteen oblique coronal slices (0 mm gap thickness) were acquired centered over the central sulcus (CS) and covering cortical regions: primary somatosensory cortex (SI) region, posterior part of the lateral sulcus, and thalamus. A SENSE acceleration factor of 3, and volume selective 2^{nd} or 3^{rd} order shimming using a pencil-beam method were employed. All EPI images were corrected for distortion using a B_0 field-map obtained at the start of scanning using two gradient echo scans (Jezzard and Balaban, 1995).

Five or six functional runs were acquired per subject, three during the resting state (rs: -Run 1, -Run 2, and -Run 3) and two to three during the thermal stimulation protocol (Pain-Run 1, Pain-Run 2, and/or Pain-Run 3). Following the acquisition of

reference, T1-weighted structural, and B_0 scans, the functional runs were acquired beginning with the first resting state run, rs-Run 1, acquired in 195 volumes (390 s). Rs-Run 1 was followed by Pain-Run 1 (195 volumes) and Pain-Run 2 (and Pain-Run 3 in Subject 1). The last Pain run was collected in 295 volumes (590 s), with the pain stimulation protocol for the first 195 volumes (Pain-Run 2 (or 3), and the last 100 volumes were acquired as resting state data, rs-Run 2. This run was followed by the last functional run, rs-Run 3 in 195 volumes. During the resting state runs, subjects were instructed to lay still with their eyes closed and remain in a neutral affective and cognitive state.

There is an augmentation of physiological effects at higher MR-fields, so the respiratory and cardiac cycles were monitored and recorded during the entire imaging session ((Triantafyllou et al., 2005)). A respiratory bellow was strapped around the subject's chest in a taut manner so as to not restrict the subject's breathing, and a pulse oximeter was clamped to the subject's left thumb. The monitoring devices were connected to the scanner, and the physiological data were recorded.

fMRI Data Analysis

The pre-processing and imaging analysis was implemented in Matlab, SPM5, AFNI, and BrainVoyager QX but differed between the resting state and stimulus driven runs. For the stimulus driven runs, pre-processing included slice scan time correction using a cubic spline, motion correction in three dimensions, slice alignment using an intra-session registration, and temporal filter using a 7-mHz high-pass filter and linear trend removal.

For the resting state runs, similar to the stimulus driven runs, slice scan time correction using a cubic spline, motion correction in three dimensions, and slice alignment using an intra-session registration were implemented. The physiological

effects were regressed out of the functional imaging data using RETROICOR ((Glover et al., 2000)), this negated the need to regress out the global time course which dampens correlation coefficients in correlated regions of functional connectivity analysis, yet is common practice in resting state functional connectivity analysis. A temporal filter was applied using a 0.01-0.1-Hz temporal band-pass filter.

The functional images were interpolated into 1x1x1-mm^3 voxels for visualization. To preserve the high spatial resolution, spatial smoothing of the functional images was not applied, and warping into stereotactic space was not performed on any of the data. All analysis was performed on the individual subject level. Two general linear models (GLM) were fitted to the data and t-maps were created. The first GLM fitted to the data was based on the convolution of the hemodynamic response function (HRF, in BrainVoyager the default is a two-gamma function that models the initial undershoot) with temperature blocks in the thermal stimulation protocol. Multiple contrast maps, e.g. (Warm+ModeratePain+HighPain)–Rest, (ModeratePain+HighPain)–Rest, (ModeratePain+HighPain)–Warm, and HighPain–Warm, were examined. The second GLM was based on the subject specific pain rating. The subjects' ratings were decimated in Matlab into 2-s interval time course, matching the 2-s TR of the EPI. The time course of the subject's rating was uploaded into BrainVoyager and applied as the regressor in the GLM analysis. Activation maps were created by using the pain ratings as the regressor.

Defining Regions of Interest

Regions of interest (ROIs) for the functional connectivity analysis were defined based on the rating activation maps. An adaptive threshold was employed due to the high degree of variability in BOLD activation magnitude across subjects and between hemispheres in a single subject ((Zhang et al., 2008)). The peak voxels (highest t-value)

in both contralateral and ipsilateral SI were identified, and a p-value threshold corresponding to approximately 50 % of the peak t-value was applied to the appropriate hemisphere. The adaptive p-value threshold was always greater than p (uncorr) < 0.05, and a cluster minimum was set to 4 voxels. Bilateral regions of interest (ROIs) within SI and along the lateral sulcus were defined. The BOLD signal time course was extracted from each ROI and was investigated to ensure that the temporal dynamics of the BOLD pattern reflected the subject's rating (Figure 2). ROIs that did not reflect the increases in noxious temperature or pain intensity sensation were not included, i.e. noisy ROIs with random fluctuations in BOLD signal were not used in the functional connectivity analysis.

Identification of SI and Lateral Sulcus Subdivisions

SI cortex can be divided into four distinct cytoarchitectural regions, Brodmann Areas 3a, 3b, 1, and 2 ((Brodmann, 1909), (Vogt and Vogt, 1919)). The location of the SI hand region is identified by the omega-shaped folding (visible in the axial plane) of the postcentral gyrus ((Moore et al., 2000), (White et al., 1997)). We used the operational definitions described by Geyer at al to delineate the boundaries between subregions within SI (Geyer et al., 2000). Area 3a is located within the fundus of the CS, area 3b is located along the posterior bank of the CS, area 1 is located at the crest of the postcentral gyrus, and area 2 is located on the anterior bank of the postcentral sulcus (medial) (Geyer et al., 2000; Krause et al., 2001; Kurth et al., 2000; Nelson and Chen, 2008).

The Sylvian Fissure, or lateral sulcus, is the sulcus that divides the parietal, temporal, and insular lobes. The parietal operculum (OP) lies along the upper bank of the lateral sulcus, the temporal operculum lies along the lower bank of the lateral sulcus, and the insular cortex lies deep within the fold of the lateral sulcus, hidden by the opercula. Cytoarchitecturally OP can be subdivided onto four areas, OP1, OP2, OP3,

and OP4 ((Eickhoff et al., 2006a), (Eickhoff et al., 2006b)). Each of these areas is a homologue to well-characterized areas within nonhuman primates: OP1 corresponds to secondary somatosensory cortex (SII), OP2 corresponds to parietoinsular vestibular cortex, OP3 corresponds to ventral somatosensory area, and OP4 corresponds to parietal ventral area. Eickhoff and colleagues derived brain templates and probability maps correlating these cytoarchitectural subdivisions within OP with MR structural images. We used these templates and maps as a guide to structurally classify functional activations along the lateral sulcus. Due to our restricted imaging volume, all activations within the insular cortex could be classified as posterior insular cortex.

Resting State Correlations

The BOLD signal time courses from the resting state runs, rs-Run 1-3, were extracted from the voxels within each defined ROI, and were segmented into lengths of 190 s (corresponding to 95 functional volumes) for further evaluation. Specifically, rs-Run 1 and rs-Run 3 were divided into two segments, using the first 95 volumes (RS0 and RS3) and last 95 volumes (RS1 and RS4), and for rs-Run 2 using the last 95 volumes (RS2) for all further evaluations, in order to mitigate any systematic errors from comparing across time courses of varying lengths. In a given time segment (e.g. RS0), the correlations between the ROI time courses were calculated using the Pearson's correlation coefficient, implemented in Matlab and recorded as a matrix. We created histograms to illustrate the distribution of correlation coefficients for each time segment. We transformed the R-values into Z-scores (mean=0, standard deviation=1) to compare the rs-fc across time segments (e.g. RS1-RS2, before pain and directly after pain).

We compared the rs-fc, within the neural network that we defined from the pain perception activations, across multiple time points. To test the stability of the rs-fc we compared the significance of R-matrices and difference between Z-scores from the first

and last 95 volumes of rs-Run 1 (RS0 and RS1, respectively). We next calculated the difference between the Z-scores from RS1 before pain and subsequent post-pain time points RS2, RS3, and RS4 (i.e. RS1-RS2, RS1-RS3, and RS1-RS4, respectively). For R- and Z-matrices, we also calculated the p-value corresponding to each matrix element. We present only significant ($p < 0.5$) R- and Z-values.

Results

Pain Activation Maps

For each subject, activation maps were created using a standard boxcar convolution with the HRF based on the pain stimulation protocol. From the contrasts, (PainHigh+PainModerate+Warm) – Rest, (PainHigh+PainModerate) – Warm, and others, we observed minimal activation throughout the imaging volume at q (FDR) < 0.05 (maps not shown). We lowered the statistical threshold to p (uncorrected) < 0.05, with little change in the amount of activation observed. Of the ROIs that were detected, the BOLD signal time course was evaluated, and none mimicked the thermal stimulus design.

We next used the individual subject ratings as regressors in the single subject analysis. All subjects revealed robust activation throughout the imaging volume, particularly in multiple areas along the postcentral gyrus, along the lateral sulcus, in the posterior cingulate, and within the thalamus. It is important to note that the imaging volume was acquired in a 32-mm oblique coronal slab, in a diagonal over SI and thalamus, and does not provide full brain coverage.

The rating regression maps were thresholded at q (FDR) < 0.001 to reveal focal activation in varying regions of SI, 4 voxel minimum cluster threshold. In contralateral cortex response to the painful stimulus were observed in areas 3a, 3b, 1, and 2 in four,

four, four, and two out of the four subjects. In ipsilateral cortex response to the painful stimulus were observed in areas 3a, 3b, 1, and 2 in three, four, four, and two out of the four subjects.

In Subject 2 contralateral activations were observed focally in areas 3b, 1, and 2 (Figure 2A). The activation clusters in area 1 (indicated by the blue circle labeled 1) and area 2 (indicated by the blue circle labeled 2) were located at the crest of the postcentral gyrus near the area 1/area 3b border and at the lateral anterior bank of postcentral sulcus, respectively. The activation in cluster in area 3b (indicated by the blue circle 3) was located inferior to the area 1 and 2 at the posterior bank of the central sulcus. The activations in the contralateral cortex were focal and punctate. The BOLD signal time course for a single run showed robust response to the high pain stimulus, with little response to the warm and moderate pain stimuli (Figure 2A 1-3a). The response in area 3b has an initial response to the warm stimulus that declines halfway through the stimulus duration and the response to the moderate pain stimulus is robust but smaller in magnitude than the high pain. The mean time course across the two pain runs for this subject highlight the differential response to the different temperatures (Figure 2A 1-3b).

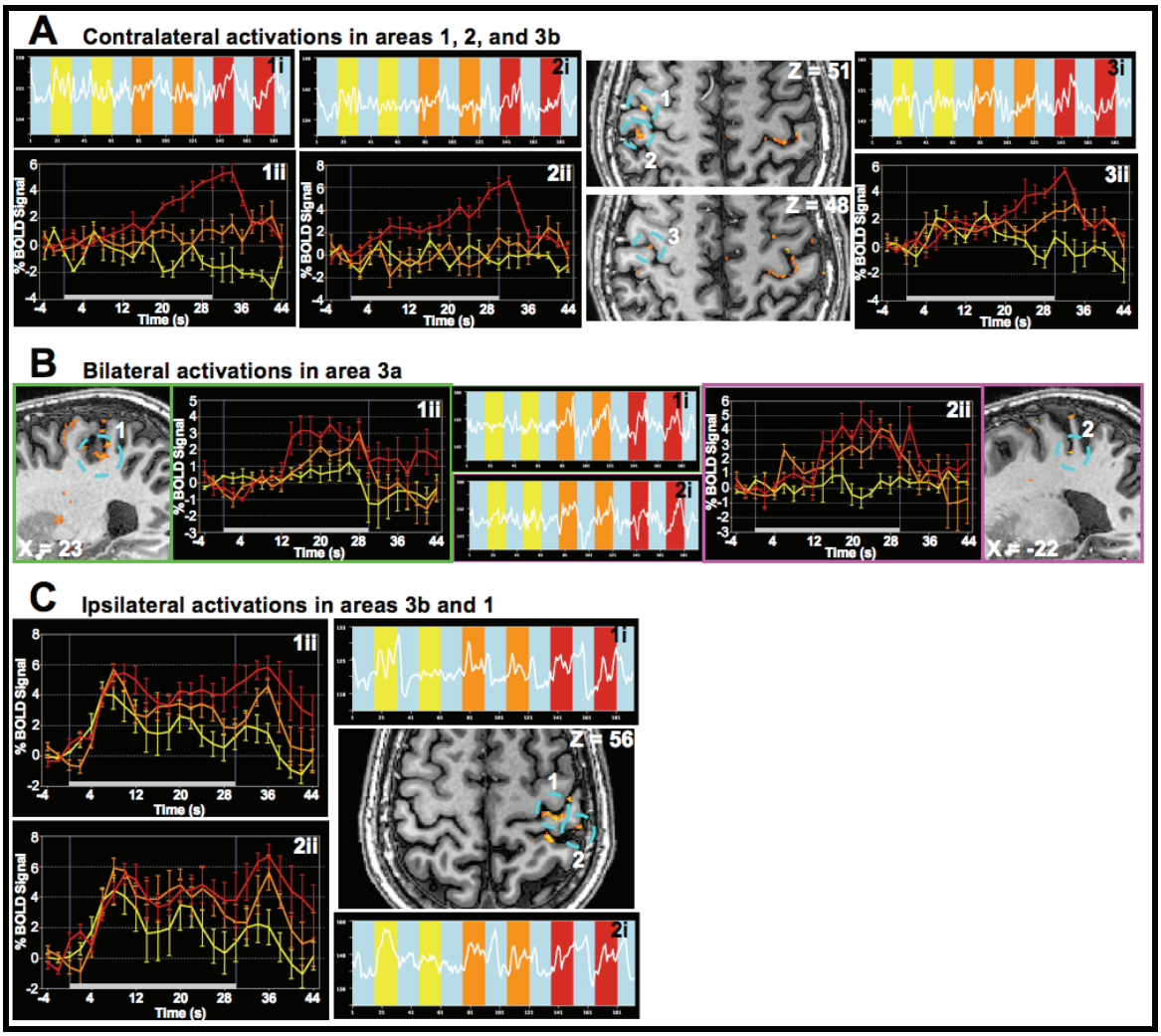

Figure 2. Activation maps and BOLD signal time courses in response to thermal stimulation. Pain activation maps (using pain rating as regressor, adaptive threshold with cluster minimum of 4 voxels) and BOLD signal time courses of activations within the postcentral gyrus. The time courses depict the BOLD signal during each of the stimuli (warm yellow, pain orange, and tolerance red) for a single run (***i***), and for the mean across blocks and runs, with the vertical bars indicating the duration of the 30s stimuli (***ii***). (***A***) The activity map for Subject 1 is overlaid on anatomical images in the axial plane; Z=51 corresponds to 51 mm superior to anterior commissure. Activations were observed in areas 1 (***1***), 2 (***2***), and 3b (***3***). A single run time course for each ROI is displayed (***i***), as well as the mean time course (***ii***). Areas 1 and 2 were selective for the tolerance temperature (***1ii*** and ***2ii***), whereas area 3b responded in graded pattern to the pain and tolerance stimuli. (***B***) Contra (***1***) and ipsilateral (***2***) activations in area 3a of Subject 3 are overlaid on anatomical images in the sagittal plane; X=23 corresponds to 23 mm right of the anterior commissure. Both ROIs responded in a graded pattern to the pain and tolerance stimuli (***1ii*** and ***2ii***). (***C***) Activations were observed in ipsilateral SI areas 3b (***1***) and 1 (***2***) for Subject 2. Both areas responded in a graded pattern to the three temperature stimuli (***1ii*** and ***2ii***).

Subject 3 showed robust response to the thermal stimuli in bilateral area 3a (Figure 2B). The activations were localized deep within the central sulcus, focal restricted to the grey matter, and more posterior. The time courses from the single runs show a robust response to both pain stimuli (Figure 2B 1-2a). The mean BOLD signal time course across runs shows a differential, graded response to the three temperatures contralaterally and a graded response to the pain temperatures ipsilaterally, with no response to the warm stimulus. There was also a significant delay in signal onset in contralateral 3a for all the temperatures, approximately 12 s after the stimulus onset, this was not seen ipsilaterally. Both subjects 2 and 3 showed an almost triangular, gradual increase in BOLD signal throughout the duration of the stimulus. The amplitude was not sustained throughout the duration of the stimulus, increasing during the duration of the stimulus.

Subject 1 showed robust activation in response to pain in the ispilateral cortex, and minimal cortical respone to pain in the contralateral hemisphere. For all subjects, the voxels with the highest t-value were detected in the ipsilateral cortex, yet not all had such little response contralateral to stimulation. There was diffuse response in area 3b, while the activation was focal, and restricted to the grey matter in area 3b, the activation was not punctate and extended throughout a large extent of area 3b (Figure 2C). Area 1 response was more focal and punctate. The time courses in the single run show a robust response to all temperatures with a more sustained response than the other two subjects (Figure 2C 1a-2a). The mean signal across the three pain runs showed a graded response to the three stimuli. The high pain stimulus is sustained through the stimulus duration. The moderate pain was less sustained and dropped off slightly throughout the duration of the stimulus, but with an increase in BOLD signal at the stimulus offset. The warm stimulus had the weakest response that waned over the duration of the stimulus.

While each subject showed a robust response to pain in the defined ROIs, each responded uniquely to the stimulation protocol. Each area either preferentially responded to pain over warm stimuli, or responded more robustly to pain than to warm stimuli.

Resting State Correlations within the Lateral Pain Network

ROIs within the lateral (sensory) pain network were defined from the activation maps correlating with subject-specific pain ratings, using an adaptive threshold. Multiple ROIs within bilateral postcentral gyrus (SI) and along bilateral lateral sulcus (LS) were identified and grouped into the four larger regions (contralateral SI, contralateral LS, ipsilateral SI, and ipsilateral LS). We measured the resting state functional connectivity (rs-fc) between these ROIs at multiple time points by calculating the correlation coefficients. We tested the stability of the rs-fc within this intrinsic sensory pain network by comparing the correlation coefficients at RS0 (first 95 volumes of rs-Run 1) and RS1 (last 95 volumes of rs-Run 1) for each subject (Figure 3A-D: Subjects 1-4). The significant ($p < 0.05$) R-values for RS0 (Figure 3i) and RS1 (Figure 3ii) were displayed, with the colorbar indicating positive correlations in warm tones, negative correlations in cool tones, and zero correlation in black. All subjects possessed strong positive rs-fc with few exceptions.

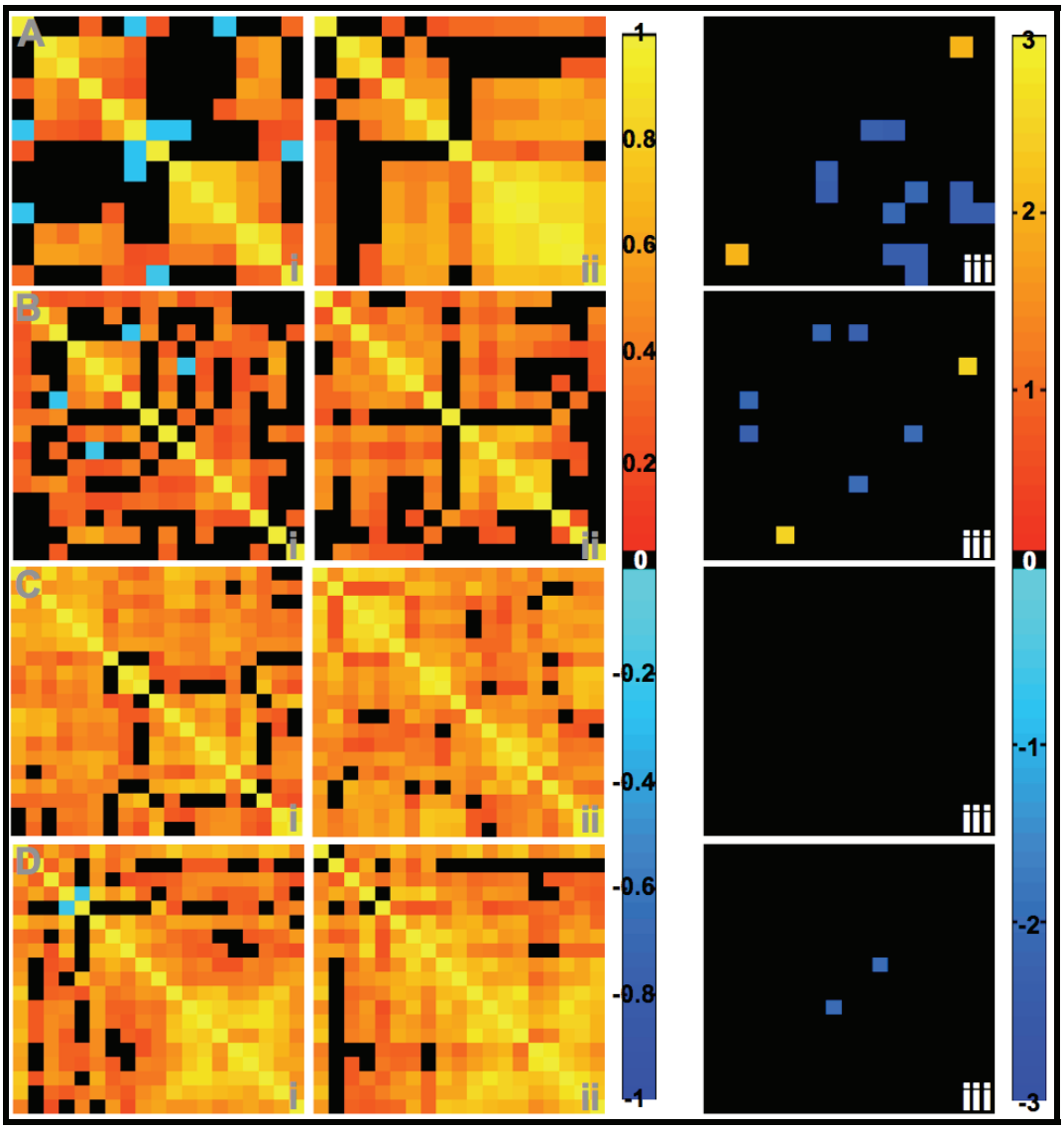

Figure 3. Resting state-functional connectivity within areas of the lateral pain network, for all subjects (***A***-***D***). The correlation coefficients between ROIs at two time intervals (***i***) and (***ii***) before the perception of pain are displayed in the matrices, with non-significant correlations in black. Positive correlations are presented in warm tones and negative correlations in cool tones as indicated by the colorbar to the right of the R-matrices. The R-matries were transformed into Z-scores, and the difference in correlations between the two time intervals (Z_{RS0}-Z_{RS1}) was calculated and displayed in a difference matrix (***iii***) to assess the stability of the rs-fc. Only significant differences were displayed in color, with the colorbar to the right of the Z-matrices.

The R-values were converted to Z-scores and the difference between the Z-scores (RS0-RS1) were calculated, with the significant differences displayed (Figure

3iii). The colorbar indicates positive differences in fc in warm tones, negative differences in cool tones, and no difference in black. Most often positive differences indicate a decrease in rs-fc, and negative differences indicate an increase in rs-fc. Subjects 3 showed no significant difference between the two time segments (Figure 3Ciii), while only one comparison showed a significant difference for Subject 4 (Figure 3Diii). Subject 1 (Figure 3Aiii) and Subject 2 (Figure 3Biii) showed more variation in rs-fc between the two time segments, with seven and four comparisons having a significant difference, respectively. While some variance was observed, the intrinsic lateral pain network exhibited stability in the resting state prior to the experience of pain.

Functional Connectivity Modulated by Pain

We next tested whether the experience of pain altered the functional connectivity within the defined network. For each subject we calculated the correlation coefficients over multiple time segments, RS1 (directly before pain), RS2 (40 s after the pain stimulus offset), RS3 (approximately 5 min after pain stimulus offset), and RS4 (approximately 8.5 min after pain stimulus offset), and we plotted the distribution of R-values for each time segment. We next converted the R-values into Z-scores so that we could directly compare the fc across time segments by the following operations, Z_{RS1}-Z_{RS2}, Z_{RS1}-Z_{RS3}, and Z_{RS1}-Z_{RS4}.

For Subject 1, the rs-fc within the lateral pain network, as measured by the correlation coefficients, was positive and significant before the pain stimulus, yet diminished in significance over time, and exhibited weak negative correlations by RS4 (Figure 4A). The R-value distribution histogram illustrates the decrease in rs-fc over time, as demonstrated by the shift in R-values toward zero when compared to RS1 (Figure 4B). The direct comparison of Z-scores showed little significance from RS1 to RS2 and RS3, but showed a great decrease in rs-fc between RS1 and RS4 (Figure 4C).

The main effects were seen between contralateral LS and ipsilateral SI, and within ipsilateral SI. These were the result of a decrease in the strength of positive correlation coefficients and a switch from positive to slightly negative correlation coefficients. For example, the ipsilateral area 3a ROI had a strong positive correlation to ipsilateral area 1 pre-pain, but this diminished to no significance by RS4. Ipsilateral area 3a also had a positive correlation to ipsilateral area 2 pre-pain, but this changed to a negative correlation by RS 4.

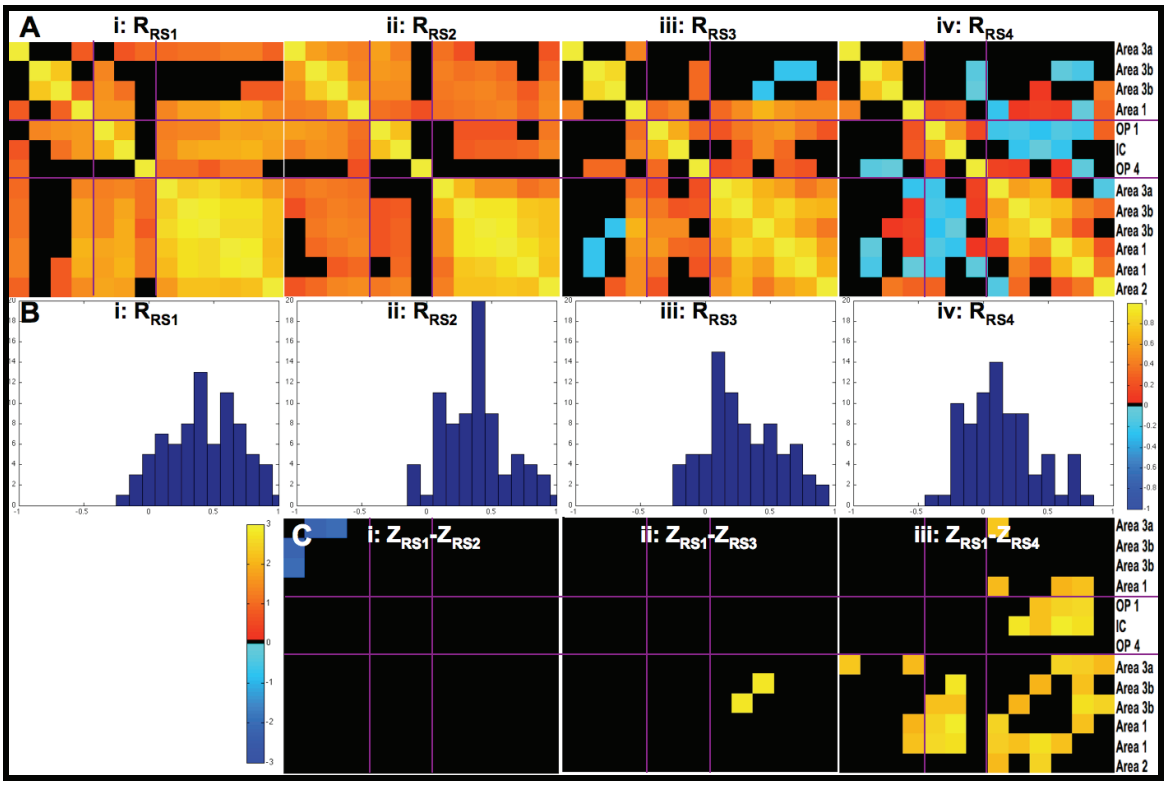

Figure 4. Resting state-functional connectivity within areas of the lateral pain network before and after pain, for Subject 1. (***A***) The correlation coefficients between ROIs at four time intervals: (***i***) before pain, R_{RS1}; (***ii***) 40 s after pain, R_{RS2}; (***iii***) 5 min after pain, R_{RS3}; and (***iv***) 8.5 min after pain, R_{RS4}. Positive correlations are presented in warm tones, negative correlations in cool tones, and non-significant correlations in black as indicated by the colorbar below and to the right of the R-matrices. (***B***) The distributions of the correlation coefficients at the four time intervals (***i***: R_{RS1}, ***ii***: R_{RS2}, ***iii***: R_{RS3}, ***iv***: R_{RS4}) are displayed in the histograms in the middle panel. (***C***) The R-matries were transformed into Z-scores, and the differences in correlations between the before pain interval and after pain intervals (i: Z_{RS1}-Z_{RS2}, ii: Z_{RS1}-Z_{RS3}, iii: Z_{RS1}-Z_{RS4}) were calculated and displayed in difference matrices. Only significant differences were displayed in color, with the colorbar to the left of the Z-matrices. The ROIs from different regions are separated by purple lines, with contralateral SI in the first section, contralateral lateral sulcus in the second section, and ipsilateral SI in the third section. Abbreviations: OP 1, SII; OP 4, parietal ventral area; IC, insular cortex.

Similar to Subject 1, Subject 2 demonstrated significant rs-fc within the lateral pain network before the experience of pain, yet this connectivity diminished over time. The correlation coefficients in both RS1 and RS2 were positive and significant, while the significance of these correlations diminished in RS3 and RS4, with slight changes to negative connectivity (Figure 5A). The shift in R-values toward zero and negative values is illustrated in by the R-distribution histograms in RS3 and RS4 (Figure 5B). There was

an overall increase in the strength of connectivity from RS1 to RS2 that is less obvious in the R-distribution histograms, but is well illustrated by the Z_{RS1}-Z_{RS2} matrix (Figure 5Ci). Contralateral area 1 and area 2, and multiple ROIs within the ipsilateral cortex increased in connectivity (blue pixels). By RS3 and RS4, however, the connectivity significantly diminished.

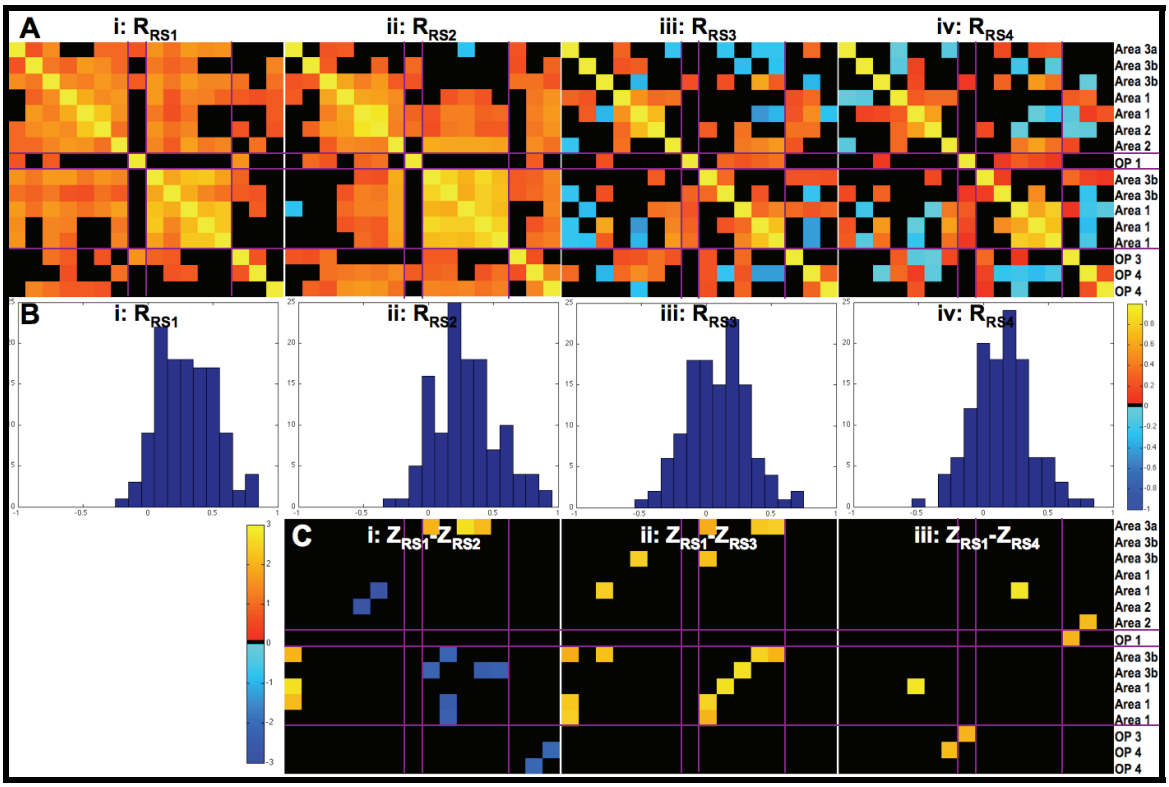

Figure 5. Resting state-functional connectivity within areas of the lateral pain network before and after pain, for Subject 2. (***A***) The correlation coefficients between ROIs at four time intervals: (***i***) before pain, R_{RS1}; (***ii***) 40 s after pain, R_{RS2}; (***iii***) 5 min after pain, R_{RS3}; and (***iv***) 8.5 min after pain, R_{RS4}. Positive correlations are presented in warm tones, negative correlations in cool tones, and non-significant correlations in black as indicated by the colorbar below and to the right of the R-matrices. (***B***) The distributions of the correlation coefficients at the four time intervals (***i***: R_{RS1}, ***ii***: R_{RS2}, ***iii***: R_{RS3}, ***iv***: R_{RS4}) are displayed in the histograms in the middle panel. (***C***) The R-matries were transformed into Z-scores, and the differences in correlations between the before pain interval and after pain intervals (i: Z_{RS1}-Z_{RS2}, ii: Z_{RS1}-Z_{RS3}, iii: Z_{RS1}-Z_{RS4}) were calculated and displayed in difference matrices. Only significant differences were displayed in color, with the colorbar to the left of the Z-matrices. The ROIs from different regions are separated by purple lines, with contralateral SI in the first section, contralateral lateral sulcus in the second section, ipsilateral SI in the third section, and ipsilateral lateral sulcus in the forth section. Abbreviations: OP 1, SII; OP 3, ventral somatosensory area; OP 4, parietal ventral area.

Subject 3 showed much less variation in rs-fc than all other subjects. The correlation coefficients overall remained positive and significant over time (Figure 6A). The R-distribution histograms illustrated a decrease in connectivity from RS1 to RS2, and increase in connectivity from RS1 to RS3, and a decrease from RS1 to RS4 (Figure 6B). There was little significant difference between Z-score except for Z_{RS1}-Z_{RS3}, where most of the increase in connectivity was seen in contralateral SI (Figure 6C). The R-matrix for RS3 illustrated this increase in connectivity as demonstrated by yellow pixels within the upper quadrant (Figure 6Aiii).

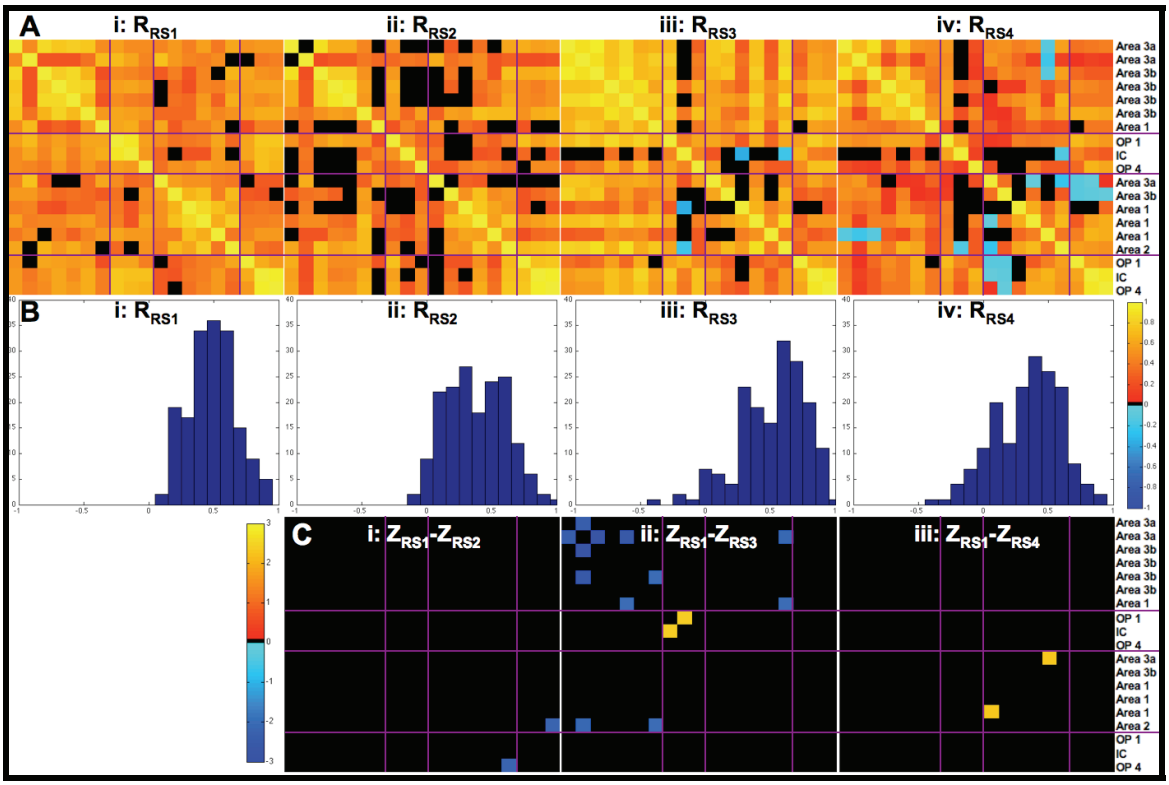

Figure 6. Resting state-functional connectivity within areas of the lateral pain network before and after pain, for Subject 3. (***A***) The correlation coefficients between ROIs at four time intervals: (***i***) before pain, R_{RS1}; (***ii***) 40 s after pain, R_{RS2}; (***iii***) 5 min after pain, R_{RS3}; and (***iv***) 8.5 min after pain, R_{RS4}. Positive correlations are presented in warm tones, negative correlations in cool tones, and non-significant correlations in black as indicated by the colorbar below and to the right of the R-matrices. (***B***) The distributions of the correlation coefficients at the four time intervals (***i***: R_{RS1}, ***ii***: R_{RS2}, ***iii***: R_{RS3}, ***iv***: R_{RS4}) are displayed in the histograms in the middle panel. (***C***) The R-matries were transformed into Z-scores, and the differences in correlations between the before pain interval and after pain intervals (i: Z_{RS1}-Z_{RS2}, ii: Z_{RS1}-Z_{RS3}, iii: Z_{RS1}-Z_{RS4}) were calculated and displayed in difference matrices. Only significant differences were displayed in color, with the colorbar to the left of the Z-matrices. The ROIs from different regions are separated by purple lines, with contralateral SI in the first section, contralateral lateral sulcus in the second section, ipsilateral SI in the third section, and ipsilateral lateral sulcus in the forth section. Abbreviations: OP 1, SII; OP 4, parietal ventral area; IC, insular cortex.

In contrast to Subject 3, Subject 4 showed the greatest change in rs-fc over time. The correlation coefficients for the lateral pain network were positive and significant pre-pain, but diminished in significance over time (Figure 7A). This is well illustrated by the number of black pixels within the R_{RS2}, R_{RS3}, and R_{RS4} matrices, as well as the negative shift in the R-distribution histograms (Figure 7B). There were also many pixels with significant differences between Z-scores pre- and post-pain (Figure 7C). As in Subject 1,

some of these positive changes in Z-scores were the result of a decrease in significance from one time point to another, yet others were the result of a switch from positive to negative correlations pre- and post-pain. One region that did not change in correlation over time was ipsilateral SI. The correlation coefficients remained significantly (positive) correlated throughout time with few exceptions.

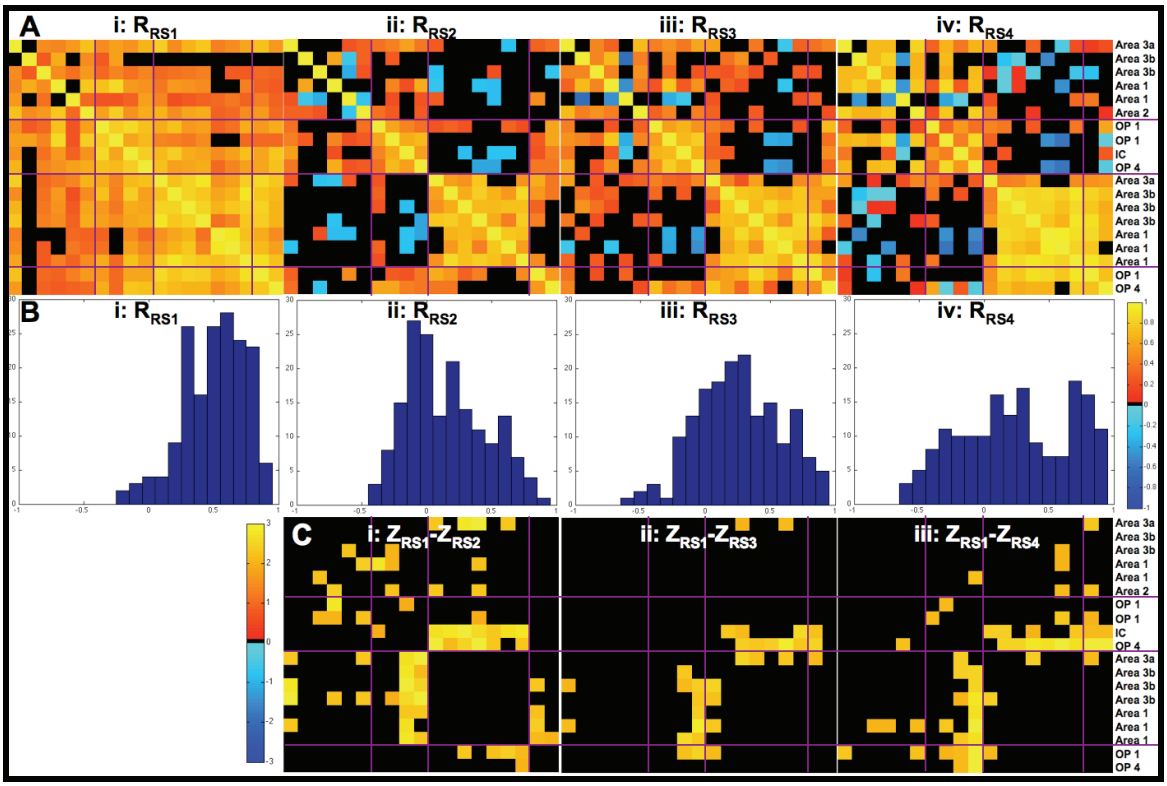

Figure 7. Resting state-functional connectivity within areas of the lateral pain network before and after pain, for Subject 4. (***A***) The correlation coefficients between ROIs at four time intervals: (***i***) before pain, R_{RS1}; (***ii***) 40 s after pain, R_{RS2}; (***iii***) 5 min after pain, R_{RS3}; and (***iv***) 8.5 min after pain, R_{RS4}. Positive correlations are presented in warm tones, negative correlations in cool tones, and non-significant correlations in black as indicated by the colorbar below and to the right of the R-matrices. (***B***) The distributions of the correlation coefficients at the four time intervals (***i***: R_{RS1}, ***ii***: R_{RS2}, ***iii***: R_{RS3}, ***iv***: R_{RS4}) are displayed in the histograms in the middle panel. (***C***) The R-matries were transformed into Z-scores, and the differences in correlations between the before pain interval and after pain intervals (i: Z_{RS1}-Z_{RS2}, ii: Z_{RS1}-Z_{RS3}, iii: Z_{RS1}-Z_{RS4}) were calculated and displayed in difference matrices. Only significant differences were displayed in color, with the colorbar to the left of the Z-matrices. The ROIs from different regions are separated by purple lines, with contralateral SI in the first section, contralateral lateral sulcus in the second section, ipsilateral SI in the third section, and ipsilateral lateral sulcus in the forth section. Abbreviations: OP 1, SII; OP 4, parietal ventral area; IC, insular cortex.

Summary

The rs-fc of each subject altered over time, and this difference in connectivity, following the experience of pain, was greater than the difference in rs-fc between RS0 and RS1. In general the connectivity within the lateral pain network decreased over time, and after pain, did not normalize back to the connectivity measured before pain in the time we evaluated them.

Discussion

SI Activation Correlated with Pain Ratings

Much of noxious information is processed in the periphery and spinal cord, yet it is hypothesized that the processing of pain perception is located in the brain. One key aspect to the perception of sensory input is intensity estimation, especially for painful experiences. We asked subjects to rate their pain intensity throughout the duration of the pain runs, permitting us to use the ratings as a regressor in the GLM, similar to the 3-T group study by Baliki and colleagues, ((Baliki et al., 2008)). A single subject often rated the same temperature stimulus a different intensity, so using the ratings mitigated the variability and noise associated with the often-unpredictable psychophysics of repeated painful stimulation. Similar to this prior study, we observed activation correlated with intensity estimation of pain in SI, IC, and OP. In addition to the pain stimulus, subjects in the Baliki study were given a motor task to control for motor activation. While the authors did not specify whether the motor task elicited activity in SI, they found that SI activation was not more significant in the pain task than the motor task. A comparable motor task should be implemented with our study design to rule out motor confounds. It is possible that our increased spatial resolution and sensitivity to BOLD signal at 7 T will indicate specific subregions within SI that are not confounded by motor activation.

Resting State Correlations with SI Cortex

The first fMRI study that examined functional connectivity mapped both activations and resting state correlations within the sensorimotor cortex ((Biswal et al., 1995)). This study demonstrated that a map, almost identical to an activation map created from a finger-tapping task, could also be generated measuring the correlation of the low frequency BOLD signal in the rest time blocks. A similar technique was implemented here to demonstrate that activation clusters detected by a pain task, also had high correlation within the resting state, even in areas not anatomically connected. Many of the correlations that we measured within the lateral pain network were $R>0.5$, higher than the prior study reporting correlation coefficient of $R>0.35$. The strength of the resting state correlations within the network that we defined is greater in amplitude than the correlations that have previously been described.

Stability of Resting State Functional Connectivity

Resting state functional connectivity has been used to compare patient and control populations, however, little research on the stability of these correlations over time has been considered. If the correlations we measure to make inferences about neural networks in both healthy and patient populations are unstable, this becomes problematic. A recent study by Chang and Glover found that the resting state functional connectivity within the "default mode network" (posterior parietal cortex and other nodes) was not static and recommended that this variability be considered in analysis and deduction ((Chang and Glover, 2010)). Here, we tested the stability of the resting state functional connectivity within the lateral pain network at two time points before pain. We observed a static network in two of our subjects, yet we also detected a small degree of variability between some of the areas within the lateral pain network.

Pain Perception Modulation of Functional Connectivity

Recently resting state functional connectivity has become a popular method for investigating psychiatric and neurological disorders. These types of analyses are not limited to a single task or cortical region, and moreover, they have the ability to explore multiple neural networks. While this is the first study to specifically examine the strength of correlations within areas of the lateral pain network and how these correlations are modulated by pain perception, other studies have examined other networks in chronic pain patients ((Baliki et al., 2008), (Cauda et al., 2010), (Napadow et al., 2010), (Rocca et al., 2010), (Tagliazucchi et al., 2010), (Upadhyay et al., 2010)). In our healthy subject population, we observed diminished functional connectivity following a painful stimulus. Multiple chronic pain populations have been studied, multiple procedures were executed, and multiple analysis methods were implemented. There is no consensus on which networks are altered by pain and whether the functional connectivity is increased or decreased in the chronic pain population. Resting state functional connectivity studies at 7 T are uniquely suited to study this patient population. The inconclusive prior results are likely due to the inhomogeneity of the population being studied. Here, the pain network was mapped for each individual, based on his/her own anatomy and experience. Similar studies should be conducted in the chronic pain population.

Conclusion

We have demonstrated that areas of the lateral pain network have strong functional connectivity in the resting state. The correlation coefficients between these areas are very high before the perception of pain, and tend to diminish in magnitude after a painful experience. There was little consistency across subjects about the

strength of specific areal connections (i.e. contralateral area 3b and ipsilateral 3b) within the network, and the modulation of specific connections varied across subjects. This is not surprising since the pain network is highly complex and each subject experiences the same painful stimulus differently. To better understand the area-specific functional connectivity, psychophysical evaluations of the pain stimuli should be performed prior to the scanning session, directly after each pain stimulus, and after the scanning session. The quality of the experience is different for every subject, so accounting for this variability in our analysis could lead to a better understanding of this intrinsic network.

References

Baliki, M.N., Geha, P.Y., Apkarian, A.V., Chialvo, D.R., 2008. Beyond feeling: chronic pain hurts the brain, disrupting the default-mode network dynamics. J Neurosci 28, 1398-1403.

Biswal, B., Yetkin, F.Z., Haughton, V.M., Hyde, J.S., 1995. Functional connectivity in the motor cortex of resting human brain using echo-planar MRI. Magn Reson Med 34, 537-541.

Brodmann, K., 1909. VergleichendeLocalisationslehre der Gro Hhirnrinde. Barth, Leipzig.

Cauda, F., D'Agata, F., Sacco, K., Duca, S., Cocito, D., Paolasso, I., Isoardo, G., Geminiani, G., 2010. Altered resting state attentional networks in diabetic neuropathic pain. J Neurol Neurosurg Psychiatry 81, 806-811.

Chang, C., Glover, G.H., 2010. Time-frequency dynamics of resting-state brain connectivity measured with fMRI. Neuroimage 50, 81-98.

Eickhoff, S.B., Amunts, K., Mohlberg, H., Zilles, K., 2006a. The human parietal operculum. II. Stereotaxic maps and correlation with functional imaging results. Cereb Cortex 16, 268-279.

Eickhoff, S.B., Schleicher, A., Zilles, K., Amunts, K., 2006b. The human parietal operculum. I. Cytoarchitectonic mapping of subdivisions. Cereb Cortex 16, 254-267.

Geyer, S., Schormann, T., Mohlberg, H., Zilles, K., 2000. Areas 3a, 3b, and 1 of human primary somatosensory cortex. Part 2. Spatial normalization to standard anatomical space. Neuroimage 11, 684-696.

Glover, G.H., Li, T.Q., Ress, D., 2000. Image-based method for retrospective correction of physiological motion effects in fMRI: RETROICOR. Magn Reson Med 44, 162-167.

Hashmi, J.A., Davis, K.D., 2008. Effect of static and dynamic heat pain stimulus profiles on the temporal dynamics and interdependence of pain qualities, intensity, and affect. J Neurophysiol 100, 1706-1715.

Jezzard, P., Balaban, R.S., 1995. Correction for geometric distortion in echo planar images from B0 field variations. Magn Reson Med 34, 65-73.

Kennedy, D.P., Courchesne, E., 2008. The intrinsic functional organization of the brain is altered in autism. Neuroimage 39, 1877-1885.

Krause, T., Kurth, R., Ruben, J., Schwiemann, J., Villringer, K., Deuchert, M., Moosmann, M., Brandt, S., Wolf, K., Curio, G., Villringer, A., 2001. Representational overlap of adjacent fingers in multiple areas of human primary somatosensory cortex depends on electrical stimulus intensity: an fMRI study. Brain Res 899, 36-46.

Kurth, R., Villringer, K., Curio, G., Wolf, K.J., Krause, T., Repenthin, J., Schwiemann, J., Deuchert, M., Villringer, A., 2000. fMRI shows multiple somatotopic digit representations in human primary somatosensory cortex. Neuroreport 11, 1487-1491.

Moore, C.I., Stern, C.E., Corkin, S., Fischl, B., Gray, A.C., Rosen, B.R., Dale, A.M., 2000. Segregation of somatosensory activation in the human rolandic cortex using fMRI. J Neurophysiol 84, 558-569.

Napadow, V., LaCount, L., Park, K., As-Sanie, S., Clauw, D.J., Harris, R.E., 2010. Intrinsic brain connectivity in fibromyalgia is associated with chronic pain intensity. Arthritis Rheum 62, 2545-2555.

Nelson, A.J., Chen, R., 2008. Digit somatotopy within cortical areas of the postcentral gyrus in humans. Cereb Cortex 18, 2341-2351.

Price, D.D., Hu, J.W., Dubner, R., Gracely, R.H., 1977. Peripheral suppression of first pain and central summation of second pain evoked by noxious heat pulses. Pain 3, 57-68.

Rocca, M.A., Absinta, M., Moiola, L., Ghezzi, A., Colombo, B., Martinelli, V., Comi, G., Filippi, M., 2010. Functional and structural connectivity of the motor network in pediatric and adult-onset relapsing-remitting multiple sclerosis. Radiology 254, 541-550.

Rogers, B.P., Morgan, V.L., Newton, A.T., Gore, J.C., 2007. Assessing functional connectivity in the human brain by fMRI. Magn Reson Imaging 25, 1347-1357.

Tagliazucchi, E., Balenzuela, P., Fraiman, D., Chialvo, D.R., 2010. Brain resting state is disrupted in chronic back pain patients. Neurosci Lett 485, 26-31.

Torebjork, E., 1985. Nociceptor activation and pain. Philos Trans R Soc Lond B Biol Sci 308, 227-234.

Triantafyllou, C., Hoge, R.D., Krueger, G., Wiggins, C.J., Potthast, A., Wiggins, G.C., Wald, L.L., 2005. Comparison of physiological noise at 1.5 T, 3 T and 7 T and optimization of fMRI acquisition parameters. Neuroimage 26, 243-250.

Upadhyay, J., Maleki, N., Potter, J., Elman, I., Rudrauf, D., Knudsen, J., Wallin, D., Pendse, G., McDonald, L., Griffin, M., Anderson, J., Nutile, L., Renshaw, P., Weiss, R., Becerra, L., Borsook, D., 2010. Alterations in brain structure and functional connectivity in prescription opioid-dependent patients. Brain 133, 2098-2114.

Vogt, C., Vogt, O., 1919. Allgemeiner Ergebnisse unserer Hinforschung. Journal Psychology and Neurology 25, 279-462.

White, L.E., Andrews, T.J., Hulette, C., Richards, A., Groelle, M., Paydarfar, J., Purves, D., 1997. Structure of the human sensorimotor system .1. Morphology and cytoarchitecture of the central sulcus. Cerebral Cortex 7, 18-30.

Zhang, N., Gore, J.C., Chen, L.M., Avison, M.J., 2007. Dependence of BOLD signal on tactile stimulus intensity in SI of primates. Magnetic Resonance Imaging 25, 784-794.

CHAPTER V

CONCLUSIONS AND FUTURE DIRECTIONS

Conclusions

The studies presented in this work provide insight into the organization and function of the primary somatosensory cortex (SI). SI, comprised of four cytoarchitecturally distinct regions (3a, 3b, 1, and 2), plays a critical role in the processing of somatic and noxious sensation, with each subregion contributing differently to the encoding of sensory information. Until recently, most contributions to the understanding of SI organization and function have been made through invasive techniques in various mammalian species, excluding humans. We have shown how ultra-high field imaging may be used to explore cortical processing with fine-scale precision and high sensitivity to signal.

We have demonstrated digit somatotopy in both areas 3b and 1 and shown that the topographical maps differ in precision, with area 1 having greater overlap of digit representation. The distance between adjacent digits was calculated along the folds of cortex, following the grey matter, and the separation of digits was roughly 1.7 times greater in area 3b than in area 1. The response fields were measured, and found to be the same size in both areas 3b and 1, suggesting that the overlap of digit responses observed in area 1 is due to the smaller volume of cortex that area 1 is represented in, not a larger response field. In contrast to our other findings, the size of the response field is not in agreement with the nonhuman primate literature that finds larger response fields in area 1.

While SI's role in the processing of pain information is controversial, we were able to detect bilateral responses to thermal pain in SI. Using the activation clusters as

seed regions in a functional connectivity analysis, we were able to reveal an intrinsic network tightly coupled in the absence of any task. Areas within this network were unaffected by the perception of pain, while other areas showed marked changes in connectivity after the painful experience. This demonstrates our ability to use functionally defined regions from stimulus driven data to define basal networks within the cortex, and the dynamic nature of interregional correlations is BOLD signals. These data also suggest that in healthy subjects with no disease the perception of pain can disrupt an underlying intrinsic pain network.

The findings of these studies have a significant impact on the neuroimaging field in addition to the specific tasks investigated. One of the most significant findings from this work is the short scan time needed to map the cortical response to a particular task at high resolution. We found that a single digit's cortical representation could be mapped at millimeter resolution in just over two minutes, in part due to the increased sensitivity to BOLD signal changes at 7 T. This could have a profound impact on studying patient populations and young children. Many patients seeking MRI evaluations are living in some state of discomfort, or their illness prevents them from lying still for long periods of time, for reasons such as tremors or cognitive impairments. Our data show promise for these patients having a positive experience with an MR scan when the total scan time is more limited. Neuroimaging has been a helpful tool in our understanding of neural development both normal and abnormal, such as in autism or learning disabilities. Children tend to have short attention spans and have difficulty holding their heads still during long scanning sessions. The reduction in scan time should be especially beneficial to studying this population.

The ability to map the fine-scale representation of body surface is integral to our understanding of how sensory information in organized within the cortex. In a number of diseases, the cortex is reorganized, and the ability to detect this reorganization could

lead to better long-term treatment for these patients. For example during a stroke, part of the brain loses its blood supply for some duration of time, resulting in the affected area of the brain being unable to function normally. This can lead to a loss in motor control, sensation, and/or cognition, which may become permanent. In the cases of lasting neurological damage, therapy is given to patients with the goal of recovering some of the lost function. From the time at which the stroke occurs to the months of therapy following the stroke, the cortex can undergo extensive reorganization ((Brion et al., 1989)). Our data give hope to the ability to measure this cortical reorganization over time, with high precision. This could allow us to access the efficacy of different forms of therapy, or correlate the degree of reorganization with the outcome of treatment. Cortical reorganization not only occurs in stroke victims, but in other patients such as those suffering with spinal cord injury and amputation.

In conjunction with the fast scan time, we could also access the temporal dynamics of cortical reorganization. For example, transcranial magnetic stimulation (TMS) can be used to temporarily disrupt the function of a discrete area of cortex, in essence mimicking the disease state. TMS can be applied over SI while simultaneously delivering a tactile stimulus and acquiring functional MR images. The SI activation in response to the tactile stimulus can be investigated over time as the brain recovers from the TMS. Since less than three minutes are required to accurately map representation of body surface in SI, many time points can be examined. While we have focused on the somatosensory network in this body of work, other sensory, motor, cognitive, and affective networks can also be explored.

As described in Chapter I, millions of Americans suffer from pain everyday, with a costly price tag. While millions of research dollars are poured into studying pain every year, the complexity of processing noxious stimuli in the peripheral and central nervous systems has proven detrimental to new breakthroughs in our understanding of encoding

pain information and the treatment of pain perception. While effective medications are available for the treatment of acute pain in the majority of the population, long-term medication and procedures for the treatment of the chronic pain state are less successful. While the spinal cord plays vital role in nociceptive processing, the perception of pain is thought to be processed in the brain, integrating sensory, affective, and cognitive information leading to an overall unpleasant experience. The ability of fMRI to explore all of the brain structures hypothesized to play a role in pain processing renders it uniquely suited to the investigation of pain. While the groundwork for this neural mapping has been previously demonstrated ((Apkarian et al., 2005), (Peyron et al., 2000)), more precise maps (acquired at high magnetic fields) that can differentiate subtle functional differences in adjacent areas of cortex will lead to a better understanding of parallel and serial processing of pain information. The biggest drawbacks of many pharmacological agents (interacting predominately at the μ-opioid receptor) used to treat chronic pain are the deleterious side effects, such as sedation, impaired cognition, low blood pressure, shortness of breadth, constipation, addiction, and tolerance. If we could more precisely target a specific area of cortex, this could mitigate some of these side effects. For example, in the treatment of Parkinson's disease catechol-O-methyl transferase (COMT) inhibitors are often prescribed, taking advantage of the differential expression of COMT that is low in the striatum and midbrain and high in the prefrontal cortex, designing a class of drugs to selectively target COMT in prefrontal cortex. The same strategy could in principle be implemented in designing pharmaceuticals for the treatment of pain.

Another hallmark of pain is the variability in the pain experience across subjects and the variability in pain perception within a subject across time. This variability is especially true with chronic pain patients. The underlying pathology of each patient is unique, leading to heterogeneity within a patient group, which is problematic when

attempting to compare a patient group with a control group. The ability to analyze subjects individually with the increase in sensitivity to fMRI signals at high fields, correlating their unique perception with their cortical response, lessens some of the variability within the data.

The biggest drawback of using functional imaging to study chronic pain is that most fMRI studies have relied on comparing hemodynamic changes in different conditions, ie pain “on” condition versus pain “off” condition. While this allows us to study acute pain circuitry, we do not gain much insight into neural circuitry associated with chronic pain perception. Resting state functional connectivity (rs-fc) is an fMRI analysis that allows us to examine the intrinsic neural circuitry within the basal state of an individual’s brain. In this body of work we compared rs-fc in areas correlated with perception of pain intensity before and after pain. This type of procedure could be extended to chronic pain patients, with the hypothesis that the basal state of the pain network in chronic pain patients is quite different from that of normal controls. This could help us target what functional connections within the pain network are disrupted that lead to abnormal processing of pain information. Moreover, we have seen how a brief episode of pain alters the fc, which is, therefore, dynamic in nature. Studies of different dynamic properties of fc may provide a better basis for classifying chronic pain patients.

Future Directions

The studies presented here show very interesting and valuable new insights, but they also suggest some compelling possible future investigations. This research would focus on a) development of fMRI at 7T, b) ipsilateral activations, c) decreases in BOLD signal, d) secondary somatosensory cortex, and e) the dynamic nature of functional connectivity.

Development of fMRI at 7 T

All of the studies presented in this work were conducted using ultra-high field fMRI at 7 T. While these studies have demonstrated the increased sensitivity to BOLD signal and the increased spatial resolution permitted at higher fields, improvements can be made to our imaging techniques to mitigate some of the pitfalls of high field imaging. One of the leading drawbacks we faced was the distortion caused by magnetic field inhomogeneities and the limited cortical coverage. A handful of methods are being developed, implemented, and optimized on the 7-T scanner currently and in the future. Since we last imaged on the scanner, a new 32-channel head coil has been installed. Previously we used a 16-channel head coil. The head coils are arrays of receive coils that detect the MR signal. By increasing the number of receive coils, we have gained sensitivity to signal, improving the measured SNR. Additional coils, arranged in a geometry like the 32-channel coil, permit SENSE acceleration in more than one direction, allowing us to under sample the data and acquire images even more rapidly. This could result in less distortion and a larger imaging volume.

EPI sequences have been used in all our reported data. These images, however, are vulnerable to inhomogeneities within the magnetic field. Some of our early studies included an imaging sequence called a three-dimensional fast-field-echo (3D-FFE) in which the images are acquired in 3D and not 2D like the EPI sequence. The FFE sequence diminishes most of the image distortion caused by B-field inhomogeneities. While we experienced less distortion in our images, the sequence was not optimized and suffered from severe noise. Since the time of our first studies, this 3D-FFE has been optimized and will be implemented in future studies

Although not currently available within our institute, parallel transmit coils offer promise for mitigating B_1 (radio frequency pulse field (RF)) inhomogeneities. Similar to

increasing the number of receive coils, increasing the number of transmit coils can greatly improve the quality of our functional images. The excitation and inversion pulses are not uniform over the entire brain, for example the cortex and thalamus receive an inhomogenous RF pulse, causing weaker detection of signal in the thalamus. A parallel transmit coil could enable a homogenous B_1 field allowing us to target the cortex and subcortical tissue in the same image. This would greatly improve the quality of the functional data we have acquired already over the thalamus. As these improvements to our imaging methodology continue to developed, we will continue to implement them in our studies, in a continuing pursuit of optimization of our functional images.

Activation in Ipsilateral SI

Introduction

Classical models of sensory and motor processing dictate that the right hemisphere of cortex controls the left side of the sensorimotor environment (ie the left visual hemifield or left side of the body), and likewise, the left hemisphere of cortex controls the right side of the sensorimotor envirnoment. In the somatic sensory network this has been demonstrated by numerous mammalian structural and functional studies. Staining of fibers through afferent pathways of simple touch illustrate the decussation of afferent fibers at the posterior most part of the brainstem (medulla), and electrophysiological recordings from contralateral cortex reveal robust response to stimuli. Evidence, however, exists for the processing of some sensory data in the ipsilateral cortex ((Tommerdahl et al., 2005), (Tommerdahl et al., 2006)), likely originating from callosal collateral fibers that are hypothesized to act as feedback between the cortices. Staining studies have shown that there are large projections of fibers through the corpus callosum from area 2 in one hemisphere to area 2 in the other hemisphere. These fibers also exist for area 1 which are less dense, and very little for

area 3b ((Killackey et al., 1983), (Conti et al., 1986), (Toda et al., 1996). Interregionally, there are feed-forward and feedback projections between areas within SI.

With the callosal connections and fibers projecting to areas of ipislateral SI, it is not surprising that studies have demonstrated that ipsilateral SI is responsive to basic tactile stimulation at the periphery. Many early electrophysiology studies in monkey were only able to demonstrate that body surface proximal to the midline was represented bilaterally in SI ((Schwartz and Fredrickson, 1971), (Dreyer et al., 1975), (Conti et al., 1986), (Manzoni et al., 1989), (Ogawa et al., 1989)). In 1994, however, Iwamura and colleagues observed bilateral cortical response to tactile stimulation of the hand and digits in SI, most specifically area 2 that possesses dense callosal inputs ((Iwamura et al., 1994)).

Neuroimaging studies in humans have shown little activation in the ipsilateral cortex in response to digit touch stimuli ((Kurth et al., 2000), (Krause et al., 2001), (Nelson and Chen, 2008), (Weibull et al., 2008)), in part due to imaging restricted to the contralateral hemisphere ((Schweizer et al., 2008), (Sanchez-Panchuelo et al., 2010), (Maldjian et al., 1999)). Maldjian and colleagues presented activation maps with bilateral response in SI, but did not discuss the detection of ipsilateral activation ((Maldjian et al., 1999)). Only Francis and colleagues detected and discussed ipsilateral activation in SI, finding infrequent cortical response in areas 3b and 1 with only 3 out 8 subjects responding to D2 stimulation in ipsilateral cortex and 4 out of 8 subjects responding to D3 stimulation in ipsilateral cortex ((Francis et al., 2000)). Due to the predicted weak signal in ipsilateral cortex, it is not surprising that earlier fMRI studies were unable to reliably detect ipsilateral activations. With the increased sensitivity we have to BOLD signals at 7 T, and with the smaller problem of partial volume effects (effect where different signals arising from different points in space, but still part of the same larger voxel, are reduced because they are averaged together), we were able to detect

activation in the ipsilateral cortex.

Results

From the somatosensory data presented in Chapters II and III, we also investigated the response of ipsilateral SI to 2-Hz air puff stimulation on individual digits. In the single condition activity maps of all subjects we observed activation in multiple areas of SI contralateral to stimulation. Some of the subjects also showed activation in ipsilateral SI at the strict threshold q (FDR) < 0.001. We examined whether all subjects showed significant response to digit stimulation in the ipsilateral cortex. Upon relaxing the threshold to q (FDR) < 0.05 we observed activation ipsilateral to stimulation in all subjects (n = 6). The exact areas of activation varied highly among subjects. Areas 3b, 1, and 2 were all observed to be activated in multiple subjects. The zoomed-in activation map (D4-Rest) of a single subject is overlaid on the structural image in the sagittal plane (Figure 1D). The pink box over the structural image indicates the zoomed-in area of the activation map, and the central sulcus (CS) ipsilateral to stimulation is highlighted in blue (Figure 1C). There are several activation clusters within the displayed area. A handful of clusters are localized at the anterior bank of the CS and at the crest of the precentral gyrus, corresponding to primary motor cortex. Another activation cluster is located deep within the CS, corresponding to area 3a. Two more clusters are located at the posterior bank of the CS and the crest of the postcentral gyrus, corresponding to areas 3b and 1, respectively.

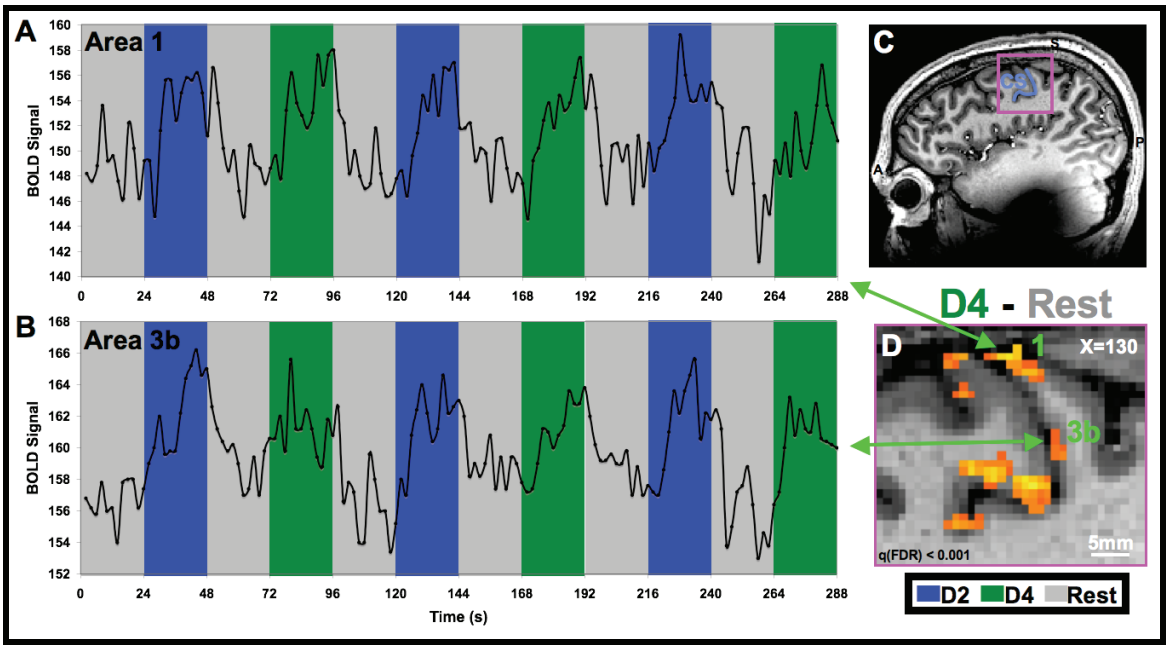

Figure 1. Activity map and time course of digit responses in ipsilateral areas 1 and 3b. (***C***) The sagittal slice of the anatomical image is displayed in the inset with the central sulcus (CS) highlighted in blue. (***D***) The activity map (D4 - Rest) is displayed in the increase field of view image, with distinct representations in areas 1 and 3b (as well as representations within the motor cortex at the anterior bank of the central sulcus). (***A*** and ***B***) The time course of BOLD signal change was extracted from the peak 5 voxels and displayed in the time course plots for a single run and shows no differential response to digit 2 and 4 in both areas 1 and 3b (green arrows indicate correspondence between activation cluster and time course); Rest grey, D2 blue, D4 green.

Due to the differences between cortical responses to digit stimulation observed in Chapter III, we further investigated the BOLD signal time courses in these ipsilateral activations in areas 3b and 1. We examined whether there was overlap of digit responses and whether the shape of the BOLD signal time course was different between these adjacent areas of cortex. We extracted the BOLD signal time course from the peak five voxels (highest t-value) within the two activation clusters. The BOLD signal time course revealed a robust response to D4 stimulation in both ipsilateral area 3b and 1. The BOLD responses from area 1 and 3b are displayed for a single run (Figure 1A&B). Both time courses demonstrate that these areas of cortex respond as robustly to D4 stimulation as they do to D2 stimulation. There is no difference in the signal amplitude between the different condition blocks. In area 3b, there is not a sustained response to

the stimulus similar to the shape of the BOLD response observed in contralateral area 3b. The BOLD response in both areas looks more similar to the transient response observed in contralateral area 1.

Discussion and Future Directions

The BOLD signal response observed in ipsilateral SI suggests that the fine-scale somatotopy detected in contralateral cortex is not present in ipsilateral cortex. While a topographic map of ipsilateral body surface is likely to exist, our data suggest that is does not exist at the resolution of individual digits. The BOLD signal time courses did not distinguish between digits, with the amplitude of BOLD response the same during stimulation of both D4 and D2, even though the regions of interest of defined from the D4-Rest single condition map. In addition, unlike contralateral digit responses, there was no detectable difference in the shape of the BOLD signal time course between areas 3b and 1. While area 3b responds robustly to both slowly and rapidly adapting neurons and area 1 responds robustly to primarily rapidly adapting despite which hemisphere is being engaged, we were not able to detect hemodynamic differences that might reflect these response preferences. This is consistent with the premise that the cortical response detected in ipsilateral cortex arises from the feedback and feedforward projections between the two hemispheres of SI through the corpus collosum.

We also detected cortical responses in all subdivisions of SI. There was variability in the detection of activations in the different areas, with different digits, and across subjects. The collosal projections into area 2 are most dense, so detection of activation in area 2 was most expected, but not observed. In the future, we will investigate the frequency of cortical responses in each of the subdivisions of SI with other analysis techniques, such as an independent component analysis (ICA). ICA has the advantage of not assuming a hemodynamic response function, so if the inability to detect activation in ipsilateral cortex is due to differences in blood flow dynamics, we

would still be able to observe the cortical response. This would also allow us to compare the differences in the shape of the BOLD signal time course across the four areas, if differences exist. We also detected decreases in BOLD signal in ipsilateral cortex that need to be further explored to understand the contribution of ipsilateral cortex to the processing of tactile information and the sensation of touch.

"Negative" BOLD Signal

Introduction

Since the first BOLD-fMRI studies were conducted, both increases and decreases in the amplitude of BOLD signal have been observed throughout the cortex. Investigating the detection of positive BOLD response (PBR) has been given more attention in the imaging field than the detection of "negative" BOLD response (NBR). The aim of most functional neuroimaging studies, however, has been to correlate positive increases in correlates to neural activity (e.g. blood flow, BOLD) with a specific task. These increases are judged relative to an arbitrary starting level of flow and activity, and so decreases in activity are readily conceived. The interpretation of decreases in BOLD, however, is potentially confounded by vasculature origins.

Two theories explaining the neural basis for the NBR have been proposed: vasculature blood steal and reduction in neural activity. The former hypothesizes that in regions of NBR there is a decrease in cerebral blood flow (CBF) to compensate for the increase in CBF in adjacent regions of neural activity. The latter hypothesizes that the reduction in CBF is caused by a decrease in the activity of neurons ((Shmuel et al., 2002)). In 2006, Shmuel and colleagues, through simultaneous fMRI and electrophysiological recordings in monkey cortex demonstrated that NBR is a response to decreases in neural activity ((Shmuel et al., 2006)). Human studies investigating responses to motor and somatosensory tasks have established decreases in the BOLD

signal in ipsilateral cortices ((Newton et al., 2005), (Kastrup et al., 2008)). These findings further substantiate the hypothesis that the decreases in neural activity lead to NBR. Here, with the increased sensitivity to BOLD signal at 7 T, we show neighboring regions of PBR and NBR.

Results

From the somatosensory data in which we stimulated individual digits with a 2-Hz air puff stimulus, we created single condition activation maps (q (FDR) < 0.001), as described in Chapters II and III. In the D2-Rest activation map for Subject 1, we detected focal clusters of activation, or positive increases in BOLD signal, in multiple locations within the postcentral gyrus (Figure 2). The activation map was overlaid on the structural image of the axial plane (Figure 2A), and the green box indicates the area over which we presented a zoomed-in image of the activity (Figure 2B). The increased-field-of-view image illustrates the restriction of activation to the posterior bank of the central sulcus (area 3b), highlighted by the pink circle, and the crest of the postcentral gyrus (area 1) along the superficial cortex. Also observable in this image is the presence of "negative" BOLD signal, restricted to the anterior bank of the central sulcus corresponding to primary motor cortex (M1). Two NBR clusters were detected in M1 directly across the central sulcus from the PBR in area 3b; these clusters were located slightly lateral/anterior, highlighted by the blue circle, and medial/posterior to the PBR. In the bottom left of the image is the scale bar indicating a 5-mm distance, a distance longer than the separation between the PBR and each of the NBRs. In the bottom right of the image is a yellow box, 3x3 mm^2, indicating the size of an in-plane voxel in a typical 3-T study. Our high spatial resolution imaging sequence means that nine of the high-resolution voxels can fit into one of the lower-resolution voxels.

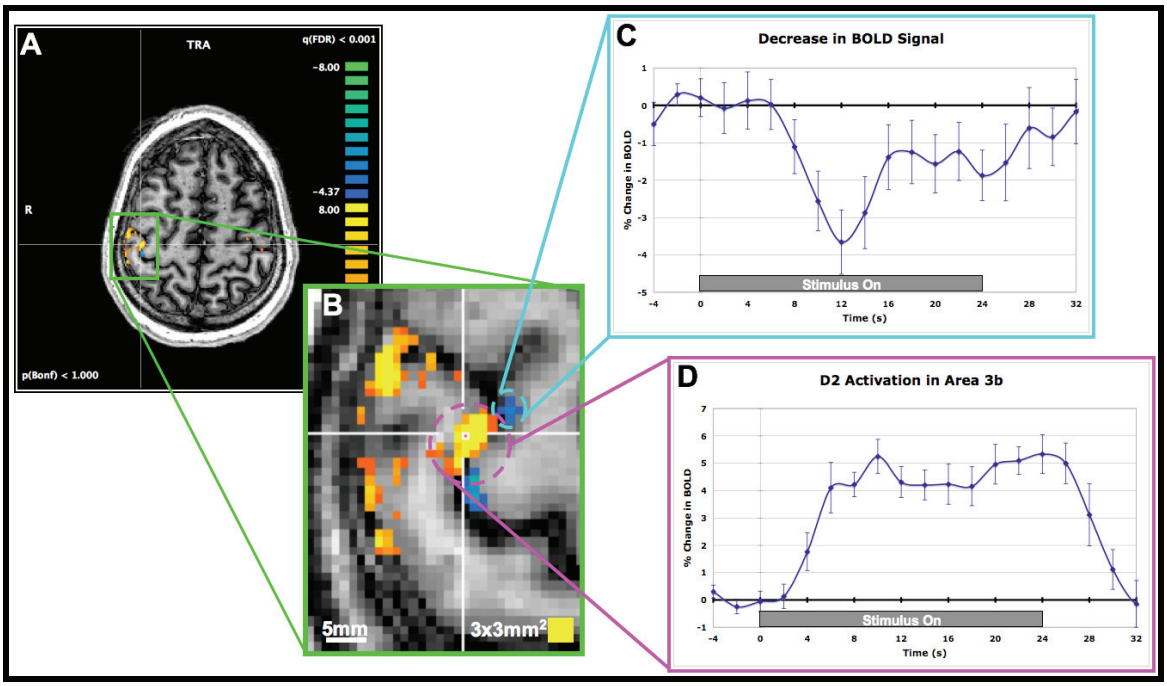

Figure 2. "Negative" BOLD signal along the anterior bank of the central sulcus (CS). (***A***) The activation map of a representative subject for D2-Rest, q(FDR) < 0.001, overlaid on the axial plane of a structural image. The green box indicates the zoomed-in area. (***B***) The activation map at an increased field-of-view, with the activation cluster on the posterior bank of the CS highlighted by the pink circle and the "negative" cluster on the anterior bank of the CS highlighted by the blue circle. The scale bar indicates 5 mm and the yellow square indicates an area 3x3 mm^2, a typical voxel size at 3 T. (***C***) The BOLD signal time course of the "negative" ROI illustrates the decrease in BOLD signal in these voxels. (***D***) The BOLD signal time course of the activation cluster demonstrates a robust positive BOLD response. The gray bar indicates the duration of the stimulus, 24 s.

To further examine whether the PBR and NBR were robust signals, we investigated the time course of the BOLD signal from these clusters. We defined the five peak (highest t-value) voxels from each of the two clusters highlighted by the pink (area 3b) and blue (M1) circles and extracted the BOLD signal time course. We calculated the mean response by averaging over the three runs and the three condition blocks within each run. The area 3b cluster (pink circle) responded robustly to the stimulation of D2, with a greater than 5% increase in BOLD signal (Figure 2D). The time course depicts the mean BOLD signal from 4 s before stimulus onset and 8 s following stimulus offset, with the gray bar indicating the duration of the D2 stimulus. The cortical response was

positive and sustained throughout the duration of stimulation. The lateral/anterior M1 cluster (blue circle) responded robustly to the stimulation of D2, but in a much different pattern than in area 3b. The time course illustrates a decrease in the mean BOLD signal in response to D2 stimulation. The NBR was less robust than the PBR, with less than a 4% decrease in BOLD signal, and the signal had a more transient pattern than the sustained pattern detected in area 3b. There was also a longer delay in BOLD signal onset, taking approximately 6-8 s to respond in M1 versus 2-4 s in area 3b.

Similar patterns of neighboring PBR and NBR were observed in other subjects in response to innocuous digit stimulation. The NBR was not restricted to M1 in all these subjects. Many of the NBRs were detected in both contralateral and ipsilateral primary somatosensory cortex adjacent to clusters of PBR. Not all subjects, however, revealed NBR.

Discussion and Future Directions

This is not the first study to observe measureable decreases in BOLD signal (Scheuml, REF). Studies within nonhuman primates have the advantage simultaneously measuring neuronal signal and BOLD signal to probe the two existing hypotheses of NBR. In the 2006 Shmuel study, the time course of the BOLD signal decrease was reported and looked remarkably similar to the BOLD signal time course from this study (Figure 2D), less the delayed lag. This monkey study also estimated what the NBR should look like based on the neuronal firing that was recorded. Again, these estimations matched their own data and ours.

In the future the NBR in all subjects will be systematically examined. The pattern of the BOLD signal across different regions of cortex will be investigated to explore where the temporal dynamics change across regions and whether this could give us insight into whether the NBR arises purely from vasculature effects or whether it is driven neuronally. In order to best estimate the hemodynamic response function

associated with the NBR in specific areas, an event-related design (instead of a block design) may be employed. As addressed in Chapter I, a block design stimulus protocol is best for signal detection, but and event-related design, in which the stimuli are delivered in jittered short blocks, is best for signal estimation. For all these studies, the higher spatial resolution from 7-T imaging is critical.

Areas beyond SI

Introduction

While SI is the principal region engaged in processing somatic sensation, it is not the only region elicited in the encoding of tactile information. Likewise, while SI was originally believed to be the primary region for processing pain sensation, we now know the secondary somatosensory cortex (SII) is the first region of cortex to receive pain information. As discussed in Chapter I, many cortical and subcortical structures are essential for the normal processing of innocuous touch and noxious heat perception.

Multiple crucial regions for the processing of touch and pain lie along the folds of the lateral sulcus (Sylvian Fissure). Most notable are the parietal operculum and insular cortex. Each of these cortical regions can be subdivided into smaller areas based on cytoarchitectural and functional differences. Studies carried out in the Zilles laboratory have subdivided the parietal operculum into four distinct areas based on the local cytoarchitecture and compared this histological data with fMRI data, creating a template for identifying these areas with MRI data alone ((Eickhoff et al., 2010), (Eickhoff et al., 2006b), (Eickhoff et al., 2006a), (Geyer et al., 1999), (Geyer et al., 2000), (Geyer et al., 2001)). The four parietal operculum (OP) areas have also been compared to well-characterized areas within nonhuman primate cortex: OP 1 is the human homologue of classic monkey secondary somatosensory cortex, OP 2 parietoinsular vestibular cortex, OP 3 ventral somatosensory area, and OP 4 parietal ventral area. At the posterior bank

of the OP is the retroinsular that is also believed to play a critical role in the processing of pain. The insular cortex lies within the folds of the lateral sulcus and can also be subdivided into multiple areas. Cytoarchitectural studies have revealed three layers of insular cortex, agranular, dysgranular, and granular, while anatomical studies have demonstrated specific connections in these three layers with other areas of the cortex and subcortex ((Kurth et al., 2010), (Augustine, 1996)). Functional differences along the anterior to posterior axis have also been observed, and are tightly coupled to the specific anatomical connections. For example, in general the posterior section of insular cortex is anatomically connected to sensory areas like SI and thus responds to sensory stimuli, while the anterior section of the insular cortex is anatomically connected to areas like the anterior cingulated and thus responds to affective stimuli.

Results

We detected multiple clusters of activation along the lateral sulcus in response to the heat-pain stimulus described in Chapter IV. The subdivisions of the OP adapted from Eickhoff *et al* are displayed for reference (Figure 3A, (Eickhoff et al., 2006b)). The activation maps using the subject ratings as a regressor are presented for two sample subjects along the lateral sulcus arranged from anterior to posterior (Figure 3B-E). The activation maps are overlaid on the structural images of each subject in the coronal plane, and the images area zoomed-in only over the area of interest. The lateral sulcus is indicated by the green line in the top and bottom images of Subject 1 (Figure 3B&D). Bilateral activation was not only detected, but more robust in the ipsilateral cortex (Figure 3D&E) than the contralateral cortex (Figure 3B&C). The activation maps were thresholded using an adaptive threshold due to the amplitude differences in signal between the two hemispheres ((Zhang et al., 2010)). The activation clusters were classified as localizing to OP 1 (green), OP 2 (blue), OP 3 (red), OP 4 (yellow), insula (purple), and retroinsula (cyan), and the classification was indicated by the colored arrow

pointing to the activation cluster.

After classifying the location of each activation cluster, we aimed to characterize the function of the cluster by examining the BOLD signal time course. The percent change in BOLD signal was plotted as a function of time, with a grey bar indicating the length of the temperature stimulus (Figure 3F). The BOLD signal response to the warm stimulus (35°C) was represented by the yellow trace, the moderate pain (5/6 on a 10 point scale) by the orange trace, and the high pain (7/8 on a 10 point scale) by the red trace. The mean BOLD signal time course was extracted from the peak five voxels in six of the activation clusters, numbered 1-6 on the activation maps and the time courses. The location of the activation cluster was written to the left of each time course. All of the time courses suggest that these areas of cortex respond to pain stimuli in a differential pattern than to innocuous warm stimuli. The exception was cluster 3 in Subject 2, located in contralateral OP 4, where the BOLD response to each of the stimuli is similar in amplitude throughout the duration of the stimulus. Other activation clusters such as cluster 4 in Subject 1, located in ipsilateral OP 3, responds robustly to the high pain stimulus and weakly, if at all, to the other temperature stimuli.

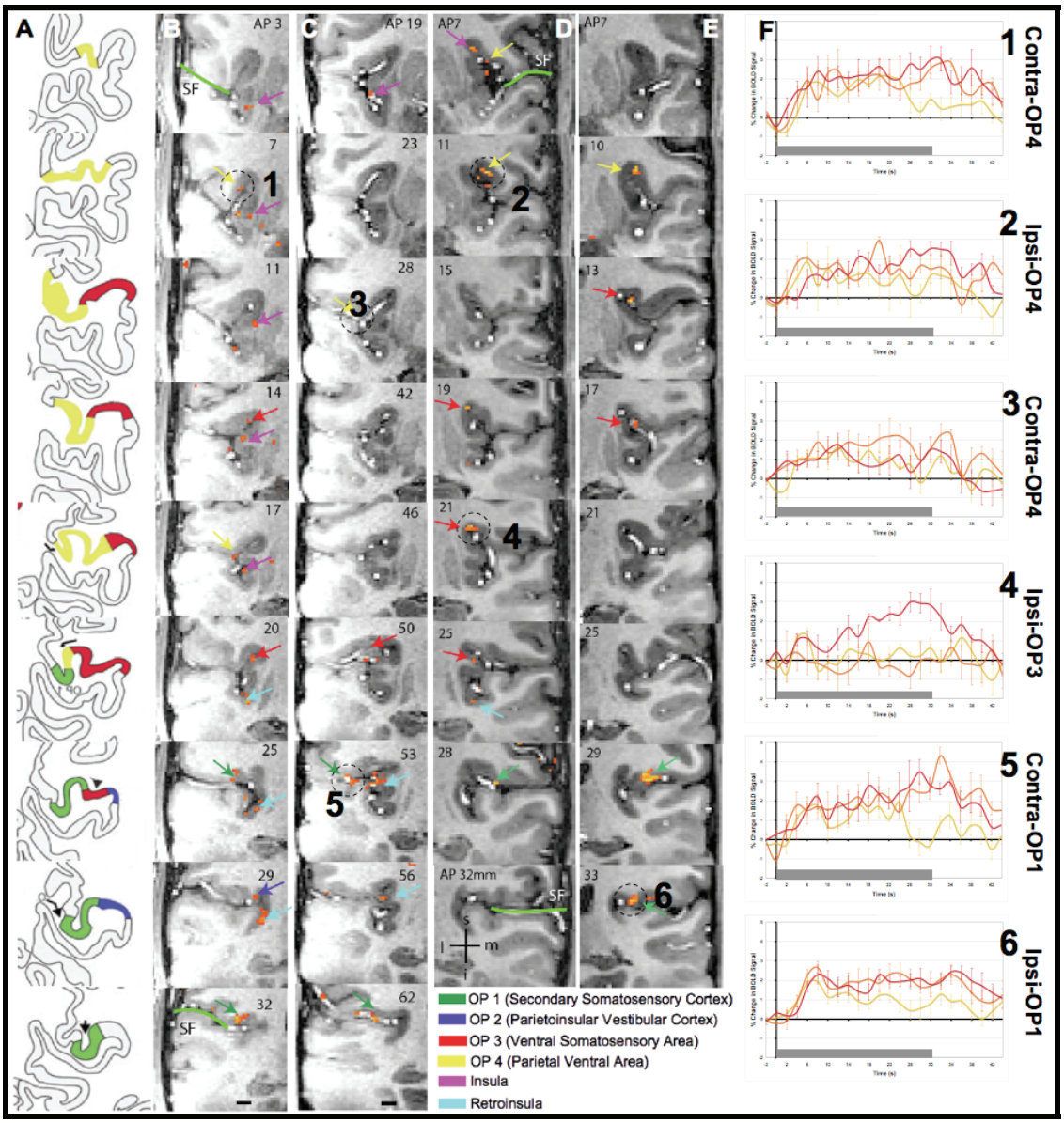

Figure 3. Activation maps (pain rating as regressor) are overlaid on anatomical images and displayed in the coronal plane to visualize cortical areas (parietal operculum (OP) and insula) along the lateral sulcus (bright green line) for two subjects. (***A***) Schematic of OP subdivisions [3] is displayed for reference. (***B*** and ***D***) Contra and ipsilateral cortex for Subject 1, adaptive threshold with cluster minimum of 4 voxels. (***C*** and ***E***) Contra and ipsilateral cortex for Subject 2, adaptive threshold with cluster minimum of 4 voxels. Numbers indicate millimeters posterior to the anterior commissure. Colored arrows indicate cytoarchitectural subdivisions along the lateral sulcus (see legend). A 6 mm scale bar is displayed in the bottom two images. (***F***) The BOLD signal time courses from multiple ROIs located along the lateral sulcus. The ROIs are indicated by the black circles and numbers (1 - 6) corresponding to the numbered time courses. The time courses depict the BOLD signal during each of the stimuli (warm yellow, pain orange, and tolerance red). The duration of the 30 s stimuli are highlighted by the grey time bar below each time course.

Discussion and Future Directions

In the future, more data must be acquired from multiple subjects in order to characterize the response to pain stimuli in these areas along the lateral sulcus. The activation maps were created using the subjects' ratings as regressors, so we need to acquire control data from a motor task without the presence of thermal stimulation. This will allow us to identify regions throughout the imaging volumes that are activated due to the motor task of rating versus the perception pain. A similar study using subjects' ratings as regressor for the creation of activation maps was performed at a lower field (3 T) and a lower spatial resolution (voxel > 30 mm^3) ((Baliki et al., 2009)). A rating motor task in the absence of pain stimulation was performed, and the activation map of the motor task and the activation map of the pain task with the rating as a regressor were compared. Robust activation was detected in the sensorimotor cortex (SI/M1), but subsequent analysis could neither identify this region as more strongly associated with the motor-rating task nor the pain-rating task. With the higher resolution images that we have acquired, we have greater ability to parse out how SI is engaged in pain processing and perception.

The activation along the lateral sulcus in response to the 2-Hz air puff also needs to be examined. Studies have observed topographical maps in human SII cortex from the face, hands, and legs ((Ruben et al., 2001), (Eickhoff et al., 2007)). While distinguishing individual digit representation in SII cortex is not likely resolvable due to the reported imprecision of these maps, we have not directly investigated this. The time course of the BOLD signal in the subdivisions along the lateral sulcus could give us insight into which aspects of the air puff stimulus are being processed by SII. Lastly, the thalamus, from which all of the cortical areas are receiving information from the periphery, needs to be investigated for touch and pain related activation.

Dynamic Nature of Functional Connectivity

Our data in addition to previous reports suggest that resting state functional connectivity (rs-fc) is not static ((Chang and Glover, 2010)). It would be detrimental to make an inference about a disease state based on the incorrect assumption that the rs-fc of a specific network is stable and invariant. Thus the stability of the resting state networks need to be investigated more systematically. In our study of rs-fc, we evaluated the stability of the lateral pain resting state network between two 190 s time intervals (prior to painful experience). We found static functional connectivity in two of our subjects and modest variance in functional connectivity in two of our subjects. The comparison of rs-fc between these time intervals could be improved by evaluating longer time intervals and multiple time intervals before the painful stimulus. By increasing the time interval we make more comparisons at the additional time point, decreasing noise (non-network specific correlation). We evaluated multiple time intervals after the painful experience, but not before. Additionally, by acquiring multiple time intervals, we can compare the correlations across various time points, resulting in a better metric of repeatability of the rs-fc in the defined network.

We have also demonstrated that the rs-fc within the lateral pain network is altered by a pain stimulus, but these modulations in the correlations vary over time and across subjects. The variance within the data is likely the consequence of studying a complex system like neural pain processing. We aim to study the functional connectivity in the less complex and better understood somatosensory system. We will acquire multiple resting state runs before and after somatic sensation. This will permit us to study areas of SI (areas 3b and 1) that have already been characterized, since the spatial and temporal BOLD responses to air-puff stimulation have been established in our previous somatosensory study (Chapter III). For example, the ROIs defined in the resting state study conducted in this work (Chapter IV) do not necessarily correlate or

respond to the same aspects of the pain stimulus in each subject, since each subject's experience is unique. On the other hand, the cortical representation of D2 is functionally similar, if not identical, across subjects. With more narrowly defined ROIs, our interpretation of the correlations between specific ROIs might be improved. We also aim to determine whether the significant modulations in rs-fc are specific to pain, or hold true for any sensory experience.

References

Apkarian, A.V., Bushnell, M.C., Treede, R.D., Zubieta, J.K., 2005. Human brain mechanisms of pain perception and regulation in health and disease. Eur J Pain 9, 463-484.

Augustine, J.R., 1996. Circuitry and functional aspects of the insular lobe in primates including humans. Brain Res Brain Res Rev 22, 229-244.

Baliki, M.N., Geha, P.Y., Apkarian, A.V., 2009. Parsing pain perception between nociceptive representation and magnitude estimation. J Neurophysiol 101, 875-887.

Brion, J.P., Demeurisse, G., Capon, A., 1989. Evidence of cortical reorganization in hemiparetic patients. Stroke 20, 1079-1084.

Chang, C., Glover, G.H., 2010. Time-frequency dynamics of resting-state brain connectivity measured with fMRI. Neuroimage 50, 81-98.

Conti, F., Fabri, M., Manzoni, T., 1986. Bilateral receptive fields and callosal connectivity of the body midline representation in the first somatosensory area of primates. Somatosens Res 3, 273-289.

Dreyer, D.A., Loe, P.R., Metz, C.B., Whitsel, B.L., 1975. Representation of head and face in postcentral gyrus of the macaque. J Neurophysiol 38, 714-733.

Eickhoff, S.B., Amunts, K., Mohlberg, H., Zilles, K., 2006a. The human parietal operculum. II. Stereotaxic maps and correlation with functional imaging results. Cereb Cortex 16, 268-279.

Eickhoff, S.B., Grefkes, C., Zilles, K., Fink, G.R., 2007. The somatotopic organization of cytoarchitectonic areas on the human parietal operculum. Cereb Cortex 17, 1800-1811.

Eickhoff, S.B., Jbabdi, S., Caspers, S., Laird, A.R., Fox, P.T., Zilles, K., Behrens, T.E., 2010. Anatomical and functional connectivity of cytoarchitectonic areas within the human parietal operculum. J Neurosci 30, 6409-6421.

Eickhoff, S.B., Schleicher, A., Zilles, K., Amunts, K., 2006b. The human parietal operculum. I. Cytoarchitectonic mapping of subdivisions. Cereb Cortex 16, 254-267.

Francis, S.T., Kelly, E.F., Bowtell, R., Dunseath, W.J., Folger, S.E., McGlone, F., 2000. fMRI of the responses to vibratory stimulation of digit tips. Neuroimage 11, 188-202.

Geyer, S., Schleicher, A., Schormann, T., Mohlberg, H., Bodegard, A., Roland, P.E., Zilles, K., 2001. Integration of microstructural and functional aspects of human somatosensory areas 3a, 3b, and 1 on the basis of a computerized brain atlas. Anat Embryol (Berl) 204, 351-366.

Geyer, S., Schleicher, A., Zilles, K., 1999. Areas 3a, 3b, and 1 of human primary somatosensory cortex. Neuroimage 10, 63-83.

Geyer, S., Schormann, T., Mohlberg, H., Zilles, K., 2000. Areas 3a, 3b, and 1 of human primary somatosensory cortex. Part 2. Spatial normalization to standard anatomical space. Neuroimage 11, 684-696.

Iwamura, Y., Iriki, A., Tanaka, M., 1994. Bilateral hand representation in the postcentral somatosensory cortex. Nature 369, 554-556.

Kastrup, A., Baudewig, J., Schnaudigel, S., Huonker, R., Becker, L., Sohns, J.M., Dechent, P., Klingner, C., Witte, O.W., 2008. Behavioral correlates of negative BOLD signal changes in the primary somatosensory cortex. Neuroimage 41, 1364-1371.

Killackey, H.P., Gould, H.J., 3rd, Cusick, C.G., Pons, T.P., Kaas, J.H., 1983. The relation of corpus callosum connections to architectonic fields and body surface maps in sensorimotor cortex of new and old world monkeys. J Comp Neurol 219, 384-419.

Krause, T., Kurth, R., Ruben, J., Schwiemann, J., Villringer, K., Deuchert, M., Moosmann, M., Brandt, S., Wolf, K., Curio, G., Villringer, A., 2001. Representational overlap of adjacent fingers in multiple areas of human primary somatosensory cortex depends on electrical stimulus intensity: an fMRI study. Brain Res 899, 36-46.

Kurth, F., Eickhoff, S.B., Schleicher, A., Hoemke, L., Zilles, K., Amunts, K., 2010. Cytoarchitecture and probabilistic maps of the human posterior insular cortex. Cereb Cortex 20, 1448-1461.

Kurth, R., Villringer, K., Curio, G., Wolf, K.J., Krause, T., Repenthin, J., Schwiemann, J., Deuchert, M., Villringer, A., 2000. fMRI shows multiple somatotopic digit representations in human primary somatosensory cortex. Neuroreport 11, 1487-1491.

Maldjian, J.A., Gottschalk, A., Patel, R.S., Detre, J.A., Alsop, D.C., 1999. The sensory somatotopic map of the human hand demonstrated at 4 Tesla. Neuroimage 10, 55-62.

Manzoni, T., Barbaresi, P., Conti, F., Fabri, M., 1989. The callosal connections of the primary somatosensory cortex and the neural bases of midline fusion. Exp Brain Res 76, 251-266.

Nelson, A.J., Chen, R., 2008. Digit somatotopy within cortical areas of the postcentral gyrus in humans. Cereb Cortex 18, 2341-2351.

Newton, J.M., Sunderland, A., Gowland, P.A., 2005. fMRI signal decreases in ipsilateral primary motor cortex during unilateral hand movements are related to duration and side of movement. Neuroimage 24, 1080-1087.

Ogawa, H., Ito, S., Nomura, T., 1989. Oral cavity representation at the frontal operculum of macaque monkeys. Neurosci Res 6, 283-298.

Peyron, R., Laurent, B., Garcia-Larrea, L., 2000. Functional imaging of brain responses to pain. A review and meta-analysis (2000). Neurophysiol Clin 30, 263-288.

Ruben, J., Schwiemann, J., Deuchert, M., Meyer, R., Krause, T., Curio, G., Villringer, K., Kurth, R., Villringer, A., 2001. Somatotopic organization of human secondary somatosensory cortex. Cereb Cortex 11, 463-473.

Sanchez-Panchuelo, R.M., Francis, S., Bowtell, R., Schluppeck, D., 2010. Mapping human somatosensory cortex in individual subjects with 7T functional MRI. J Neurophysiol 103, 2544-2556.

Schwartz, D., Fredrickson, J., 1971. Tactile direction sensitivity of area 2 oral neurons in the rhesus monkey cortex. Brain Research 27, 397-401.

Schweizer, R., Voit, D., Frahm, J., 2008. Finger representations in human primary somatosensory cortex as revealed by high-resolution functional MRI of tactile stimulation. Neuroimage 42, 28-35.

Shmuel, A., Augath, M., Oeltermann, A., Logothetis, N.K., 2006. Negative functional MRI response correlates with decreases in neuronal activity in monkey visual area V1. Nat Neurosci 9, 569-577.

Shmuel, A., Yacoub, E., Pfeuffer, J., Van de Moortele, P.F., Adriany, G., Hu, X., Ugurbil, K., 2002. Sustained negative BOLD, blood flow and oxygen consumption response and its coupling to the positive response in the human brain. Neuron 36, 1195-1210.

Toda, T., Taoka, M., Iwamura, Y., 1996. Transcallosal connections of the upperarm/shoulder region of the monkey postcentral somatosensory cortex. Japanese Journal of Physiology 46(Suppl.), S159.

Tommerdahl, M., Simons, S.B., Chiu, J.S., Favorov, O., Whitsel, B., 2005. Response of SI cortex to ipsilateral, contralateral and bilateral flutter stimulation in the cat. BMC Neurosci 6, 29.

Tommerdahl, M., Simons, S.B., Chiu, J.S., Favorov, O., Whitsel, B.L., 2006. Ipsilateral input modifies the primary somatosensory cortex response to contralateral skin flutter. J Neurosci 26, 5970-5977.

Weibull, A., Bjorkman, A., Hall, H., Rosen, B., Lundborg, G., Svensson, J., 2008. Optimizing the mapping of finger areas in primary somatosensory cortex using functional MRI. Magn Reson Imaging 26, 1342-1351.

Zhang, N., Wang, F., Turner, G.H., Gore, J.C., Avison, M.J., Chen, L.M., 2010. Intra- and inter-subject variability of high field fMRI digit maps in somatosensory area 3b of new world monkeys. Neuroscience 165, 252-264.